



Eduardo Henrique Filizzola Colombo

**Collective behavior of living beings under
spatiotemporal environment fluctuations**

Tese de Doutorado

Thesis presented to the Programa de Pós-graduação em Física of PUC-Rio in partial fulfillment of the requirements for the degree of Doutor em Física.

Advisor: Prof. Celia Beatriz Anteneodo de Porto

Rio de Janeiro
March 2018



Eduardo Henrique Filizzola Colombo

**Collective behavior of living beings under
spatiotemporal environment fluctuations**

Thesis presented to the Programa de Pós-Graduação em Física of PUC-Rio in partial fulfillment of the requirements for the degree of Doutor em Ciências – Física. Approved by the undersigned Examination Committee.

Profa. Celia Beatriz Anteneodo de Porto

Advisor

Departamento de Física – PUC-Rio

Prof. Marcos Gomes Eleuterio da Luz

UFPR

Prof. Roberto Andre Kraenkel

UNESP

Prof. Edgardo Brigatti

UFRJ

Prof. Welles Antonio Martinez Morgado

Departamento de Física – PUC-Rio

Prof. Márcio da Silveira Carvalho

Vice Dean of Graduate Studies

Centro Técnico Científico – PUC-Rio

Rio de Janeiro, March 16th, 2018.

All rights reserved.

Eduardo Henrique Filizzola Colombo

Received his bachelor and master degree in Physics from the Pontifícia Universidade Católica do Rio de Janeiro (Rio de Janeiro, Brazil) in 2012 and 2014, respectively. Awarded with the FAPERJ-Nota10 fellowship for outstanding students. Research interests include topics in complex systems with application to biological problems, such as population dynamics and evolution.

Bibliographic data

Filizzola Colombo, Eduardo Henrique

Collective behavior of living beings under spatiotemporal environment fluctuations / Eduardo Henrique Filizzola Colombo; advisor: Celia Beatriz Anteneodo de Porto. – Rio de Janeiro: PUC-Rio, Departamento de Física, 2018.

v., 117 f: il. color. ; 30 cm

Tese (doutorado) - Pontifícia Universidade Católica do Rio de Janeiro, Departamento de Física

Inclui bibliografia

1. Física – Teses. 2. Física estatística de não equilíbrio;. 3. Matéria ativa;. 4. Sobrevivência de populações.. I. de Porto, Celia Beatriz Anteneodo. II. Pontifícia Universidade Católica do Rio de Janeiro. Departamento de Física. III. Título.

CDD: 530

Acknowledgments

First of all, I would like to thank my advisor for her support over the last years of research. Since my bachelor studies, I have relied on the guidance of prof. Celia Anteneodo and have been in contact with the methodology and presentation that are expected of the scientific studies. I am grateful for her availability, for helping me find my research interests and also for the valuable advices and talks we have had in the process of this study.

I am thankful to professors Edgardo Brigatti, Marcos da Luz, Roberto Kraenkel, Welles Morgado and Daniel Stariolo for composing the evaluation committee for this thesis. I appreciate their reading and their availability to discuss the present work.

During my years at PUC-Rio, I had courses conducted by several enthusiastic and inspiring professors such as Geraldo Sigaud, Carla Göbel and Hiroshi Nunokawa, who were of significant impact on the formation of myself as a researcher. Specially, I would like to thank Prof. Welles Morgado for introducing me to the scientific career and for the many enlightening discussions on the subjects we have already studied together. I would also like to thank professors Leandro da Silva, Sabrina Camargo and Nuno Crokidakis for the various conversations and advices during my time as a doctorate student.

I thank all the participants of the PUC-Rio Complex Systems research group for the motivating exchange of information.

To professors Emilio Hernández-García and Cristóbal López, I am grateful for the hospitality during my visit to the Institute for Cross-Disciplinary Physics and Complex Systems (IFISC), for the conversations and for the collaboration we have established.

Over the past years, I could count on the friendship and support of many colleagues who have had great importance to my understanding of what we do as scientific researchers. For that, I would like to thank Lucianno, João, Michael, Marlon and Carlos.

The Physics Department of PUC-Rio, I thank for the continued support during my bachelor, master and doctoral degrees studies, that is possible due to the dedication of the staff personel, such as Giza, Marcia, Julio, Juliana, who daily help process all the necessary bureaucracy. I also appreciate Prof. Hiroshi Nunokawa dedication to the postgraduate studies' coordination.

Nothing would be possible without my parents, Perla and Oscar, who gave me the conditions to pursue my vocation. I also thank my partner Elisa for her constant support and for sharing with me important moments during these years.

Finally, I thank the funding agencies CAPES, CNPq and FAPERJ, that granted me the financial support that made this research viable. I would also like to thank the PUC-Rio Physics Department, National Institute of Science and Technology for Complex Systems and the IFISC for providing the necessary infrastructure and financial support during the research process.

Abstract

Filizzola Colombo, Eduardo Henrique; de Porto, Celia Beatriz Anteneodo (Advisor). **Collective behavior of living beings under spatiotemporal environment fluctuations**. Rio de Janeiro, 2018. 117p. Tese de doutorado – Departamento de Física, Pontifícia Universidade Católica do Rio de Janeiro.

Living entities have their own means of locomotion and are capable of reproduction. Furthermore, the habitat in which organisms are embedded is typically heterogeneous, such that environment conditions vary in time and space. In this thesis, theoretical models to understand the collective dynamics of living beings have been proposed and investigated aiming to address relevant questions such as population organization and persistence in the environment, using analytical and numerical techniques. Initially, considering an homogeneous habitat, in which the statistical properties of the environmental conditions are time and space independent, we study how spatiotemporal order can emerge in the population distribution due to nonlocal interactions and investigate the role of environment fluctuations in the self-organization process. Further, we continue our investigation assuming an heterogeneous environment, starting with the simplest case of a single habitat domain, and we obtain the critical conditions for population survival for different population dynamics. Considering a class of nonlinear equations, introducing temporal oscillations and interactions among the organisms, we are able to provide a general picture of population stability in a single habitat domain, challenging previous ecological concepts. At last, assuming a fragmented complex landscape, resembling realistic properties observed in nature, we additionally assume that individuals have access to information about the spatial structure. We show that individuals survive when patches of viable regions are clustered enough and, counter-intuitively, observe that population size is maximized when individuals have partial information about the habitat. Finally, since, analytical exact results are not feasible in many important situations, we propose an effective approach to interpret experimental data. This way we are able to connect environment heterogeneity and population persistence.

Keywords

Non-equilibrium statistical physics; Active matter; Population survival.

Resumo

Filizzola Colombo, Eduardo Henrique; de Porto, Celia Beatriz Anteneodo. **Comportamento coletivo de organismos vivos sob flutuações espaço-temporais do meio ambiente**. Rio de Janeiro, 2018. 117p. Tese de Doutorado – Departamento de Física, Pontifícia Universidade Católica do Rio de Janeiro.

Organismos vivos têm seus próprios meios de locomoção e são capazes de se reproduzir. Além disto, o habitat no qual os organismos estão inseridos é tipicamente heterogêneo, de modo que as condições ambientais variam no tempo e no espaço. Nesta tese, são propostos e investigados modelos teóricos para compreender o comportamento coletivo de organismos vivos, visando responder questões relevantes sobre a organização e preservação da população utilizando técnicas analíticas e numéricas. Inicialmente, considerando um habitat homogêneo, em que as propriedades estatísticas das condições ambientais são independentes do tempo e do espaço, estudamos como padrões espaço-temporais podem emergir na distribuição da população devido a interações não-locais e investigamos o papel das flutuações ambientais neste processo. Em seguida, assumindo um meio ambiente heterogêneo, analisamos o caso de um único domínio de habitat. Considerando uma classe de equações não lineares, introduzindo flutuações temporais e interações entre os organismos, fornecemos uma perspectiva geral da estabilidade de populações neste caso, desafiando os conceitos ecológicos anteriores. Em um segundo passo, assumindo uma paisagem complexa fragmentada, consideramos que os indivíduos têm acesso a informações sobre a estrutura espacial do meio. Mostramos que os indivíduos sobrevivem quando as regiões espaciais viáveis estão suficientemente aglomeradas e observamos que o tamanho da população é maximizado quando os indivíduos utilizam parcialmente a informação do meio ambiente. Finalmente, como resultados exatos analíticos não são factíveis em muitas situações importantes, propomos uma abordagem efetiva para interpretar os dados experimentais. Assim, somos capazes de conectar a heterogeneidade do ambiente e a persistência da população, caracterizada pela distribuição de probabilidade para os tempos de vida.

Palavras-chave

Física estatística de não equilíbrio; Matéria ativa; Sobrevivência de populações.

Table of contents

1	Introduction	10
2	Basic concepts and tools	13
3	Homogeneous environment	18
3.1	Local dynamics	18
3.2	Dispersal	22
3.3	Nonlocal interactions	25
3.3.1	Instability conditions	28
3.3.2	Impact of noise	31
3.3.2.1	When patterns are present in the deterministic case	33
3.3.2.2	When patterns are absent in the deterministic case	34
3.3.2.3	Temporal correlations	37
4	Single habitat domain	41
4.1	Nonlinear population dynamics	44
4.1.1	Density-dependent feedback	45
4.1.2	Nonlinear asymptotic behavior	48
4.1.3	Steady states and critical habitat size	52
4.1.4	Role of initial conditions	56
4.2	Higher order interactions	57
4.3	Habitat temporal behavior	60
4.3.1	Static refuge case	63
4.3.2	Slow and fast limits	65
4.3.3	Spatial response	66
4.3.4	Recolonization process	69
5	Metapopulation dynamics	71
5.1	Dispersal guided by habitat information	73
5.2	Complex landscape	74
5.3	Deterministic dynamics	77
5.4	Stochastic dynamics	79
5.4.1	Spatially extended system	80
5.4.2	Habitat topology and coupling range	83
5.4.3	Density of favorable patches	83
5.5	Extracting metapopulation heterogeneity from ensemble data	87
6	Final remarks on population dynamics	93
A	Master equation	95
B	Mean extinction time	96
C	Time-dependent habitat	98
C.1	Population growth in heterogeneous static environment	98

<i>Table of contents</i>	9
C.2 Slow and fast limits with harsh conditions outside the refuge	99
D Metapopulation stability	101
E Numerical method for partial differential equations	103
Bibliography	105

1 Introduction

Statistical physics has been providing a path to connect the microscopic dynamics to the macroscopic observable phenomena. In the pursuit of this connection, the discipline has crossed the traditional boundaries, reaching other fields such as Chemistry, Biology and Sociology [1–3]. The collective dynamics of living beings is one of the cross-interdisciplinary subjects that has received attention recently. In considering different fundamental living entities (e.g. bacteria, ants, birds and humans), some particular features are introduced in the system. Here, in contrast to the classical case where particles are passive, the elementary units are self-propelled and endowed with the remarkable capacity of reproduction [2, 4].

The microscopic dynamics of living beings depends on a large web of processes through a wide range of scales. Due to the complexity involved in the constitution of the individuals and on the mechanisms of interaction, the relevant macroscopic behavior is disconnected from the low level physics underneath [5]. Nevertheless, macroscopic laws can be defined for a density field in its own scale [6–8]. The mathematical approach adopted in this work is based on writing a dynamical equation for the temporal evolution of the population density distribution $\rho(x, t)$. For example, the number of insects per square meter, where x is a location in space and t a time instant. Besides that, any population is intrinsically coupled to the environment, which controls many of the biological processes. Therefore, we assume that the density distribution is subjected to external conditions represented by $M(x, t)$ (e.g. nutrient concentration, temperature, humidity, soil and so on) which is typically heterogeneous in space and time.

In this thesis, given the rules of the dynamics, such as laws for movement, reproduction, interactions and environment coupling, we investigate the set of environment conditions for which population survival occurs. We will develop mathematical models, gradually incorporating fundamental features of living organisms and the ones observed in natural habitat, such as fragmentation, seasonality and randomness. The collection of results presented provide a general picture about the stability of biological populations with applications to conservation biology.

The theoretical investigation of population dynamics in heterogeneous environment has always been a central issue to spatial ecology [9–11]. In 1951, J. Skellam [12] noticed that the habitat should have size L above a certain threshold L_c to allow population survival ($L > L_c$). Later, in 1979, this problem was revised to determine the occurrence of an species invasion (such as a plague) [13]. For both cases, the conditions investigated assumed that the external conditions M generate a single time-independent habitat domain surrounded by harmful conditions. Subsequent models introduced different individual movement and growth laws [14]. More recently, this topic has also received renewed attention [15–21], revealing additional features of the dynamics. In all these cases, it is a robust feature that population survives for $L > L_c$, where the particular value of L_c depends on each model detail.

The investigation of population persistence in more complex habitats started around 1967 with the theory of island biogeography by R. MacArthur and E. O. Wilson [9], followed by S. Levin’s work on population dynamics in heterogeneous habitat [10], culminating with I. Hanski et al. [22], giving rise to the so called metapopulation theory [11, 22, 23]. In these cases, it is considered that the habitat is fragmented, being composed not by one but by many spatial domains, known as *patches*, in which the individuals find suitable condition for reproduction, such shelter, food, etc. These subpopulations remain coupled due to individual dispersal, creating a population network [24]. In this scenario, the critical spatial condition appears condensed in the form of the metapopulation capacity [22], which takes into account the major component of the spatial patch distribution (related to the maximum eigenvalue of the network adjacency matrix). Similarly to the single domain case, in the fragmented landscape, there is a threshold related to its connectivity.

It is worth to stress that biodiversity ensures ecosystem robustness against environmental changes [25]. Understanding this issue is relevant in times when habitats are getting smaller and fragmented and climate [26]. Human activity has been considered one of the main causes of these recent changes, defining the *antropocene* epoch [27]. Notable examples of human impact on habitat spatiotemporal patterns are deforestation and urbanization processes [24, 28]. On the other hand, human intervention can also be constructive, for instance, implementing proper design and management of habitats to promote population conservation [14, 29].

This thesis will be divided as described hereafter. In Chapter 2, we present the mathematical framework used to describe the system. We also define important concepts about the environment modeling and a proper definition of the population persistence is presented.

In Chapter 3, we assume that environmental properties are homogeneous, i.e., the environment conditions might change in time, but local statistical properties are invariant in time and space. First, we introduce the local (Sec. 3.1) and spatial (Sec. 3.2) components of the dynamics. Further, we take the opportunity to consider interesting scenarios where spatiotemporal order emerges exclusively due to individual interaction (Sec. 3.3). We will investigate how environment fluctuations interfere in the stability of pattern formation in the population density distribution.

In Chapter 4, we will start our discussion regarding population conservation, reviewing the classical single habitat domain case and then extending the model by assuming different population dynamics and also considering environment seasonality. Our results show how different scenarios affect the population persistence criteria. Investigating a general nonlinear case (Sec. 4.1), we find that, for a certain class of dynamics, the ecological establishment that the critical habitat size is a lower bound for population survival breaks down. Counter-intuitively, we find cases in which the population survives when the habitat size is smaller than a critical value $L < L_c$, or for any habitat size $L > 0$. Furthermore, we analyze the role of higher order interaction (Sec. 4.2) and habitat temporal fluctuations (Sec. 4.3) and show that both considerably affects the value of the critical habitat size.

In chapter 5, we investigate the persistence of a population with information based dispersal (Sec. 5.1) in a complex habitat (Sec. 5.2). In nature, fractality might appear due to power-law correlations between environment resources [24,28,30,31] or due to complex transformations, such as urbanization processes [32]. One of our results shows that there is a threshold for habitat clusterization (fractal dimension) for which the population can survive (Sec. 5.3). Moreover, we discuss the role that the habitat spatial information plays in the dispersal of the individuals (Sec. 5.4). We show that population size is maximized for a specific balance between random and directed movement towards more viable locations. In the last section (Sec. 5.5) we propose an effective model to interpret metapopulation experimental data, bypassing analytical difficulties in solving exactly nonlinear spatial stochastic processes [8].

The results presented in the upcoming chapters can be found in the following publications: Chapter 3 in Ref. [33]; Chapter 4 in Refs. [34,35] and Chapter 5 in Ref. [36].

Final remarks on population conservation are presented in the last chapter. We also state a summary of our findings and the general picture of the results.

2 Basic concepts and tools

In order to be precise about the system that we will study, we present below the mathematical tools and concepts that are fundamental to the next chapters.

The fundamental object that defines the population state is the individuals' position set $X = \{x_n\}_{\forall n < N}$, including the full information about population spatial structure and size N . The temporal evolution of X depends on the rules for the biological processes that drive displacement, creation and annihilation of the elements in the set [37].

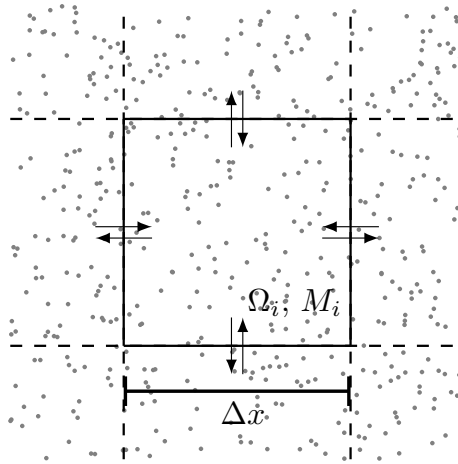


Figure 2.1: Illustration of the coarse-grained perspective. Dots represent particles, while lines separate cells Ω_i with environment conditions M_i and area Δx^2 . Arrows indicate that particles might flow between cells.

Instead of dealing with a potentially large set, $N \gg 1$, the system can be described in a coarse-grained perspective. We start by subdividing the environment domain $\Omega \subseteq R^d$ in identical regions Ω_i with area $(\Delta x)^d$ arranged in a lattice. The habitat dimension d is typically $d = 2$, although in some cases $d \approx 1$, when the dynamics occurs in narrow corridors or channels [17]. Then, we define the population density at region i as $\rho_i \equiv n_i / (\Delta x)^d = \frac{1}{\Delta x^d} \sum_i^N \mathbb{1}_{\Omega_i}(x_i)$, where the indicator operator $\mathbb{1}_{\Omega_i}(x_i) = 1$ if $x_i \in \Omega_i$, and zero otherwise [8].

Locally, we will assume that individuals reproduce, die and compete, increasing or decreasing population size, respectively. The spatial coupling between regions Ω_i arises due to fluxes between locations or due to nonlocal

interactions. Individuals change location by their own means, moving through the ecological landscape (flux between adjacent cells), being constantly affected by the habitat; or, differently, as in the case of birds that can fly over the landscape, nonlocal fluxes can also occur [11]. Moreover, individuals might interact at distance, due to communication or hidden mechanisms (see Fig. 3.3). In Fig. 2, we illustrate this coarse-grained perspective, recalling that to each region Ω_i is associated with an environment condition M_i .

Thus, we construct the general model with local and nonlocal terms,

$$\partial_t \rho_i = F(\rho_i | M_i) + \Gamma[\rho | M], \quad (2-1)$$

where F is the net growth per capita at region i and Γ the changes due to individual flux and interaction, both written as a function of population density.

In a compact way, we can write

$$\partial_t \rho_i(t) = \mathcal{L}[\rho | M], \quad (2-2)$$

which might also be written in the continuous space form,

$$\partial_t \rho(x, t) = \mathcal{L}[\rho | M]. \quad (2-3)$$

Particular forms for \mathcal{L} and environment M will be discussed in the next chapters. Diverse features of the system will be analyzed numerically with methods described in Appendix E and also analytically, with methodology discussed separately in Chapters 3, 4, 5. We will mainly focus on the asymptotic behavior of the population density distribution and the condition for population survival.

Environment spatiotemporal structure

The combination of different environment factors result in a macroscopic quantity $M(x, t)$, that provides habitat quality for a given species. In ecology, this is known as the *ecological landscape* [28]. The landscape represents the mesoscopic view of the environment, taking into account only the major variations of the habitat quality. An habitat domain is defined when a particular location meets the species requirement, having a particular microbioma, such as a bog, bush, tree, or even created artificially [28,30,38,39]. In some models, for instance, the landscape is considered a binary lattice with cells being suitable or not to population development [24].

The spatial structure of the landscape can be diverse. For the following chapters, three major categories are relevant: homogeneous, single domain

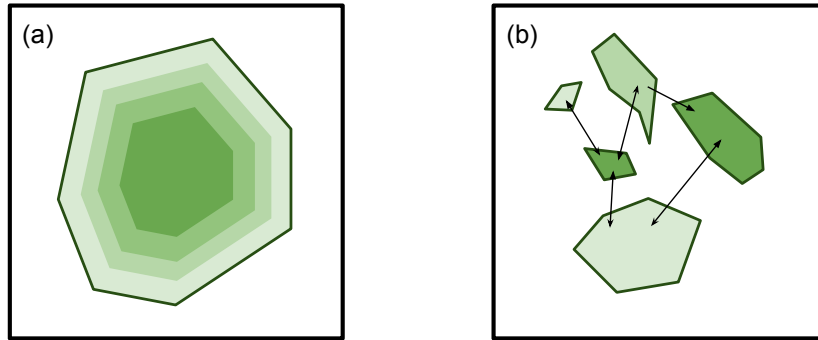


Figure 2.2: Pictorial representation of (a) single habitat domain and (b) metapopulation network. The shades of green represent possible variations in habitat quality and black lines the delimitation of the habitat domains.

and fragmented. The homogeneous case refers to the situations in which environment conditions are constant in space and time. In Fig. 2.2a, we illustrate the single domain case and in Fig. 2.2b the fragmented habitat case.

For instance, a single habitat domain can be created for bacteria, combining a background of abundant resources that promotes population growth and a heterogeneous field of UV-light that increase the death rate (see Sec. 4.3). In this case, there exists a single domain where the population is protected from the harmful radiation [17]. In the ecological scale this single domain might be generated by public policies, delimiting reserves, with the implementation of fishing and hunting regulations.

In nature, the landscape is typically fragmented, being composed by many habitat domains that are patches of the landscape [24]. A clear example is an archipelago, where the geographical constraints set the landscape spatial structure. More sophisticated landscapes arise, for instance, in the case of butterflies, where only particular locations fulfill the basic requirements for population development, such as level of humidity, temperature, water, sun light [24, 28]. Further details will be discussed in chapters 4 and 5.

Moreover, we should have in mind that the landscape is also in constant change. At short scales, the parameters that quantify the environment conditions have high uncertainty in short scales due to the complexity of the environment dynamics. At longer scales, ecosystems follow the circadian rhythm (day-night cycles) and seasons, generated by the one year oscillation of sun light. We illustrate this with the data for temperature at Copacabana beach (Rio de Janeiro, Brazil) in Fig. 2.3. The temporal evolution of the temperature is shown on the left for several years (with the one year cycle highlighted), while the right plot shows the power spectrum with peaks at the year and half-year frequencies. Despite the annual periodicity, there is

also a small semiannual oscillation, which is known to occur in some globe locations [40]. The spectrum has also an exponential tail (red line), indicating that correlation decays as a power-law for at least for short time scales. This features are not particular to the temperature, but typically observed in many other environment parameters [28,31].

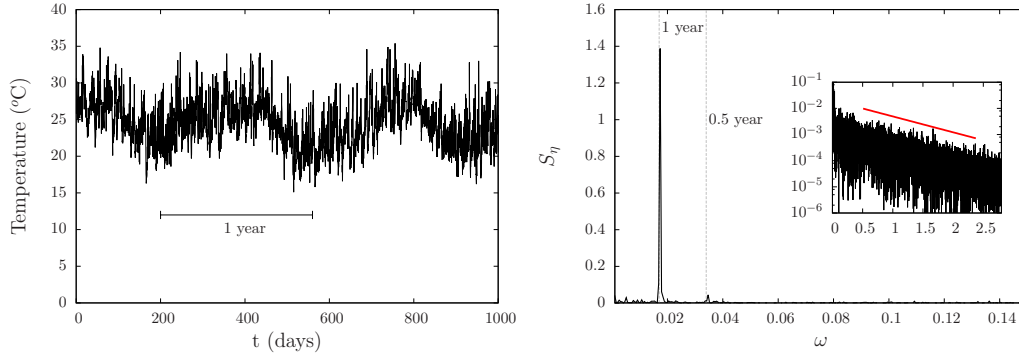


Figure 2.3: From the INMET dataset from Rio de Janeiro, we extract the period from 1961-2014 which contain temperature records every 12 hours. On the top, we show the evolution of the average daily temperature. On the bottom, we show the power spectrum for the average daily temperature with inset indicating the behavior exponential ($\tau_c \simeq 0.7$) behavior for short wave length in log scale. Semiannual oscillations [40] are also detected. Performing a detrending analysis [41] of the time series on the top, we observe a Gaussian like probability distribution and variance $\langle \eta^2 \rangle \in [1, 3]$.

For the cases investigated in the following chapters, we will focus on the fundamental aspects of the environment temporal behavior, discussing the role of seasonality and uncorrelated random fluctuations. The impact of other details shown in Fig. 2.3 are addressed when necessary, but in general, are not expected to affect qualitatively the presented results.

Extinction characterization

The core results of the following chapters depend on the definition of the extinction criteria. Extinction will be determined analyzing the asymptotic dynamics of the total population size,

$$N(t) = \int_{\Omega} \rho(x, t) dx . \quad (2-4)$$

We consider that an extinction event occurred if, when starting from a positive initial condition $N(0) > 0$, the population size becomes null ($N(t) = 0$) at a given instant t . However, in some cases, the null steady state is approached asymptotically, so $N > 0$ for all times. In these cases, after a transient, the

total population typically will either grow towards a constant value or decay according to a certain law. Then, we will assume that extinction (survival) occurs when $\frac{\dot{N}}{N} < 0$ ($\frac{\dot{N}}{N} \geq 0$).

Furthermore, when we consider stochastic fluctuations, population persistence needs to be characterized by the statistical properties of the population lifetimes \mathcal{T} . This will be discussed in details in Sec. (3.1). In the limit of infinite number of individuals, there is a clear choice, since the population average extinction time diverges for some range of environment parameters [21, 42], meaning full persistence. For other cases, in which extinction times are finite, we say that population will get extincted. However, when the number of individuals is small, survival is never fully achieved [21, 42]. In these cases, one should look to relevant changes in the dependency of the extinction times with environmental parameter. Assuming a suitable microscopic description of the system [21], previous results show that the deterministic analyzes point out the correct threshold for environment conditions that delimits the extinction-survival phases [21]. It is worth to mention, that other extinction criteria might be more relevant [42], but only quantitative corrections should be added.

For the cases that will be investigated in Chapter 4 and 5, there is clear surface M_c in environment parameter space that separates the extinction and survival phases. Nevertheless, in general, the extinction and survival phases in the environment parameter space, could be more complicated, since there is no guarantee that the interface between phases is well defined. Then, perhaps, in a broader perspective, we should define that in the set of all possible environment conditions, there exists a subset M_s , for which if $M \in M_s$, population survives, meanwhile, if the environment conditions belongs to the complement $M_e \equiv M \setminus M_s$, population will get extincted (eventually).

3

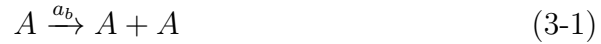
Homogeneous environment

In this chapter, we will investigate population dynamics in a homogeneous environment. We will assume that habitat is made of random fluctuations, but assuming its statistical properties are time and space independent. We start introducing basic elements in the mathematical model, such as birth-death and dispersal processes, in Sec. 3.1 and 3.2. The homogeneous case allows us to understand population spatial distribution without any habitat bias. In the last section, we will show that nonlocal interactions triggers population selforganization, generating spatiotemporal patterns in the population density distribution. Further, we show how environment fluctuations can affect the pattern formation process.

3.1

Local dynamics

The first ingredients that we introduce in the dynamics are the elementary processes: reproduction, death and competition that occur locally. Those processes can be written in terms of reactions,



where the a_b and a_d are the birth and death rates and b the competition term, when the population interact in pairs for resources.

Following the master equation approach (for details see Appendix A), the implementation of the above reaction chain gives us a Fokker-Planck equation for the number of individuals n ,

$$\partial_t P = -\partial_n [f(n)P] + (1/2)\partial_{nn} [g(n)P], \quad (3-4)$$

with

$$f(n) = (a - bn)n,$$
$$g(n) = (a_b + a_d)n + bn^2,$$

where $a \equiv a_b - a_d$.

In the limit of large n , the population statistics is well described by its first and second cumulants. This is not true in general, particularly for the extremely small and large population sizes, the Fokker-Planck equation (3-4) has minor but significant deviations from the exact solution. A more accurate prediction of the probability density distribution for population size n can be made following more sophisticated methods such as a WKB approximation [43, 44].

The first term in Eq. (3-4) takes into account the drift, driven by the deterministic forces $f(n) = (a - bn)n$. At low densities, population grows exponentially and then reaches a saturation point $n_0 = a/b$, for which reproduction and resource availability balance, $f'(n_0) = 0$. The particular form of f in Eq. 3-4 is known as logistic growth or Verhulst model [6, 45]. The second term of Eq. (3-4), introduces the fluctuations of the birth-death processes.

The temporal evolution of the population size can also be posed as a Langevin equation,

$$\dot{n} = f(n) + \sqrt{g(n)} \circ \xi(t), \quad (3-5)$$

where n is treated as a continuous variable and intrinsic stochasticity is implemented introducing a zero mean unit variance noise ξ . Since ξ enters in Eq. (3-5) as multiplicative noise, we introduce the notation of a small circle (\circ) to recall that ξ should be interpreted following Ito prescription, since demographic noise is nonanticipative, being strictly uncorrelated [46].

Despite the fact that we obtain a quadratic g in Eq. (3-4), typically fluctuations associated to the competition process are neglected in the literature [44, 47–49]. Then, in the following chapters, we considered that $g(n) \propto n$.

In the next step, we consider that the environment is fluctuating in time. We assume that the reproduction rate $a \rightarrow a + \eta$, where η is a zero mean Gaussian white noise,

$$\dot{n}(t) = f(n) + \eta(t) \bullet n(t) + \xi(t) \circ \sqrt{n(t)}. \quad (3-6)$$

Equivalently, substituting $n = \rho \Delta x^d$ and setting new scaled parameters, the above equation can be written for the population density [44],

$$\dot{\rho}(t) = f(\rho) + \eta(t) \bullet \rho + \xi(t) \circ \sqrt{\rho}. \quad (3-7)$$

Eq. (3-7), with these two components of randomness, is known as the *canonical model* [44]. The notation applied to the multiplicative noises reminds their origins, giving a modeling consistency to Eq. (3-7). The environmental noise is produced by the complex ecosystem dynamics, which makes the

evolution of the environment conditions behave erratic in time. Nevertheless, produced by a dynamical system any environment property should exhibit a nonnull time correlation, even if arbitrarily small. This leads us to interpret η following Stratonovich prescription (\bullet) [46]. Differently, as mentioned above, demographic noise is internal to the dynamics (\circ), being nonanticipative [33, 46]. Despite the fact that there is a mathematical equivalence between both approaches, we keep this distinction between noises η and ξ in Eq. (3-7) to highlight the model structure. The consequences of each noise prescription to the dynamics will be tackled in the last section.

In the limit of large population size demographic noise can be neglected, since it goes as the square of the population size, while environmental noise and f certainly contain higher order terms. This approximation is typically used in the case of microorganisms, where entities are numerous [17] and it will be used in Chapter 4.

In order to understand the different roles of η and ξ , we set their variance to σ_η and σ_ξ , respectively. From the stochastic differential equation Eq. (3-6), we can obtain the associated Fokker-Planck

$$\partial_t p(n) = -\frac{\partial}{\partial n} (f(n) + \sigma_\eta^2 n/2) p(n) + \frac{\sigma_\xi^2}{2} \frac{\partial^2}{\partial n^2} (n p(n)) + \frac{\sigma_\eta^2}{2} \frac{\partial^2}{\partial n^2} (n^2 p(n)). \quad (3-8)$$

which extends Eq. (3-4), including environment fluctuations η . Ignoring the occurrence of extinctions, that is, neglecting the flux of probability that leaves the system at $n = 0$, Eq. (3-8) admits a steady solution

$$\begin{aligned} p_s(n) &\propto \frac{1}{(\sigma_\xi^2 + \sigma_\eta^2 n)n} \exp\left(\int^n \frac{f(z) + \sigma_\eta^2 z/2}{\sigma_\xi^2 z + (\sigma_\eta z)^2} dz\right), \\ &\propto (\sigma_\xi^2 + \sigma_\eta^2 n)^{[a+b\sigma_\xi^2/\sigma_\eta^2]} \exp\left[\frac{-bn}{\sigma_\xi^2 + \sigma_\eta^2}\right]. \end{aligned} \quad (3-9)$$

In the limit of low population density $n \rightarrow 0$,

$$p_s(0) \propto \sigma_\xi^{2[a+b\sigma_\xi^2/\sigma_\eta^2]}. \quad (3-10)$$

This shows that demographic stochasticity ξ is the main mechanism of extinction. That is, if only environmental stochasticity is present ($\sigma_\xi = 0$), the null state is a natural boundary, being automatically inaccessible starting from $N_0 > 0$ [50]. In this case, mathematical modeling becomes incomplete and an artificial mechanism of extinction needs to be implemented (e.g. consider extinction occurs when the total population density goes below a certain value) [50].

In order to have a more realistic scenario, we can introduce an effective term to account for the flux exchange with the surroundings. For instance,

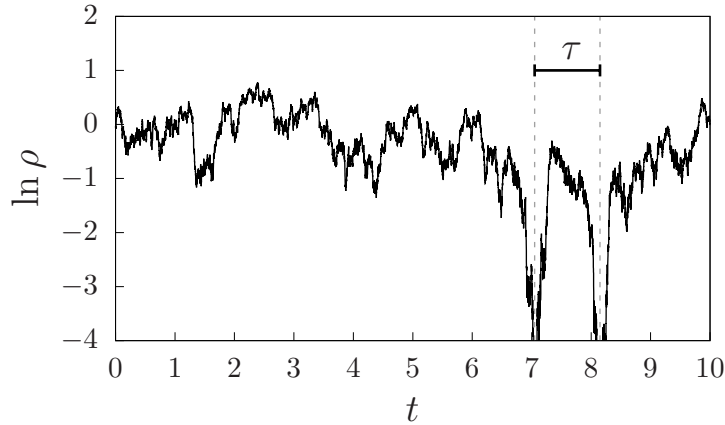


Figure 3.1: Temporal evolution of the local population density for the canonical model (3-7) plus the additive migration term. The interval τ highlights a lifetime event.

below we consider an extra additive term ζ in Eq. (3-7),

$$\dot{\rho}(t) = f(\rho) + \eta(t) \bullet \rho(t) + \xi(t) \circ \sqrt{\rho(t)} + \zeta(t), \quad (3-11)$$

with ζ as a Gaussian white noise. The protocol ζ is the pressure that drives the migration inwards and outwards of the system. Since ζ can assume positive values, the null state is not absorbent anymore and an extinction dynamics is established (see Fig. (3.1)). In this case, there is a steady state such as the one found in Eq. (3-9).

Taking into account all the elementary features of the canonical model, we see that an isolated population will be certainly extincted at some time. From Eq. (3-7), for the population density ρ , we can obtain the mean population extinction time (see Appendix B for derivation)

$$\mathcal{T} = \int_0^{\rho(0)} \int_z^\infty \frac{\exp(\int_z^v \Psi(u) du)}{V(v)} dv dz, \quad (3-12)$$

where $\Psi(\rho) = 2M(\rho)/V(\rho)$, with $M(\rho) = a\rho - b\rho^2 + \sigma_\eta^2\rho/2$ and $V(\rho) = \sigma_\eta^2\rho^2 + \sigma_\xi^2\rho + \sigma_\zeta^2$ (see Eq. (3-8)). In Fig. (3.1) we show the comparison between the theoretical prediction given by Eq. (3-12) and numerical simulation of Eq. (3-7) (see Appendix E). In this scenario, averages are performed over an ensemble of realizations starting from $\rho(0)$.

Other possible extensions of the canonical model might be implemented to include more realistic features of the natural systems. The canonical model introduced environmental stochasticity in a standard way. Nevertheless, environment is known to have two remarkable features: randomness and seasonality. Typically, environment conditions have nontrivial statistical

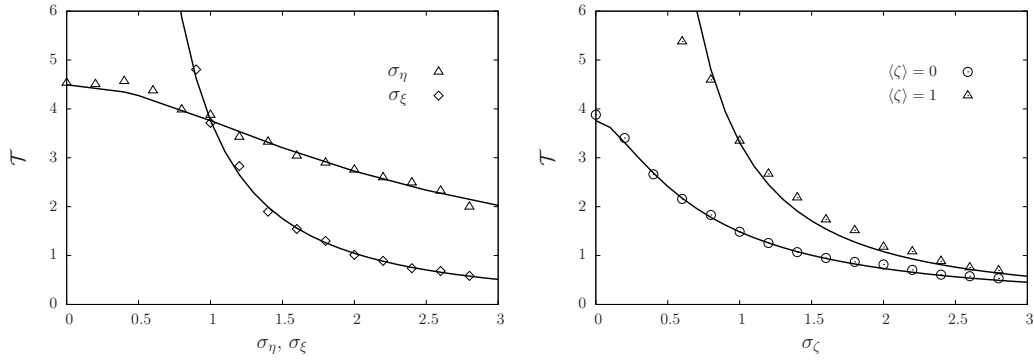


Figure 3.2: Mean lifetime \mathcal{T} starting from $\rho(0) = 1$ as a function of σ_η , σ_ξ with $\sigma_\zeta = 0$ (left) and σ_ζ for $\langle \zeta \rangle = 0$ and $\langle \zeta \rangle = 1$ with $\sigma_\eta = \sigma_\xi = 1$ (right). Remaining parameters are $a = b = 1$. Solid line represents the result from Eq. (3-12) and dots the direct integration of Eq. (3-11).

properties [28,31]. As an example, in Fig. 2.3, we showed the temporal evolution of the temperature at Copacabana beach (“posto 6”). The power spectrum shows the evident one year cycle accompanied by colored random fluctuations.

Typically, many environment conditions will possess similar temporal behavior, embodying these two fundamental features of the environment. Then, one might be interested, in assuming that

$$a(t) = a_0 + A \sin(\Omega t) + \eta(t). \quad (3-13)$$

In this case, even for small A , stochastic resonance phenomenon might tune the extinction times [51].

In the following chapter, we will investigate the role of both aspects in population conservation. However, seasonality and randomness will be considered in simplified forms to avoid unnecessary complications.

3.2 Dispersal

Population spread due to organism active motion, walking, swimming, and so on, or passively, as it occurs in seed dispersal, when displacement is promoted by wind and active agents, such as birds [7]. These mechanisms produce statistical fingerprints in individuals’ movement that can be obtained experimentally.

Microscopically, individuals’ trajectory might be modeled as a stochastic process composed by runs and tumbles [52]. In the case of bacteria, coordination of the flagella allows directional movement. However, at some times, when flagella dynamics is not synchronized, bacteria tumble and change orientation. The alternation between these two stages generates a random walk.

Note that since we are dealing with active entities, changes in momentum can occur despite of collisions or any type of interaction, since they have their mechanisms of motion.

In the coarse-grained perspective, movement is described as fluxes between the sites Ω_i (see Fig. 2). In the limit of small Δx , below we derive some preliminary results about dispersal assuming simple behavior (for details about the discrete version, see Appendix E).

To start, we assume that individuals behave randomly, performing uncorrelated jumps with sizes sorted according to a given probability distribution γ . In this case, in one-dimension, during an interval Δt the density change due to dispersal can be written as

$$\Gamma[\rho] = -\rho(x) \int_{-\infty}^{\infty} \gamma(|x - x'|) dx' + \int_{-\infty}^{\infty} \gamma(|x - x'|) \rho(x') dx', \quad (3-14)$$

$$= -\rho(x) + \int_{-\infty}^{\infty} \gamma(|x - x'|) \rho(x') dx'. \quad (3-15)$$

The first term represents the outward flow from position x , while the second term represents the incoming flow from the neighborhood. The normalized kernel γ sets that the flux exchange is a function of distance. Typically, the flux intensity decays with the distance, meaning that individuals tend to move to locations near their current patch. For instance, for active individuals, such as butterflies, but also for passive entities, such as seeds, γ is set to an exponential [7, 11]. But power-laws, and other forms have also been investigated [7, 53–55].

In the limit of small jumps, we might expand the convolution term,

$$\Gamma[\rho] = -\rho(x) + \int_{-\infty}^{\infty} \gamma(x') \rho(x - x') dx' \quad (3-16)$$

$$= -\rho(x) + \sum_{n=0}^{\infty} \frac{(\partial_x)^n \rho(x)}{n!} \int_{-\infty}^{\infty} (x')^n \gamma(x') dx' \quad (3-17)$$

$$= \sum_{i=1}^{\infty} \frac{\mu_i}{i!} (\partial_x)^i \rho(x) \quad (3-18)$$

$$= \frac{1}{2} \mu_2 (\partial_x)^2 \rho + \frac{1}{24} \mu_4 (\partial_x)^4 \rho + \dots \quad (3-19)$$

where μ_i are the moments of the kernel γ (only the even ones are non-null since γ is symmetric). The traditional diffusion equation emerges when the expansion of Eq. (3-19) is truncated at first order, considering that $\mu_2 \gg \mu_4 \gg \mu_6 \gg \dots$. The above expansion sums up the contributions of different scale components represented by derivatives of different order (see Appendix E).

Neglecting the presence of other processes, the changes exclusively due to dispersal evolve population density distribution as

$$\partial_t \rho = -\rho + \int_{-\infty}^{\infty} \gamma(x-x') \rho(x') dx' = \Gamma[\rho]. \quad (3-20)$$

Performing the Fourier transform of the above equation, we obtain

$$\partial_t \tilde{\rho} = -\tilde{\rho} + \tilde{\gamma} \tilde{\rho} = (\tilde{\gamma} - 1) \tilde{\rho}, \quad (3-21)$$

where the notation $\tilde{\gamma}$ represents the Fourier transform of the given function, $\tilde{\gamma}(k) = \int_{-\infty}^{\infty} \gamma(r) e^{-ikr} dr$. Note that since γ is normalized, the growth of the total population ($k = 0$) is null, since no reproduction or death is taking place.

The solution of Eq. (3-20) can be written explicitly,

$$\tilde{\rho}(k, t) = \tilde{\rho}(k, 0) e^{(\tilde{\gamma}-1)t}, \quad (3-22)$$

in which the mode growth rate is given by the *dispersion relation*

$$\lambda(k) \equiv \tilde{\gamma} - 1. \quad (3-23)$$

It is clear from Eq. (3-23) that dispersal damps fluctuations, with stronger effects for high frequencies. For instance, if $\gamma(r) \propto \exp(-|r|)$, $\lambda(k) = 1/(1 + k^2) - 1$.

Now, noting that,

$$\langle x^2 \rangle = - \left. \frac{d^2 \tilde{\rho}}{dk^2} \right|_{k=0}, \quad (3-24)$$

we can see that the nonlocal dispersal in Eq. (3-20) generates diffusion-like evolution of the second moment

$$\langle x^2 \rangle = - \left(\frac{d^2 \tilde{\gamma}}{dk^2} \right) t = \frac{\mu_2}{2} t, \quad (3-25)$$

where the second moment of kernel γ determines an effective diffusion coefficient. This matches the diffusion term in Eq. (3-19). The temporal evolution of higher momentum can be obtained with similar procedure.

This result ignores the influence of environment properties M and other factors that might interfere in dispersal. As we will investigate further, individuals movement might be biased by the environment (Sec. 5.1) and also influence by the local density that might increase or decrease individual mobility (Secs. 4.1 and 4.2). In general, in the continuous space formulation, the term Γ can be written in a general form as

$$\Gamma[\rho|M] = \sum_i^{\infty} j_i(\rho|M) (\partial_x)^{2i} \rho. \quad (3-26)$$

At last, recalling the growth term $f(\rho) = a\rho - b\rho^2$ from Eq. (3-7) and additionally assuming standard diffusion $\Gamma \sim \nabla^2$, the temporal evolution of the population distribution is given by

$$\partial_t \rho = D \nabla^2 \rho + a\rho - b\rho^2. \quad (3-27)$$

The above equation is known as the *Fisher-KPP* equation, named after the biologist R. Fisher and commonly followed by the names of the mathematicians A. Kolmogorov, I. Petrovsky, N. Piskunov [56,57]. Eq. (4-1) is a paradigmatic model for population biology due to the fact that it includes the elementary features of the dynamics, i.e., spread, growth and competition. It is worth to point out that Eq. (4-1) has also been applied to describe the evolution of genes in phenotype space [56]. In this situation, spatial dispersal is translated in terms of mutations which promote random changes in individuals characteristics (e.g. size, color, speed), enlarging its diversity. This brings an interesting ambiguity to the results presented, in the sense that there is a direct translation to the context of the genetic evolution.

In the following section, we will investigate other types of spatial coupling that represents, for instance, individual interaction at distance. We will see that, when there is a particular combination of interaction scales, spatial and temporal order can appear in the population distribution. In details, for a particular model, we show how spatial patterns can appear. Further, we investigate the role of environment random fluctuations in this self-organization phenomenon.

3.3 Nonlocal interactions

In the previous section, we presented the role of dispersal in the evolution of the population density distribution. Those simple models predict the relaxation towards an homogeneous steady state. However, the temporal evolution of biological populations can present complex spatiotemporal patterns, a signature of self-organization, as can be observed in populations of slime mold, bacteria, ants, birds, fishes and human beings [3, 58–61]. Self-organization may arise due to non-local interactions [6, 62–67] or other mechanisms introducing a spatial scale, and can be triggered by different phenomena that drive a system far from equilibrium towards a spatiotemporal organization. The environment certainly interferes in most of those processes. For example, for microorganisms, the environment temperature can affect the reproduction rate [68] and many other processes [69] such as spatial spread. Competition is intrinsically mediated by the environment due to its limited resource availability (carrying capacity) [45]. Now, due to the inherent complexity, an environment parameter is typically subjected to a complex web of diverse processes, varying at different scales, both in space and time. Therefore, it is interesting to consider that environment conditions fluctuate randomly as discussed in Sec. 3.1, changing the reproduction rate.

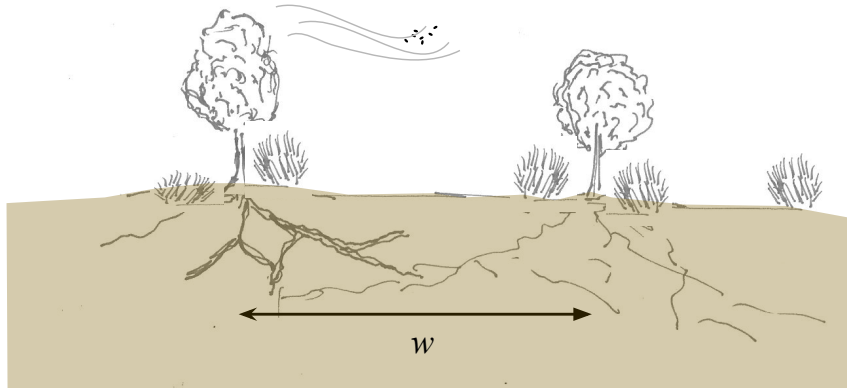


Figure 3.3: Illustration of nonlocal competition in plants promoted by roots in semi-arid regions and nonlocal reproduction rates induced by seed dispersal. The length w delimits the competitive interaction for water, mediated by the roots.

Also, as mentioned, external fluxes appear as an extra term in the canonical local equation (3-11), then the environment may also influence the system evolution through additive noise fluctuating forces (see Fig. 3.1). It is our goal to investigate the impact of such fluctuations on the system dynamics, particularly on the self-organization process. In order to do that, we will consider a single species scenario in one-dimension [33].

A standard deterministic model that takes into account the above mentioned governing rules is the generalized Fisher-KPP equation [56, 57, 65], namely, the integro-differential equation

$$\frac{\partial \rho(x, t)}{\partial t} = a \rho(x, t) - b \rho(x, t) \Gamma[\rho](x, t) + D \frac{\partial^2}{\partial x^2} \rho(x, t), \quad (3-28)$$

where $\Gamma[\rho](x, t) = \int_{\Omega} \gamma(x - x') \rho(x', t) dx'$ and f describes the influence of two interacting infinitesimal elements at a distance $|x - x'|$. This generalized form of Eq. (4-1) embodies nonlocal competition. In models similar to Eq. (3-28), nonlocal competition appears, for instance, in the context of vegetation, where the biomass concentrated at a given point consumes water around a neighborhood using its roots. In fact, this has been shown to be one of the main causes of self-organization in semi-arid regions [62, 70, 71]. In Fig. 3.3 we illustrate this situation. In fact, a derivation of the nonlocal interaction from the vegetation-water dynamics is possible in particular cases [63].

It is also worth to mention that non-locality might be present on the reproduction term, $a \rightarrow a \int \gamma_d(x - x') \rho(x', t) dx'$. In the context of Fig. (3.3), γ_d would represent the seed dispersal kernel [7, 64]. But here we proceed only with the nonlocal competition term, since it is the minimum mechanism for pattern

formation. That is, other processes interfere but are not necessary conditions for pattern formation. Further comments will be addressed in Sec. (3.3.1).

In Eq. (3-28), the environment participates in defining all the set of control parameters $\{a, b, D\}$. The inclusion of small fluctuations (or noise) allows to reflect the realistic spatiotemporal variability of the environment. In a first step, as in Eq. (3-11), we will focus on the effects of an additive noise $\sigma_\zeta \zeta(x, t)$ and a fluctuating growth rate, resorting to the transformation $a \rightarrow a + \sigma_\eta \eta(x, t)$. We consider both ζ and η independent Gaussian noises, with null averages $\langle \zeta(x, t) \rangle = \langle \eta(x, t) \rangle = 0$, and white in space-time, i.e., $\langle \zeta(x, t) \zeta(x', t') \rangle = \delta(x - x') \delta(t - t')$ and $\langle \eta(x, t) \eta(x', t') \rangle = \delta(x - x') \delta(t - t')$. In this section, we choose to neglect demographic fluctuations, assuming large population size. In this way, we can investigate pattern in the long time limit, where certainly there is a stationary state. However, its qualitative role could be predicted from the following calculations.

Therefore, our object of study is the dynamical equation that can be cast in the following form:

$$\begin{aligned} \frac{\partial \rho(x, t)}{\partial t} = & \left(a + \sigma_\eta \eta(x, t) \right) \rho(x, t) + \sigma_\zeta \zeta(x, t) + \\ & - b \rho(x, t) \Gamma[\rho] + D \frac{\partial^2}{\partial x^2} \rho(x, t) . \end{aligned} \quad (3-29)$$

Since the shape of the influence function does not lead to substantially different results [65], throughout this section, we will use a Heaviside influence function defined as $\gamma(x-x') = \frac{1}{2w} \Theta(w - |x-x'|)$ for the sake of simplicity. In the previous expression, w is a positive constant, defining the range of the interactions. Moreover, for the multiplicative white noise term, one must state an additional prescription, typically, either Itô or Stratonovich [46].

As discussed in Sec. 3.1, we argued that environment should be taken into account following Stratonovich interpretation. This is suitable since when fluctuations come from the environment, it is expected that temporal correlation might be weak but non-null (see Fig. 2.3). Indeed, the derivation of the Stratonovich prescription is based on performing this limit in a general noise [46]. This means that environment is not sensed in a nonanticipative manner by the individuals [72]. Below, we extend our results considering also the Itô prescription. This will show in a didactic way how both noises differ when interacting with the dynamics of Eq. (3-28).

3.3.1 Instability conditions

In the deterministic case [65], i.e., when $\sigma_\zeta = \sigma_\eta = 0$, one can determine the instability condition for the emergence of periodic structures by following the standard procedure of linearizing Eq. (3-28) around the homogeneous solution $\rho_0 \equiv a/b$, assuming $\rho(x, t) = \rho_0 + \varepsilon(x, t)$, where $\varepsilon(x, t) = \varepsilon_0 \exp[ikx + \lambda(k)t]$ is a small perturbation around the uniform state ρ_0 under periodic boundary conditions. This procedure leads to the dispersion relation

$$\lambda(k) = -a\tilde{\gamma}(k) - Dk^2, \quad (3-30)$$

where $\tilde{\gamma}$ is the Fourier transform of the influence function, that in the particular case of the Heaviside influence becomes $\tilde{\gamma}(k) = \sin(wk)/[wk]$. The relation (3-30) indicates instability with respect to a certain mode k , if $\lambda(k) > 0$. Then, in general, patterns are expected if the dispersion relation satisfies two conditions: (i) $\lambda(0) < 0$, to avoid instability of the total population size, and (ii) there must exist a positive global maximum at certain $k^* > 0$ [73], to give rise to an emergent characteristic mode. For Eq. (3-30), this maximum exists if $\tilde{\gamma}$ changes its sign for different values of k . Following the dispersion relation (3-30), we show in Fig. 3.5 that, when the diffusion coefficient is reduced with the other parameters kept constant, the homogeneous solution can become unstable and patterns emerge in the population [33, 65]. Then, both instances are depicted in Fig. 3.5, for fixed parameters a, b, w . Notice that in both cases $\lambda(0) < 0$, but, for small D , $\lambda(k)$ takes positive values, while for D above a threshold value $\lambda(k)$ is always negative indicating the stability of the homogeneous state.

In general, it is necessary to have oscillations in $\tilde{\gamma}$ to obtain a maximum $\lambda(k^*) > 0$. This occur if the kernel γ is compacted enough. A precise definition of this degree of compactness is only known in particular cases. For instance, if $\gamma(r) = \exp(-|r|^p)$, it is known that patterns can only be formed for $p > 2$ [74]. For infinitesimal interaction, it can be shown that the kernel's kurtosis must be below a certain value [75]. For q -Gaussian profile, $\gamma(r) \propto [1 + (1 - q)x^2]^{1/(1-q)}$, patterns only emerge if $q < 0$, even if for $q < 1$ q -Gaussians have the compact support property. But only at $q < 0$ the derivative is discontinuous border of the interaction range. The triangular kernel is the marginal case $q = 0$. For this particular case, in Fig. 3.3.1, we show the profile shapes for different values of q , together with the respective Fourier transform.

From the examples above, there is not a clear constraint to γ in position space. Nevertheless, there is an indicative that the kurtosis of γ plays an important role on pattern formation.

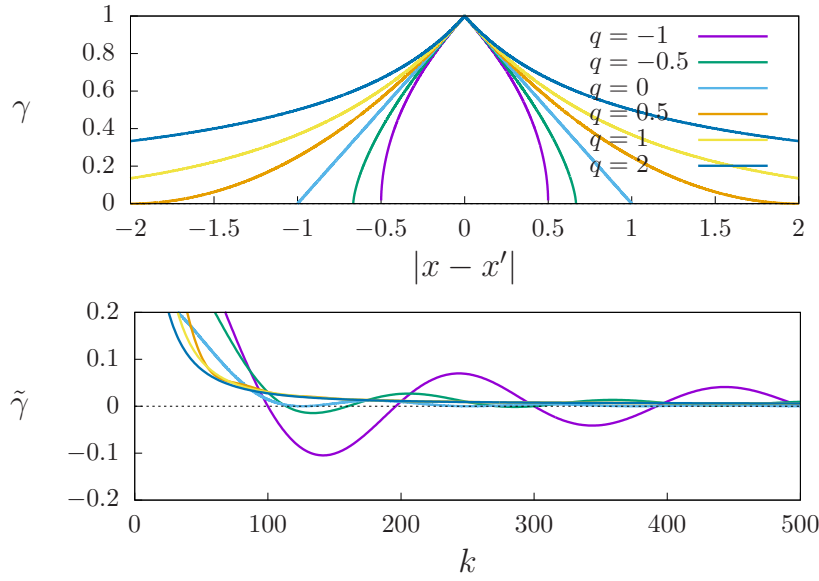


Figure 3.4: q -Gaussian kernel $\gamma(r) \propto [1 + (1 - q)x^2]^{1/(1-q)}$ profiles for different values of q and correspondent Fourier transform. Oscillations in $\tilde{\gamma}$ appear for $q < 1$, but only for $q < 0$ a change in sign occurs.

Here, we proceed with the homogeneous form $\Theta(w - |x - x'|)/(2w)$, focusing in understanding the role of environment stochastic fluctuations.

Now let us turn to the stochastic version of the nonlocal Fisher-KPP equation. By linearizing Eq. (3-29) around $\rho_0 = a/b$, in the small noise approximation, we have

$$\begin{aligned} \frac{\partial \varepsilon(x, t)}{\partial t} = & -a\Gamma[\varepsilon] + D \frac{\partial^2}{\partial x^2} \varepsilon(x, t) + \\ & + \sigma_\eta \varepsilon(x, t) \eta(x, t) + \sigma_\eta \rho_0 \eta(x, t) + \sigma_\zeta \zeta(x, t), \end{aligned} \quad (3-31)$$

where the deterministic terms are represented in the first line of the right hand side of Eq. (3-31), while the second line contains the multiplicative and additive noise terms. A suitable way to verify pattern formation is to measure the spatial autocovariance $C(r, t) = \int \langle \varepsilon(x, t) \varepsilon(x + r, t) \rangle dx$ (which does not depend on t if stationarity holds) or, alternatively, its Fourier transform, that is the structure function

$$S(k, t) \equiv \langle \hat{\varepsilon}(k, t) \hat{\varepsilon}(-k, t) \rangle, \quad (3-32)$$

where $\hat{\varepsilon}$ is the Fourier transform of ε .

Following the lines of Refs. [76, 77], we derive the evolution equation of $S(k, t)$ under the Stratonovich interpretation. Starting from the Fourier transform of Eq.(3-31), considering $\partial_t(\hat{\varepsilon}\hat{\varepsilon}') = \hat{\varepsilon}\partial_t(\hat{\varepsilon}') + \hat{\varepsilon}'\partial_t(\hat{\varepsilon})$, where $\hat{\varepsilon} \equiv \hat{\varepsilon}(k, t)$ and $\hat{\varepsilon}' \equiv \hat{\varepsilon}(-k, t)$, and averaging, we obtain

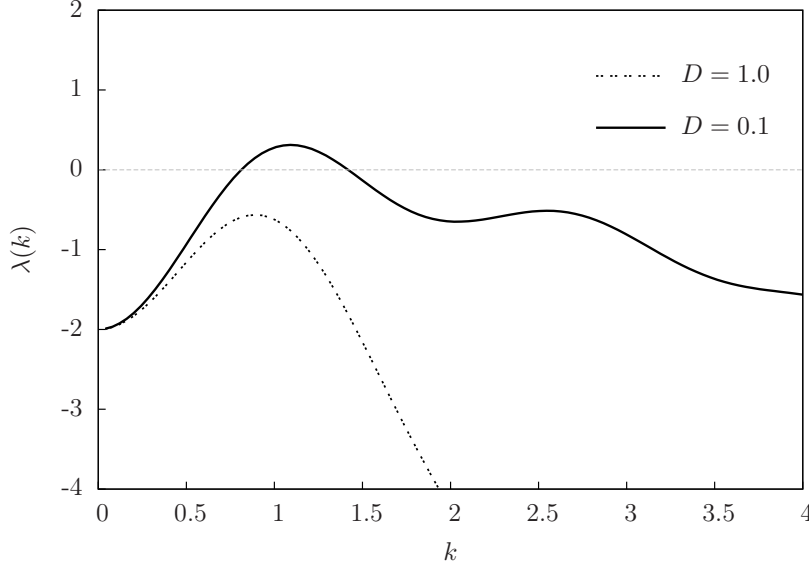


Figure 3.5: Dispersion relation Eq. (3-30) for $a = 2$, $b = 1$, $w = 4$, and two values of the diffusion coefficient D indicated on the figure.

$$\frac{1}{2} \frac{\partial}{\partial t} S(k, t) = \lambda(k) S(k, t) + \sigma_\eta \langle \hat{\varepsilon}' \widehat{\eta} \rangle + \sigma_\eta \rho_0 \langle \hat{\varepsilon}' \hat{\eta} \rangle + \sigma_\zeta \langle \hat{\varepsilon}' \hat{\zeta} \rangle. \quad (3-33)$$

In order to evaluate the average of multiplicative terms, we resort, for the case of the Stratonovich interpretation, to the so-called Furutsu-Novikov theorem [78], namely

$$\langle \chi(q) B[\chi] \rangle = \int dy \langle \chi(q) \chi(y) \rangle \left\langle \frac{\delta [B(q)]}{\delta \chi(y)} \right\rangle, \quad (3-34)$$

where $B(q')$ is functionally dependent on the Gaussian stochastic process χ , such as η and ζ . Hence, the averages of interest, in the small noise approximation, are

$$2 \langle \hat{\varepsilon}' \widehat{\eta} \rangle = \sigma_\eta K_\eta S(k, t), \quad (3-35)$$

$$2 \langle \hat{\varepsilon}' \hat{\eta} \rangle = \sigma_\eta \rho_0, \quad (3-36)$$

$$2 \langle \hat{\varepsilon}' \hat{\zeta} \rangle = \sigma_\zeta, \quad (3-37)$$

where K_η is to be interpreted as the spatial correlation function of the noise for $x = x'$, numerically computed as $K_\eta = 1/\Delta x$, where Δx is the lattice spacing.

Finally, substituting the averages into Eq. (3-33), the dynamical equation for the structure function reads

$$\frac{\partial}{\partial t} S(k, t) = 2\Lambda_\nu(k) S(k, t) + \sigma_\eta^2 \rho_0^2 + \sigma_\zeta^2, \quad (3-38)$$

with

$$\Lambda_\nu(k) = -a\tilde{\gamma}(k) - Dk^2 + \frac{1}{2}\nu\sigma_\eta^2 K_\eta(0). \quad (3-39)$$

where, the factor ν allows to select either the Itô ($\nu = 0$) or Stratonovich ($\nu = 1$) rules.

Notice that Eq. (3-39) can be identified as the stochastic generalization of the dispersion relation given by Eq. (3-30). If $\Lambda_\nu(k)$ is positive in some range of k , then perturbations grow, indicating that the homogeneous state ρ_0 is unstable. Otherwise, i.e., if $\Lambda_\nu(k) < 0$ for all k , the state ρ_0 is stable and perturbations vanish. The contribution of noise is given by the last term in Eq. (3-39), that is always nonnegative and independent on k . No such effect is predicted when noise is interpreted under the Itô rule ($\nu = 0$). In any case, the additive noise does not affect the dispersion relation. Also notice that, although the multiplicative noise η is destabilizing in the Stratonovich case, it will affect all modes. Then, the dispersion relation obtained by the linear analysis already points out that noise can reveal the instability built by the nonlocal competitive interactions.

Additional information can be obtained from the structure function. Under stationarity, Eq. (3-38) leads to

$$S(k) = \frac{\sigma_\eta^2 \rho_0^2 + \sigma_\zeta^2}{-2\Lambda_\nu(k)}. \quad (3-40)$$

Therefore, although the analysis of the signal of $\Lambda_\nu(k)$ predicts no effects caused by noise under the Itô prescription, the structure function reveals that noise can induce some kind of coherence. The numerical analysis in the next sections will clarify this issue.

3.3.2 Impact of noise

Let us remark that the stationary amplitude $S(k^*)$, of the dominant mode k^* grows with both noise intensities. Moreover, note that k^* is defined by the deterministic component only, hence by the dispersion relation (3-30). It is in that sense that noise reveals the instability of a hidden dominant mode that has been built by the nonlocal interactions and suppressed by the homogenizing diffusion process.

It is also noteworthy that, according to Eq. (3-40), noise has a constructive role only if $\rho_0 > 0$. Otherwise, if the homogeneous state is null, only the presence of additive noise can induce patterns.

The above analytical statements allow to predict the stability of the homogeneous state in the presence of noise in the dynamic rules. That analysis tacitly assumes the stability of the homogeneous distribution in the absence

of noise (i.e., $\lambda(k) < 0$ for all k), a case that will be numerically investigated in subsection 3.3.2.2.

On the other hand, it is also important to know how noise affects the asymptotic state of the population in the situations where patterns emerge in the deterministic limit (i.e., $\lambda(0) < 0$ and $\lambda(k^*) > 0$), hence when the homogeneous state is unstable leading to growing patterns in that limit. This case is analyzed in subsection 3.3.2.1.

In order to go beyond small noise and linear approximations, numerical integration of Eq. (3-28) can be performed to shed light on the far from equilibrium and nonlinear dynamics. We follow the Heun algorithm for stochastic equations [79], discretizing space and time, with $\Delta x = 10^{-1}$ and $\Delta t < 10^{-3}$ (for more details see Appendix E)

In all cases, we quantify spatial coherence, at a given time t , by means of the structure function, which is an ensemble average. Actually, since we verified ergodicity, ensemble averages have been substituted by temporal ones. From the structure function, one can extract the dominant mode k^* and its corresponding amplitude. After a transient period, stationarity of the structure function is attained. The stationary characteristic mode is well predicted by Eq. (3-40), as illustrated in Fig. 3.6 where we show a comparison between the numerical result for the stationary structure function and the linear theory prediction for the Itô case, given by Eq. (3-40) with $\nu = 0$.

For Stratonovich, the scenario is qualitatively similar, as soon as the noise intensity is below the critical value.

Through numerical simulations, one can observe that the dominant mode k^* adopts a typical value, in the whole noise intensity range, showing that the uncorrelated noise introduced in the dynamics appears in a correlated manner.

The maximum value $S^* = S(k^*)$ gives a measure of the intensity of the dominant mode. In the inset of Fig. 3.6 we show a normalized histogram of S_1^* for an individual realization. Then, although there exists a good agreement between the numerical structure function and its theoretical prediction, there is a large dispersion as depicted by means of an individual realization (dotted line) and also by the distribution of values of $S_1^* = S_1(k^*)$, where $S_1(k)$ is the power spectrum of each single realization.

The structure function measures coherence in Fourier space, what definitely provides information about the presence of patterns with a characteristic spatial scale. However, it does not guarantee that those patterns are persistent in position space. In subsection 3.3.2.2 we shall exploit this aspect, by directly measuring the temporal correlation and its dependency on noise intensity σ_η .

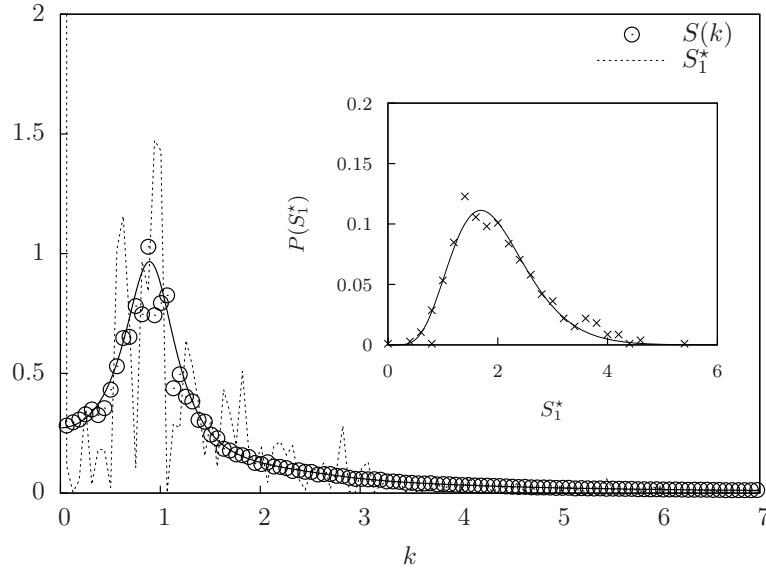


Figure 3.6: Stationary structure function $S(k)$, for $a = 2$, $b = 1$, $w = 4$, $D = 1$, $\sigma_\zeta = 0$ and $\sigma_\eta = 0.5$ (Itô noise), obtained numerically (symbols) and through Eq. (3-40) with $\nu = 0$ (solid line). For comparison, we also display the stationary power spectrum for an individual realization $S_1(k)$ (dotted line). The inset shows the distribution of values of $S_1^* = S_1(k^*)$: numerical (symbols) and gamma distribution fit as a guide to the eyes (solid line).

3.3.2.1

When patterns are present in the deterministic case

Let us consider values of the parameters for which patterns arise in the absence of noise. Then, we consider for instance the values used in Fig. 3.5 (solid line). We perform an analysis of the spatial coherence by means of the steady value of S^* , for different noise intensities. We analyze the stochastic equation under both Itô and Stratonovich prescriptions.

Let us first consider the Itô case. In Fig. 3.7, we represent the steady value of the spatial average density $\langle u \rangle$, together with S^* . The results show that multiplicative noise plays a destructive role in the coherence level up to $\sigma_\eta \simeq 1$. For higher values of the noise intensity, the reduction of S^* is due to the concomitant reduction of the population average size. In fact, for the set of parameters chosen, there exists a threshold value, $\sigma_\eta^e \approx 1.8$ in the case of the figure, that represents the *extinction threshold*. This means that, for noise intensities greater than the threshold, the population becomes extinguished. Through the deterministic mechanisms the system would go towards a stationary state that is represented by a well defined population distribution pattern, meanwhile the presence of multiplicative noise in the dynamic forces, even at low intensity, spoils that spatial order.

In the Stratonovich case, we observe a quite different behavior, as

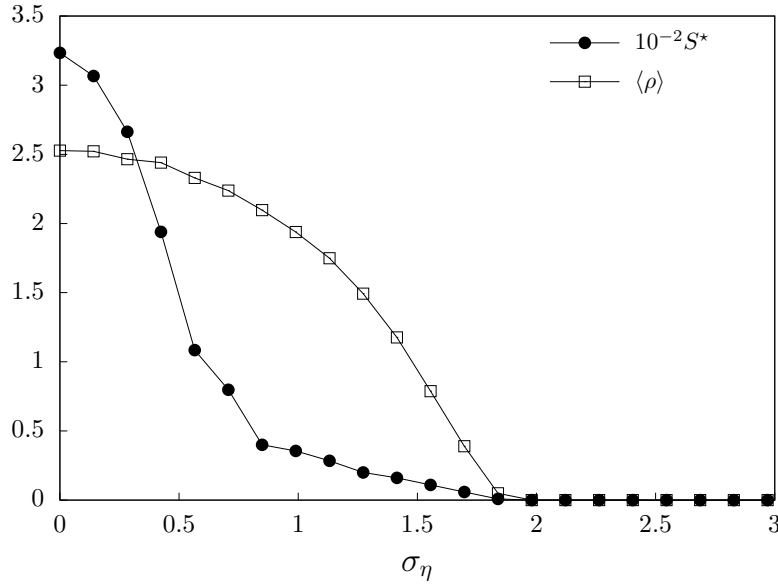


Figure 3.7: Analysis of the spatial coherence. Steady values of the intensity of the dominant mode $S^* = S(k^*)$ and of the average population density, $\langle u \rangle$, as a function of σ_η (under the Itô prescription), for the choice: $a = 2$, $b = 1$, $w = 4$, $D = 0.1$ and $\sigma_\zeta = 0$. The intensity of the dominant mode was scaled by a factor 10^{-2} just to employ a unique axis scale. The dotted lines are guides to the eyes.

displayed in Fig. 3.8. Increasing the noise intensity σ_η induces growth both of the average level and of the intensity of the dominant mode, in such a way that also the ratio $S^*/\langle u \rangle$ increases. However, as shown in the inset of the same figure, while the amplitude of the patterns grows with increasing noise, their shape becomes more irregular, indicating that the other modes also grow together with the dominant one, as predicted by Eq. (3-39).

One can cast a Stratonovich stochastic differential equation into the form of an Itô equation with an effective (or spurious) drift. For our Eq. (3-29), this implies the change $a \rightarrow a + \frac{K_\eta(0)}{2} \sigma_\eta^2$. Because the additional term is positive, this change amounts to increasing the growth rate a . On the other hand, increasing a , with the other parameters fixed, does not alter the stability condition. This situation would lead to increase the average density and to strengthen patterns, which is in fact the outcome observed in Fig. 3.8, indicating that the destructive role observed for Itô noise (Fig. 3.7) is not enough to spoil the constructive effect of the spurious drift.

3.3.2.2

When patterns are absent in the deterministic case

In this subsection we concentrate in our main case of interest, that is when the homogeneous solution is stable despite nonlocality. The purpose of

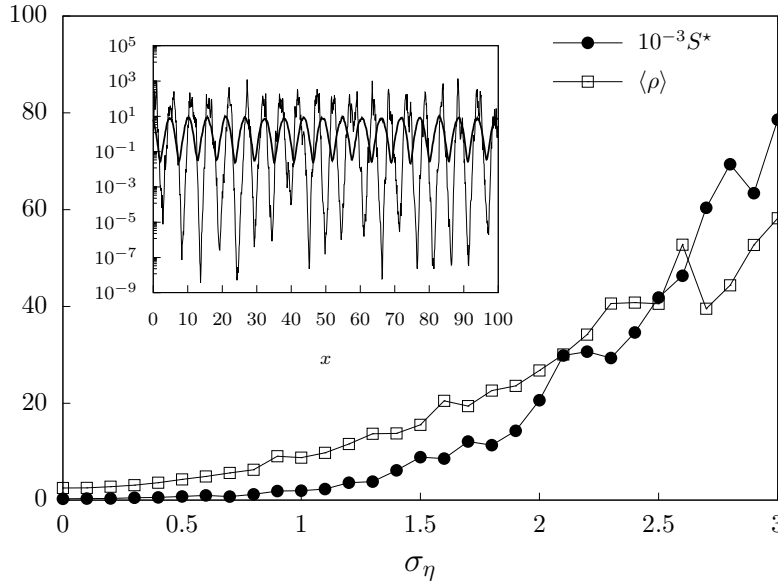


Figure 3.8: Analysis of the spatial coherence for the choice: $a = 2$, $b = 1$, $w = 4$, $D = 0.1$ and $\sigma_\zeta = 0$ (under the Stratonovich prescription). The intensity of the dominant mode was scaled by a factor 10^{-3} just to use the same axis scale. In the inset we exhibit typical patterns for low (solid line) and high (dotted line) noise intensities, namely for $\sigma_\eta = 0.1$ and 1.9 , respectively. The dotted lines are guides to the eyes.

analyzing this situation is to verify if the introduction of noise in the dynamic rules can reveal the characteristic scale of interaction.

Let us first analyze the Itô case. In Fig. 3.9, we observe how the dominant mode intensity S^* changes as a function of the noise intensity σ_η . Our results point out that when noise intensity is small enough ($\sigma_\eta < 1.0$), the behavior $S \propto \sigma_\eta^2$ predicted by Eq. (3-40) occurs. However, when we increase the noise intensity beyond the linear regime, we note that there is a break in the monotonic behavior of S^* with a peak that characterizes an optimum value $\sigma_\eta^o \approx 2.0$. Above this optimum value, noise starts to play a destructive role in spatial coherence. As a consequence, the dominant mode becomes less intense until it is completely destroyed. Actually, this is due to the concomitant decrease and extinction of the population, as shown by the quotient $S^*/\langle u \rangle$ also exhibited in Fig. 3.9.

On the one hand, noise in the reproduction rate affects the number of individuals in the population, as expected. There exists a value $\sigma_\eta^c \approx 3$ that represents the *extinction threshold*: if a noise intensity greater than this value is set, population vanishes. This implies a shift transition [50] for the critical growth rate that now competes with noise.

This is a strongly nonlinear effect dependent on the noise intensity. It is noteworthy that, in the local mean-field approximation described by the

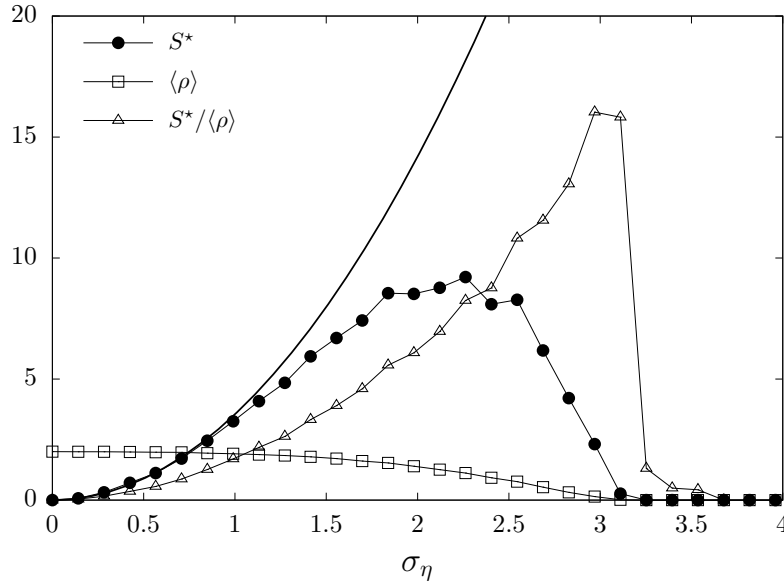


Figure 3.9: Analysis of the spatial coherence for the choice: $a = 2$, $b = 1$, $w = 4$, $D = 1$ and $\sigma_\zeta = 0$, for Itô noise. The symbols correspond to numerical results. The quotient $S^*/\langle u \rangle$ is also plotted. The solid line corresponds to the theoretical prediction given by Eq. (3-40), the dotted lines are guides to the eyes.

equation $\frac{d\rho}{dt} = (a - b\rho)\rho + \sigma\eta\rho$, one can show that the ensemble average stationary density is given by $\bar{\rho} = \frac{a}{b} - \frac{\sigma^2}{2}$, indicating a critical threshold.

On the other hand, although noise does not shift the dispersion relation, it forces an anticipation of mode instability, which is illustrated by the bursts of coherence displayed by density inhomogeneities in Fig. 3.11.

Now we perform the same analysis for the Stratonovich case. Figure 3.10 displays the analysis of spatial coherence, while the time evolution is depicted in Fig. 3.12. In the inset of the last figure we also show the theoretical prediction given by Eq. (3-40), which is only valid up to a critical value, $\sigma_\eta^c \simeq 0.33$ in the case of the figure, point at which the theoretical structure function becomes divergent, although its numerical computation is possible.

In terms of a spurious drift, Stratonovich noise would essentially lead to a larger growth rate, with the concomitant increase of the average density. Moreover, that spurious drift has the effect of shifting the dispersion relation, yielding Eq. (3-39). But, in contrast to Sec. 3.3.2.1, increasing noise intensity can shift the maximum of the dispersion curve from the stability to the instability region for sufficiently large noise intensity (above its critical value). When this happens, differently to the Itô case for the same value of the parameters, persistence of spatial patterns emerges. The resulting profiles are similar to those observed for the parameter region in which patterns already occur in the deterministic limit.

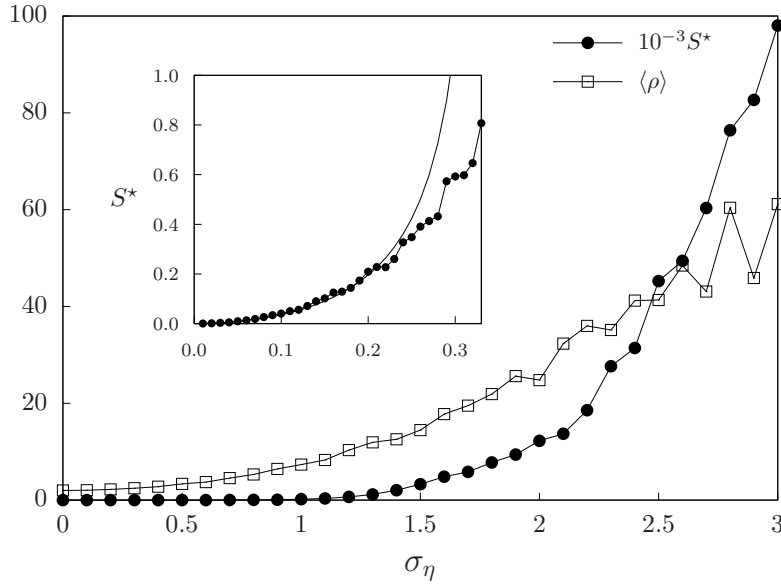


Figure 3.10: Analysis of the spatial coherence for the choice: $a = 2$, $b = 1$, $w = 4$, $D = 1$ and $\sigma_\zeta = 0$, for Stratonovich noise. The symbols correspond to numerical results. The inset shows a blow up of the vicinity of the origin, where the solid line corresponds to the theoretical prediction given by Eq. (3-40).

Although for both noises one has $S^* > 0$, indicating the presence of coherence, in the Stratonovich case, $\Lambda_1(k^*) > 0$, while in the Itô case $\Lambda_0(k^*) = \lambda(k^*) < 0$. That is, despite some kind of coherence is always revealed by noise, in the Stratonovich case there is persistence of the patterns, while in the Itô case they are weakly correlated in time. Moreover, comparison of the profiles shown in Figs. (3.11) and (3.12), reveals a greater regularity and more pronounced peaks in the distribution $\rho(x, t)$ in the Stratonovich case.

3.3.2.3

Temporal correlations

In order to quantify the degree of persistence, we measured the spatial average of the time autocorrelation function of $\rho(x, t)$, $R(\tau)$ as a function of the time lag τ . The autocorrelation function presents an exponential behavior after an abrupt decay, then, we considered different effective correlation times (as defined in Fig. 3.13), as measures of the degree of persistence. All these quantities plotted as a function of σ_η , under the Stratonovich interpretation, are presented in Fig. 3.13. The figure shows that persistence first increases with noise intensity, attaining a maximum, and thereafter decays with larger noise intensities for which order is spoiled. Notice that in the limit of vanishing noise intensity, the correlation times do not go to zero. The limiting values remain almost constant up to a value of σ_η that approximately coincides with the critical one predicted by the condition $\Lambda_1(k^*) = 0$ in Eq. (3-39), in the

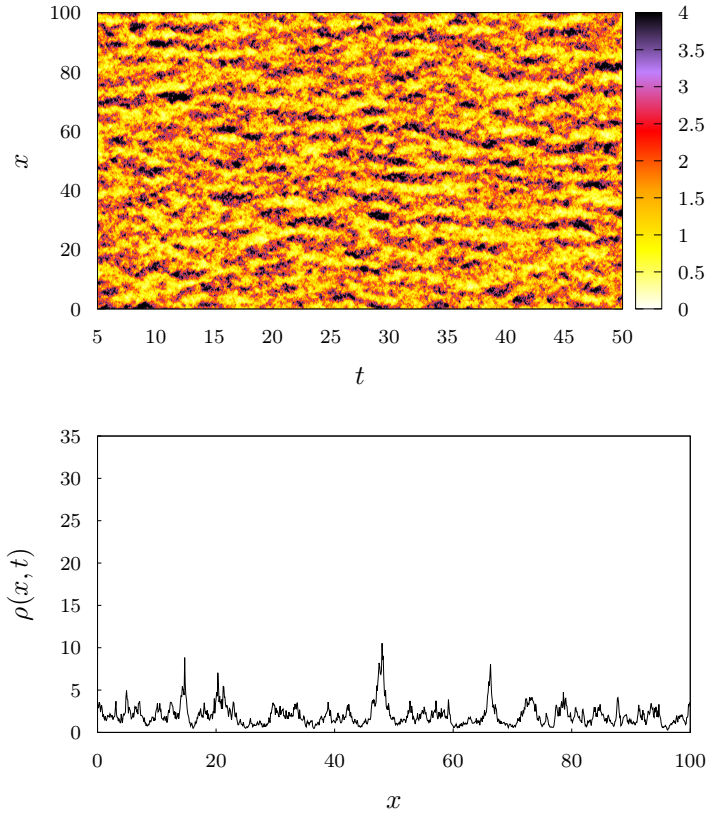


Figure 3.11: (Color online) Time evolution of the density $\rho(x, t)$ in a color map (upper panel), for $a = 2$, $b = 1$, $w = 4$, $D = 1$, $\sigma_\zeta = 0$, $\sigma_\eta = 1.0$ (Itô noise). In the lower panel we exhibit a density profile corresponding to a cut of the color map at $t = 50$.

case of the figure, the aforementioned critical value is $\sigma_\eta^c \simeq 0.33$. In fact, the kind of persistence observed in Fig. 3.12 can be attributed to a positive maximum of the dispersion relation ($\Lambda_\nu(k^*) > 0$). This condition is possible only for $\nu = 1$ (Stratonovich interpretation) and $\sigma_\eta > \sigma_\eta^c$. Notice that, under the Itô interpretation ($\nu = 0$), $\Lambda_0(k^*)$ is always negative if $\lambda(k^*) < 0$, then such kind of persistent pattern cannot occur. In fact, for the Itô simulations, we observed (not shown) that below the extinction threshold noise does not affect the correlation times that remain at the level of those at vanishing noise intensity in the Stratonovich case. Hence we can conclude that for the same parameters, the effect of Itô noise is equivalent to that of Stratonovich noise below σ_η^c .

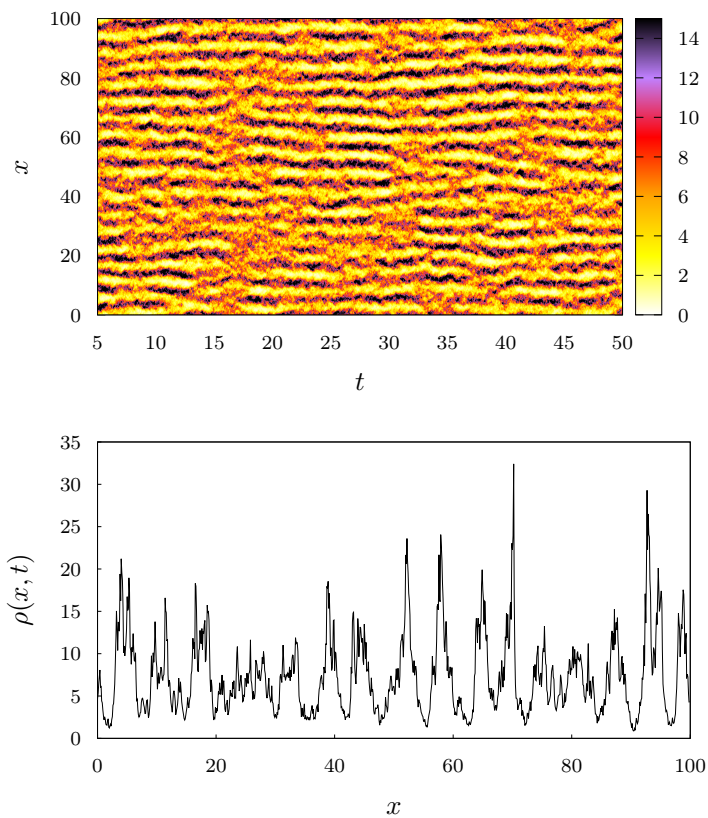


Figure 3.12: (Color online) Time evolution of the density $\rho(x, t)$ in a color map (upper panel), for $a = 2$, $b = 1$, $w = 4$, $D = 1$, $\sigma_\zeta = 0$ and $\sigma_\eta = 1.0$ (Stratonovich case). In the lower panel we exhibit a profile corresponding to a cut of the color map at $t = 50$.

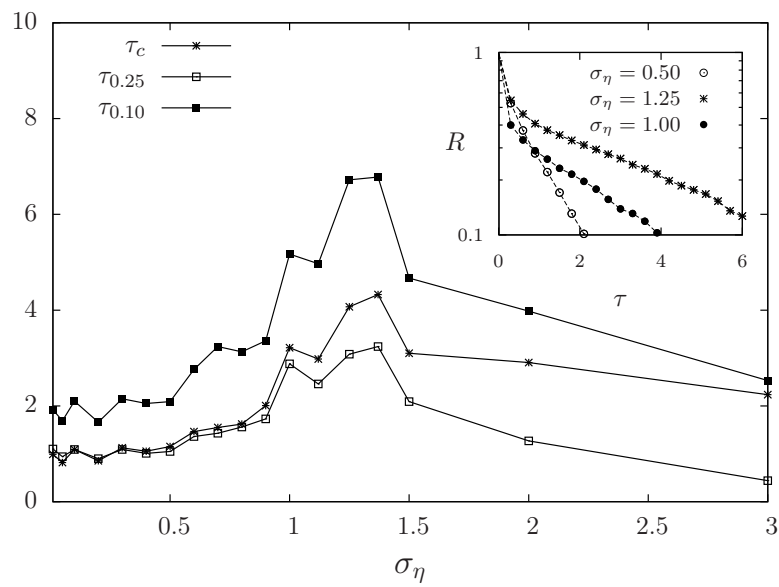


Figure 3.13: Correlation times as a function of σ_η . for $a = 2$, $b = 1$, $w = 4$, $D = 1$, $\sigma_\zeta = 0$ (with Stratonovich noise). The inset shows typical curves of the autocorrelation function vs the time lag τ , from which correlation times were extracted: τ_c is the inverse rate of exponential decay, since there is an abrupt decay before the exponential regime, we also computed $\tau_{0.25} = \tau(R = 0.25)$ and $\tau_{0.10} = \tau(R = 0.10)$.

4 Single habitat domain

In this chapter, we start our investigation regarding population persistence in heterogeneous environment. Before proceeding to more sophisticated scenarios, we should review the classical results for single habitat domain [12, 13], that will also help introduce the main concepts of the problem.

A region, like a shelter, shield, mask, etc., that allows individuals to be protected against unfavorable conditions (e.g. predation, water scarcity, sun light) [28] constitutes the habitat in the form of a refuge. This region might appear naturally due to resource spatial correlations, or artificially, for instance, in ecological reserves, or in the case of microorganisms, where artificially constructed landscapes can be made [17, 80].

For simplicity, we start with the already introduced Fisher-KPP equation in one dimension,

$$\partial_t \rho(x, t) = f(\rho) + D \nabla^2 \rho, \quad (4-1)$$

which includes random individual movements through the Laplacian term and logistic growth $f(\rho) = (a - b\rho)\rho$ without any noise terms.

Despite its simplicity, Eq. (4-1) includes the elementary processes in population dynamics and also resembles a reaction-diffusion process encountered in many different areas, such as plasma physics, combustion and physiology. Therefore, the results found for the biological problem might reach different contexts.

The most elementary definition of the landscape is to consider a single convex habitat domain surrounded by harmful regions, where negative effects are present. In one-dimension, a particular length in the line is considered the habitat. Population dynamics at the habitat boundary $\partial\Omega$ can be defined in many ways [81], for instance, establishing its permeability (von Neumann) or its influence on the local population density (Dirichlet). For this first contact, we shall consider Dirichlet boundary condition,

$$\rho(x, t)|_{x \in \partial\Omega} = 0, \quad (4-2)$$

assuming that individuals that leave the habitat domain die in short time. Under these conditions, the stability of the null state can be easily investigated.

In the low density regime, the competition term in f can be neglected, making Eq. (3-27) linear. Then, the general exact solution for the Fisher dynamics with harsh vicinity conditions can be written in terms of the allowed modes in the domain,

$$\rho(x, t) = \sum_i \tilde{\rho}(k, 0) \cos(k_i x) e^{\lambda_i t}. \quad (4-3)$$

The solution is now decomposed in the base of Fourier modes i that grow according to the rate λ_i . For the case of Eq. (3-27),

$$\lambda_i = a - Dk_i^2 \quad \text{with } k_i = \frac{\pi(i+1)}{L} \quad \text{for } i = 0, 1, 2, \dots \quad (4-4)$$

Population size will remain positive in the long time if at least one positive eigenvalue exists λ . Then, if population survives, certainly $\max\{\lambda_i\} = \lambda_0 = a - D\pi^2/L^2 > 0$. Then, the critical value for L is giving by

$$L_c = \pi \sqrt{\frac{D}{a}}. \quad (4-5)$$

For $L > L_c$, we have $\lambda_0 > 0$, then population survives. For $L < L_c$, population size decays to zero. This establishes an intuitive ecological concept that habitats need to exceed a certain minimum (critical) size to allow population development. In order to provide a concrete example, in Fig. (4.1), setting an homogeneous initial condition, we show the temporal evolution of the population density distribution for $L < L_c$, $L = L_c$ and $L > L_c$. Further details will be discussed in the next section.

In the limit of large population size, agent simulations, performed with suitable reproduction and spread with rates, show that at the critical habitat size the mean extinction time diverges and population persists at long times. Particularly, it is shown that $\mathcal{T} \sim L^2/(L_c^2 - L^2)$ (valid for $L < L_c$) [21]. This shows that the deterministic contributions are the main reference for population persistence. For small population, survival is never fully achieved due to demographic noise, however, extinction times are significantly bigger for $L > L_c$ [21].

Before proceeding beyond the linear and static case, it is necessary to introduce an alternative modeling of the habitat [17]. It is more realistic to assume that the natality rate is space dependent, such as

$$a \rightarrow a - A\Theta(|x| - L/2) \quad (4-6)$$

with $A > a$. This means that inside the habitat $\Omega = [-L/2, L/2]$, the growth rate is positive, while outside the habitat domain the population dies due to the lack of environment support with rate $|a - A|$ (see Fig. 4.11).

Aiming to investigate the stability of the null state, we linearize Eq. (3-27) which becomes

$$\begin{aligned}\partial_t \rho &= D \partial_{xx} \rho + a \rho \quad \text{for } x \in \Omega \\ &= D \partial_{xx} \rho - |A - a| \rho \quad \text{for } x \notin \Omega.\end{aligned}\quad (4-7)$$

For $L \rightarrow \infty$, the population dynamics will be dominated by the dynamics inside the domain, such that the population will survive. For $L \rightarrow 0$ the opposite behavior occurs and the population size must decay with time. Then, a critical habitat size L_c for population survival exists. Precisely at the critical value $L = L_c$, population approaches the steady solution for Eq. (4-7). The critical condition for this case emerges assuming the continuity of the population density distribution at the boundary. The imposition of the continuity of the zeroth and first order derivative can be cast setting equal the logarithm derivative of the inner and outer solution,

$$\left. \frac{\rho'_{\text{in}}}{\rho_{\text{in}}} \right|_{\partial\Omega} = \left. \frac{\rho'_{\text{out}}}{\rho_{\text{out}}} \right|_{\partial\Omega}, \quad (4-8)$$

where the prime notation indicates spatial derivative. The steady solution for Eq. (4-7) at each region is given by

$$\rho_{\text{in}}(x) \propto \cos(q_+ x), \quad (4-9)$$

$$\rho_{\text{out}}(x) \propto e^{-q_- |x|}, \quad (4-10)$$

with $q_{\pm} = \sqrt{a_{\pm}/D}$, where $a_+ = a$ and $a_- = |A - a|$.

Substituting Eq. (4-9)-(4-10) in Eq. (4-8) setting $x = L_c/2$, we obtain $\tan(q_+ L_c/2) = \frac{q_-}{q_+}$. Rearranging,

$$L_c = \frac{2}{q_+} \tan^{-1} \left(\frac{q_-}{q_+} \right) = 2 \sqrt{\frac{D}{a_+}} \tan^{-1} \left(\frac{a_-}{a_+} \right). \quad (4-11)$$

In the limit of harsh outside conditions $a_- \gg a_+$, we recover Eq. (4-5).

The methodologies used to obtain the critical size for the harsh (4-5) and smooth (4-11) boundaries, differ significantly. For the former, we could solve the eigenvalues problem for the dynamical equation, which certainly will not be easy, or possible, to do in general. This is what exactly occurs in the case of smooth habitat boundary, where we used a geometric condition to find the steady state that arises at L_c . This second strategy is more general and it should be specially useful when the eigenvalues problem cannot be solved easily, as we will see in the next section.

4.1 Nonlinear population dynamics

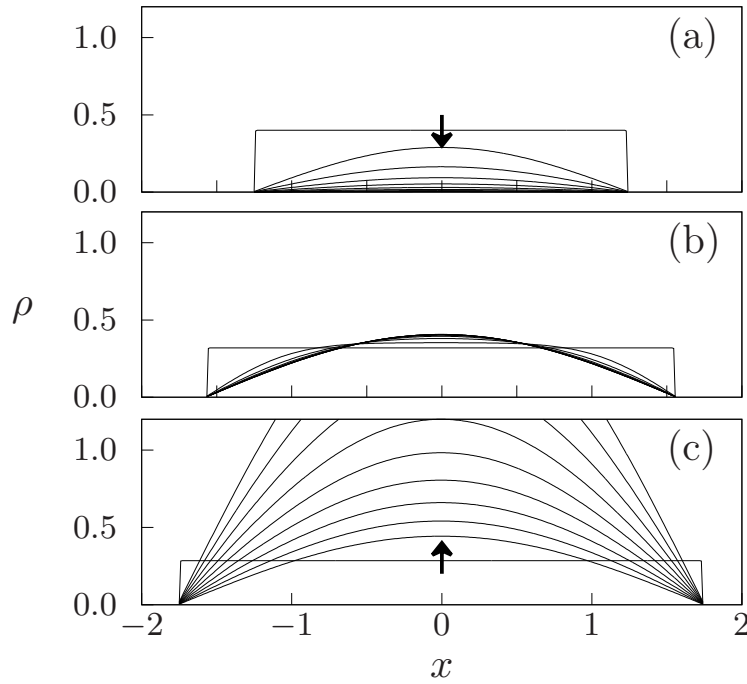


Figure 4.1: Temporal evolution of the density distribution profile, in the linear case $\nu = \mu = 1$. For (a) $L < L_c$, (b) $L = L_c = \pi$ and (c) $L > L_c$, the population becomes extinct, attains a steady state or blows up, respectively. The lines are produced with Eq. (4-16). The arrows indicate the direction of time.

Despite many studies about the critical habitat size L_c , one aspect that has been overlooked is the role of nonlinear diffusion and growth rate [14], which we address in this section. Our results will show, in particular, that the idea that the habitat size needs to overcome a critical value to allow population survival is not always valid. Depending on the kind of nonlinearities present, population survival occurs for $L > L_c$, $L < L_c$ or for any L . Additionally, nonlinearity introduces sensitivity to initial conditions, which affects the values of L_c .

We address these issues assuming a general nonlinear population dynamics taking into account, in an effective manner, density-dependent regulatory mechanisms [34]. We focus on the one dimensional case, where L is the length of the habitat. The evolution equation for the population density distribution $\rho(x, t)$ at position x and time t is given by

$$\partial_t \rho = \partial_x (\rho^{\nu-1} \partial_x \rho) + \rho^\mu, \quad (4-12)$$

where $\nu > 0$, $\mu \in \mathbb{R}$, together with the absorbing boundary condition $\rho(\pm L/2, t) = 0$ and a uniform initial condition $\rho(x, 0) = N_0/L$, where N_0 is the initial population size. The terms of Eq. (4-12) represent diffusion and growth, respectively, with diffusion coefficient $\rho^{\nu-1}$ and per capita growth rate $\rho^{\mu-1}$, which depend on ρ when $\nu, \mu \neq 1$. The boundary conditions take into account a nonviable neighborhood. Competition was neglected by assuming abundance of resources. Further details of the model and its biological motivations will be given in Sec. 4.1.1.

The emergence of these nonlinearities in population dynamics has different origins that will be discussed in Sec. 4.1.1 too. But beyond the biological motivation, the nonlinear mathematical problem can be also of interest for diverse other fields such as combustion theory, heat conduction and transport in porous media [82, 83]. It is also related to the so-called blow-up (divergence at finite time) of solutions, found in the mathematical literature [82–84].

In the next sections, our goal is to determine the critical size and characterize the regimes of extinction and survival in the general nonlinear case. In order to do that, we perform a systematic analysis, both numerically and analytically, of the asymptotic behavior of the total population $N(t) \equiv \int_{\Omega} \rho(x, t) dx$, where $\Omega \equiv [-L/2, L/2]$. For numerical integration of the partial differential Eq. (4-12), the standard forward-time centered-space discretization scheme ¹ was used.

4.1.1 Density-dependent feedback

Recalling the Fisher-KPP equation [56] ,

$$\partial_t \rho = D \partial_{xx} \rho + a \rho - b \rho^2, \quad (4-13)$$

we introduce density-dependent rates, through nonlinearities in the growth and diffusion processes. These dependencies on the density represent macroscopic feedbacks in the regulatory mechanisms, that can emerge from the complex interactions at individual level, such as cooperation, competition or homophilia (the preference to be among peers) [86], or from the interactions with a complex environment. Assuming power-law forms, we generalize Eq. (4-13) as

$$\partial_t \rho = D \partial_x (\rho^{\nu-1} \partial_x \rho) + a \rho^{\mu} - b \rho^{\mu+\delta}, \quad (4-14)$$

¹We used a forward-time centered-space (FTCS) scheme, with integration steps Δt and Δx adequate for convergence. Typically it was necessary that $\Delta t / \Delta x^2 \lesssim 10^{-3}$. See, for instance, Ref. [85]

with exponents $\nu > 0$, $\delta > 0$ and real μ .

Diffusion. In many real cases, the diffusion coefficient is not constant, which may be a consequence of the interaction between individuals [87, 88]. For instance, in populations of insects, such as grasshoppers, the diffusion coefficient is enhanced at high densities ($\nu > 1$), but, in other species, this occurs at low densities ($\nu < 1$) [88]. The adopted form of the diffusion coefficient, $D\rho^{\nu-1}$, allows to embrace all these cases. The spread of insect swarms, bacteria and other organisms has been also described through a nonlinear diffusion equation with different values of ν [82, 88–90]. When $\nu > 1$, the diffusion coefficient increases with population density. Then, large dispersal takes place in dense regions ($\rho > 1$), but low mobility occurs where the population is sparse ($\rho < 1$). This indicates that individuals become more active when they encounter more individuals, a type of positive feedback that increases with ν . In contrast, when $0 < \nu < 1$, the diffusion coefficient is enhanced in regions of low density, in comparison to highly populated ones. Then, this dispersion in open space yields long tails in the distribution of individuals [91–93], but here we are dealing with a bounded domain.

Alternatively, nonlinear diffusion may also have external origin, from the spatial heterogeneity of the environment, such as the recently investigated case of bacteria developing in porous media [94]. In fact, $\partial_t \rho = D \partial_x (\rho^{\nu-1} \partial_x \rho)$ is known as porous media equation [95, 96], which arises in other contexts too [82, 83, 97]. Let us note that the associated random dispersal yields anomalous diffusion in open space, where $x \sim t^{1/(1+\nu)}$. That means normal diffusion for $\nu = 1$, subdiffusion for $\nu > 1$ and superdiffusion for $\nu < 1$ [91, 93, 98].

Growth. A clear interpretation can also be given to the growth rate $a\rho^{\mu-1}$. For $\mu > 1$, it goes to zero as density goes to zero, which means that the population is losing its ability to survive when less individuals live in the habitat. This can be related to the feature known in ecology as *Allee effect* [86], which is reported in a wide range of scenarios. On the other hand, when $\mu < 1$, population responds to low densities increasing its growth rate, which functions as a regulatory mechanism for survival, preventing extinction. This feature is present, for instance, in parasite dynamics, where the reproduction rate increases in low density [99]. This is because, the lower the population density, the larger the female worm size, producing more eggs [99]. It is worth recalling that, when only the growth term is present ($D = b = 0$), with the initial

condition $\rho(t = 0) = \rho_0$, the average density is

$$\rho(t) = \rho_0 \left[1 + \frac{(1 - \mu)}{\rho_0^{1-\mu}} at \right]^{\frac{1}{1-\mu}}, \quad (4-15)$$

which generalizes the exponential growth, recovered for $\mu \rightarrow 1$. This solution means sub-exponential growth with time when $\mu < 1$ (linear in the case $\mu = 0$ or sub-linear for $\mu < 0$), or divergent behavior at finite times when $\mu > 1$.

Competition for resources. The last term in Eq. (4-14) represents intra-specific competition, preventing unlimited growth. Sometimes in the literature, the logistic growth is written in the form $a\rho(1 - \rho/K)$, introducing the notion of environment carrying capacity K (related to resource availability). In our case, the logistic-like term becomes $a\rho^\mu(1 - \rho^\delta b/a) = a\rho^\mu(1 - (\rho/K)^\delta)$, then $K = (a/b)^{1/\delta}$, recalling that $\delta > 0$ to ensure the limiting effect.

In the subsequent analysis, we neglect competition by setting $b \rightarrow 0$ ($K \rightarrow \infty$). This approximation corresponds to a sufficiently large carrying capacity, when resources are sustainable or unlimited, for the investigated range of ρ . Now, a simple change of variables, $x \rightarrow x\sqrt{D/a}$ and $t \rightarrow at$, turns Eq. (4-14) dimensionless, leading to Eq. (4-12), that will be the object of our study.

Evolution equations similar to Eq. (4-12), used to model population dynamics [31, 100] and transport in absorbing porous media [96], were previously investigated, but for infinite habitats, in contrast to our bounded problem. Reaction-diffusion systems governed by Eq. (4-12), such as in combustion theory and heat conduction, motivated the study of the existence of blow-up solutions [83]. The issue of the critical habitat size L has been addressed before for modified forms of Eq. (4-13), including, for instance, chemotaxis and advection [13, 14, 101]. Here we extend that problem to analyze the impact of the interplay between density-dependent diffusion coefficient and growth rate on the critical size.

Before passing to the general case, we revisit the linear problem, $\nu = \mu = 1$, for our particular setup.

For $\nu = \mu = 1$, we can propose, as solution of the problem defined in Eq. (4-12), a cosine series of the form $\rho(x, t) = \sum_{k \geq 0} c_k(t) \cos([2k + 1]\pi x/L)$, where each term satisfies symmetry around $x = 0$ and vanishes at the boundaries $x = \pm L/2$. Substituting this expression into Eq. (4-12), solving for $c_k(t)$ and adjusting the initial condition (uniform population with total size N_0), one obtains the exact solution

$$\rho(x, t) = \frac{4N_0}{\pi L} \sum_{k=0}^{\infty} \frac{(-1)^k}{2k+1} \cos([2k+1]\pi x/L) e^{\lambda_k t}, \quad (4-16)$$

where $\lambda_k = 1 - [(2k+1)\pi/L]^2$ [101].

Modes have discrete wavelength values, to obey the boundary conditions, and their amplitudes grow according to the dispersion relation λ_k . When $L < L_c = \pi$, then $\lambda_k < 0$ for all k ; as a consequence, the total population goes to zero (extinction). When $L > L_c$, one has $\lambda_k > 0$ for all modes with index $k < (L/L_c - 1)/2$ (which includes at least the fundamental mode, given by $k = 0$); then the density grows indefinitely. Only when $L = L_c$, a finite steady state $\rho(x)$ is attained, since $\lambda_0 = 0$, while $\lambda_k < 0$ for all $k > 0$, namely,

$$\rho(x) = \frac{4N_0}{\pi^2} \cos x. \quad (4-17)$$

These regimes are illustrated in Fig. 4.1.

Integration of Eq. (4-16) over the interval $\Omega = [-L/2, L/2]$ provides the total population size N as a function of time:

$$N(t) = \frac{8N_0}{\pi^2} \sum_{k=0}^{\infty} \frac{e^{\lambda_k t}}{(2k+1)^2}. \quad (4-18)$$

As time passes, the evolution becomes dominated by $\lambda_0 = \max\{\lambda_k\} = 1 - (\pi/L)^2$, then $N(t) \sim e^{\lambda_0 t}$. In particular, at the critical length, the stationary population size is $N = (8/\pi^2)N_0$, which is smaller than N_0 , because some modes decayed.

4.1.2 Nonlinear asymptotic behavior

For the nonlinear problem, the superposition principle (i.e., linear combination of solutions is solution) does not apply, hence, only limited knowledge about the dynamics is accessible analytically. Then, we resort to numerical integration and address analytically only particular classes of (ν, μ) to obtain information about the asymptotic behavior of the total population N .

Separation of variables, using $\rho(x, t) = X(x)T(t)$ into Eq. (4-12), leads to

$$\frac{T'}{T^\mu} = \frac{(X^\nu)''}{X} T^{\nu-\mu} + \nu X^{\mu-1}. \quad (4-19)$$

The spatial and temporal parts can be separated, if $\nu = \mu$ or $\mu = 1$. But, since a superposition of solutions for different modes does not apply due to the nonlinearity of Eq. (4-12), then the solution remains $\rho(x, t) = X(x)T(t)$. This would mean that the spatial profile is invariant unless a prefactor $T(t)$. But, this is not true in general. However, if after a transient time, the profile

tends to adopt a spatially invariant shape, from that moment separation is sound. The difficulty of assessing analytically the initial transient will have a quantitative, but not qualitative, impact on the results reported in the following subsections assuming the existence of an asymptotic profile.

Case $\nu = \mu$

If $\nu = \mu$, Eq. (4-19) can be separated into two ordinary differential equations, for time and space, as

$$T' = \lambda T^\mu, \quad (4-20)$$

$$\lambda = \frac{Y'' + \mu Y}{Y^{1/\mu}}, \quad (4-21)$$

where we identified $Y = X^\mu$ and λ is a separation constant, determined by the shape of the asymptotic profile.

The solution of the temporal part is

$$T(t) = T_0 \left[1 + \frac{(1 - \mu)}{T_0^{1-\mu}} \lambda t \right]^{\frac{1}{1-\mu}}, \quad (4-22)$$

which, of course, has the form of Eq. (4-15). To obtain the inverse timescale λ , we need to solve the spatial part, together with the requirements at the boundaries. However, if we assume the existence of a (symmetric) steady solution (hence $\lambda = 0$), the spatial solution of Eq. (4-21), $Y(x) = \cos(\pi\sqrt{\mu}x/L)$, yields

$$\rho(x) \propto [\cos(\pi\sqrt{\mu}x/L)]^{1/\mu}. \quad (4-23)$$

Furthermore, to obey the condition at the boundaries, L must be $L_c = \pi/\sqrt{\mu}$, which generalizes the exact result obtained in the linear case. In Fig. 4.2, we show a comparison of the profile given by Eq. (4-23) with the steady state obtained by numerical integration of Eq. (4-12), for $\nu = \mu = 0.5, 1$, and 1.5 . The agreement is very good.

The temporal evolution of the total population, N versus t , is illustrated in Fig. 4.3 (insets), for different values of the habitat size L , when $\nu = \mu = 0.5$ and 1.5 . The main frames show the corresponding data collapses near the critical size, obtained for N vs λt , where $\lambda = 1 - [L_c(\mu)/L]^2 \sim L - L_c$, like in the linear case. The observed plots are typical of an absorbing phase transition [102] at L_c , being $N \sim t^\alpha$, with $\alpha = 0$ in our case.

Moreover, in this figure, we compare the numerical results with the growth law predicted by Eq. (4-22). For $\mu < 1$, the absorbing state is attained at finite time, while for $\mu > 1$, there is blow up, at finite time.

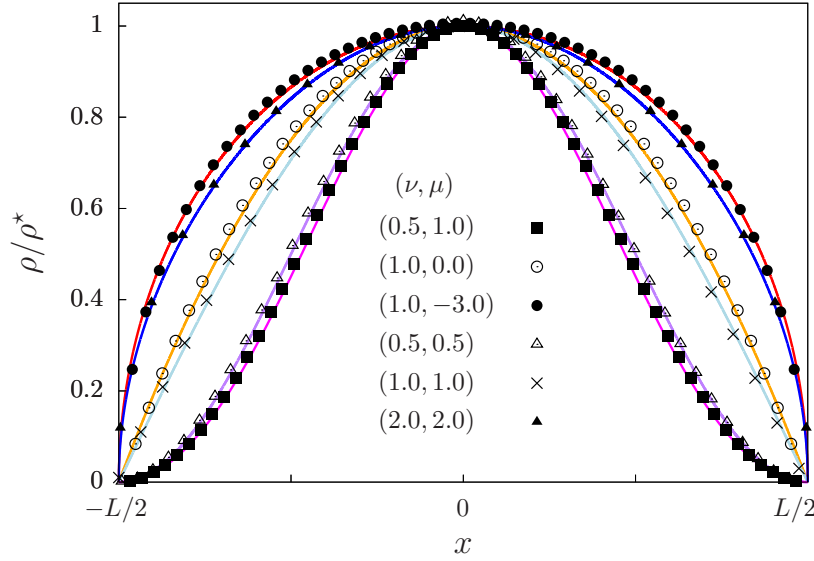


Figure 4.2: Steady state profiles, normalized by the maximal value ρ^* , for (ν, μ) indicated on the figure. The habitat size is $L = L_c$ for the cases $\mu \geq \nu$, and $L = 5$, otherwise, that is for $(1,0)$ and $(1,-3)$. Symbols correspond to numerical integration of the differential equation (4-12). Solid lines represent the analytic solutions given by Eqs. (4-17), (4-23), (4-32), (4-38), (4-39).

Case $\mu = 1$, arbitrary ν

In this case, Eq. (4-19) can be separated into

$$T' = T(\nu - \lambda T^{\nu-1}), \quad (4-24)$$

$$(X^\nu)'' = -\lambda X. \quad (4-25)$$

A nontrivial steady state exists if $T = (\nu/\lambda)^{1/(\nu-1)}$.

The solution of Eq. (4-24) is:

$$T(t) = \left[\frac{\lambda}{\nu} + \left(T_0^{1-\nu} - \frac{\lambda}{\nu} \right) e^{\nu(1-\nu)t} \right]^{1/(1-\nu)}. \quad (4-26)$$

In the large time limit, $T(t)$ tends to $(\nu/\lambda)^{1/(\nu-1)}$ for any $\nu > 1$, while the expression diverges for $\nu < 1$, except if $\lambda \geq \nu T_0^{1-\nu}$, suggesting the existence of a critical condition for the spatial shape.

In the particular case $\nu \rightarrow 1$, we recover $T(t) = T_0 e^{(1-\lambda)t}$. In the limit $\nu \rightarrow 0$, $T(t) \rightarrow T_0 + \lambda t$. Note, however, that beyond these particular cases, timescales are not dictated by λ , which interferes only in the additive and multiplicative constants in Eq. (4-26).

The spatial part will be treated within the general case of arbitrary values of μ and ν , in the following subsection.

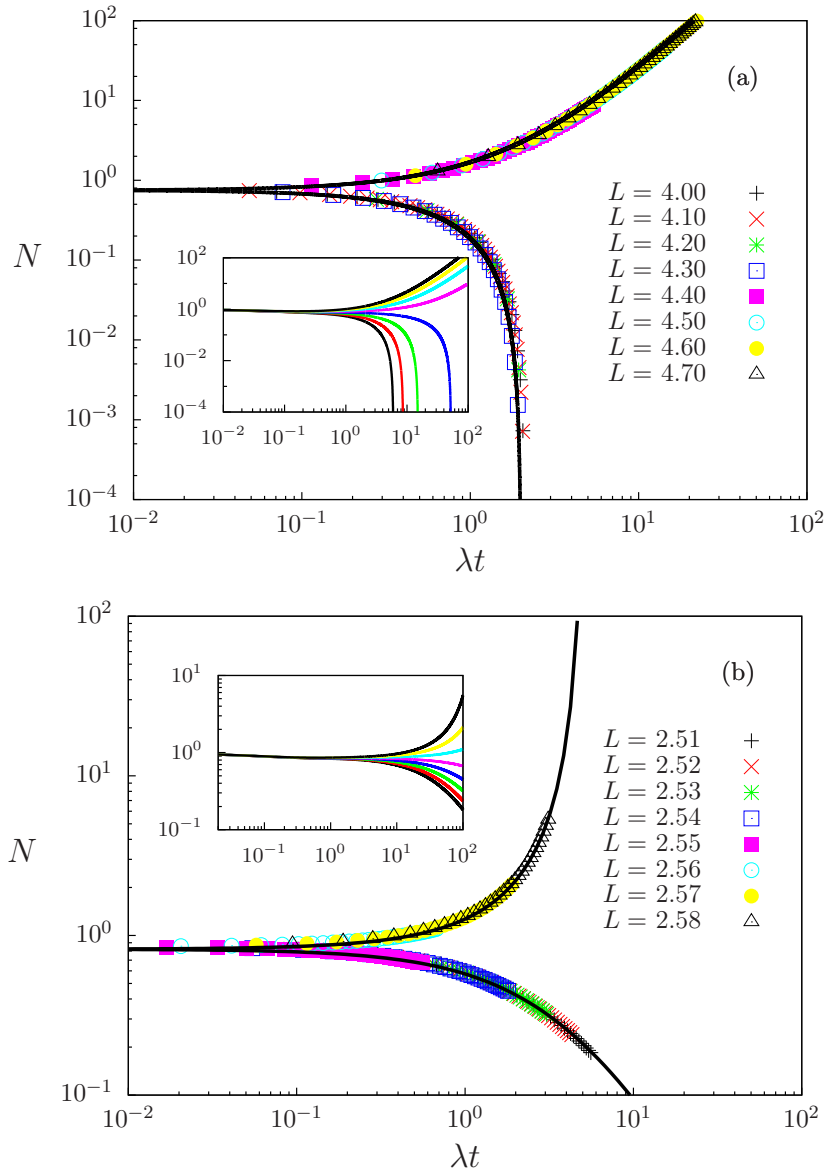


Figure 4.3: Temporal evolution of the total population size $N(t)$ when $\nu = \mu$, in the cases $\mu = 0.5$ (a) and 1.5 (b), for several values of L indicated on the figure. The scaling parameter is $\lambda = 1 - (L_c(\mu)/L)^2$. Results were obtained from numerical integration of Eq. (4-12), starting from a uniform initial distribution with $N_0 = 1$. The solid lines correspond to the scaling law (4-22), with T_0 as a fitting parameter.

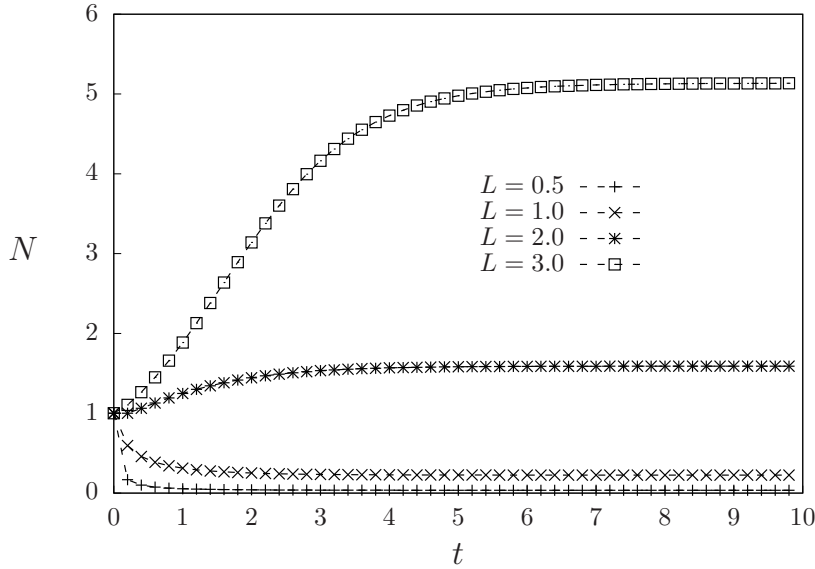


Figure 4.4: Temporal evolution of the total population size $N(t)$ for different habitat sizes L indicated on the figure, when $\mu = 1$ and $\nu = 2$, i.e., $\mu/\nu < 1$.

4.1.3

Steady states and critical habitat size

In general, we observe two main classes of behaviors. For $\mu/\nu > 1$, the dynamics behaves like in the case $\mu/\nu = 1$ illustrated in Fig. 4.3. That is, there is a critical size L_c that separates the extinction and survival regimes, while at the critical value a nontrivial steady state is reached. In this class, extinction can occur conditioned to the habitat size. Differently, for $\mu/\nu < 1$, a finite steady state solution is attained for any L , as illustrated in Fig. 4.4. That is, the effective critical value is $L_c = 0$. It is interesting that this stationary state is a result of the balance between growth and diffusion, in contrast to the steady state that emerges from a logistic rule.

Assuming that a steady state $\rho(x)$ is attained, Eq. (4-12) becomes

$$[\rho(x)^\nu]'' + \nu[\rho(x)]^\mu = 0, \quad (4-27)$$

or, alternatively, making the change of variables $Z = \rho^\nu$, then

$$Z'' + \nu Z^{\frac{\mu}{\nu}} = 0. \quad (4-28)$$

Defining $V \equiv \frac{d}{dx}Z$, hence $\frac{d}{dx}V = V\frac{dV}{dZ}$, we can rewrite Eq. (4-28) in separate differential form as

$$VdV = -\nu Z^{\frac{\mu}{\nu}}dZ. \quad (4-29)$$

Integrating over a path from the center (at $x = 0$), where $V = 0$ and $Z = Z_0$ is

the maximum value, towards its right border, up to generic (Z, V) , we obtain

$$\frac{V^2}{2} \Big|_0^V = -\nu \frac{Z^{1+\frac{\mu}{\nu}}}{1+\frac{\mu}{\nu}} \Big|_{Z_0}^Z = \left(\frac{\nu}{1+\frac{\mu}{\nu}} \right) \left[Z_0^{1+\frac{\mu}{\nu}} - Z^{1+\frac{\mu}{\nu}} \right], \quad (4-30)$$

where the case $\mu/\nu = -1$ is recovered from limiting values.

Integration of $dx = dZ/V(Z)$, taking into account the symmetry of the solutions due to the even initial condition, leads to

$$\sqrt{\frac{|\nu + \mu|}{2\nu^2}} \int_Z^{Z_0} \frac{dZ}{\sqrt{|Z_0^{1+\frac{\mu}{\nu}} - Z^{1+\frac{\mu}{\nu}}|}} = \int_0^x dx. \quad (4-31)$$

The integral in the right-hand-side can be expressed in terms of hypergeometric² function ${}_2F_1$. Then, we obtain the steady solution in implicit form. For instance, when $\alpha = \mu/\nu + 1 > 0$, we have

$$Z |{}_2F_1(1/\alpha, 1/2, 1/\alpha + 1, 2A^2\nu Z^\alpha/\alpha)| = |x|/A, \quad (4-32)$$

where $A > 0$ is an integration constant, that depends on the initial condition.

We want to obtain the possible habitat sizes, L^* , for which an steady state exists. In order to do that, we perform the change of variables $z = Z/Z_0$ and consider that $Z = 0$ at the border (where $x = L^*/2$), then we obtain

$$Z_0^{(1-\frac{\mu}{\nu})/2} \int_0^1 \frac{dz}{\sqrt{|1 - z^{1+\frac{\mu}{\nu}}|}} = \sqrt{\frac{2\nu^2}{|\nu + \mu|}} \frac{L^*}{2}. \quad (4-33)$$

Therefore,

$$L^* = Z_0^{(1-\frac{\mu}{\nu})/2} \frac{\sqrt{2|\nu + \mu|}}{\nu} \mathcal{I}(\mu/\nu), \quad (4-34)$$

where

$$\mathcal{I}(\gamma) = \begin{cases} \sqrt{\pi} \frac{\Gamma\left(1+\frac{1}{1+\gamma}\right)}{\Gamma\left(\frac{1}{2}+\frac{1}{1+\gamma}\right)}, & \text{if } 1 + \gamma > 0, \\ \sqrt{\pi} \frac{\Gamma\left(\frac{1}{2}-\frac{1}{1+\gamma}\right)}{\Gamma\left(-\frac{1}{1+\gamma}\right)}, & \text{if } 1 + \gamma < 0, \end{cases} \quad (4-35)$$

and Γ corresponds to the the Gamma function³. In the marginal case, $\mathcal{I}(\gamma \rightarrow -1) \rightarrow 1$. Hence, for $\mu/\nu = -1$, we obtain $L^* = Z_0\sqrt{2\pi/\nu}$.

In particular, when $\mu/\nu = 1$, $\mathcal{I}(1) = \pi/2$, then

$$L^* = \frac{\pi}{\sqrt{\mu}}, \quad (4-36)$$

which is independent on Z_0 , that is, a unique value arises independently of the initial condition. This value can be identified with L_c , recovering the result of

²The hypergeometric function is defined by the series ${}_2F_1(a, b; c; z) = \sum_{n=0}^{\infty} \frac{a_n b_n}{c_n} \frac{z^n}{n!}$, where $x_n = \Gamma(x+n)/\Gamma(x)$, and Γ is the Gamma function [103].

³The Gamma function can be defined as $\Gamma(z) = \int_0^{\infty} dy y^{z-1} e^{-y}$ [103].

Section 4.1.2.

In general, L^* depends on the initial condition, through Z_0 . Its connection with N_0 , that defines the initial total population size, can be obtained as follows. Recalling the change of variables $Z = \rho^\nu$, then, the maximum value of Z , occurring at the center of the habitat, is $Z_0 = [\rho_0]^\nu$, where $\rho_0 = \rho(x = 0)$. On the one hand, the stationary total population can be written as $N_s = g\rho_0 L^*$, where g is a geometric factor that depends on the shape of the steady state. On the other, we assume that $N_s = \eta N_0$, where η takes into account the transient effects that relate the initial and final population sizes. Therefore, we have $Z_0 = \rho_0^\nu = [N_s/(gL^*)]^\nu = [\eta N_0/(gL^*)]^\nu \propto (N_0/L^*)^\nu$. This is expected to be valid, if a finite steady state actually emerges, for some length L^* . Otherwise the population will go extinct ($\eta \rightarrow 0$) or suffer unbounded growth ($\eta \rightarrow \infty$). Then, when η is finite, substituting $Z_0 \propto (N_0/L^*)^\nu$ into Eq. (4-34) and solving for L^* , we obtain

$$L^* \propto \left(2 N_0^{\nu-\mu} |\nu + \mu| [\mathcal{I}(\mu/\nu)]^2 / \nu^2 \right)^{\frac{1}{2+\nu-\mu}}. \quad (4-37)$$

Note that L^* increases with the initial population size N_0 , when $\mu < \nu$ or $\mu > \nu + 2$, while it decreases otherwise, being independent only for $\mu = \nu$. Moreover, the exponent of N_0 diverges when $\mu \rightarrow \nu + 2$.

When $\mu/\nu \geq 1$, we observed in numerical simulations that a steady state exists for a unique value of L (that is, $L_c > 0$). Then, we are tempted to identify L^* with L_c . In fact, as shown in Fig. 4.5, Eq. (4-37) is in excellent accord with numerical values, except that the proportionality constant η which embodies transient effects is unknown from this analytical approach, therefore it was obtained as a fitting parameter.

Furthermore, the critical size determines whether the population will either go extinct or survive. Numerical simulations show that survival occurs for $L > L_c$, when $\nu < \mu < \nu + 2$, that is, a minimal size of the viable region is required, like in the linear case. However, when $\mu > \nu + 2$, the population survives for $L < L_c$. It is worth recalling that precisely for $\mu > \nu + 2$, the nature of global solutions changes drastically [83, 84]. This result means a violation of the usual result about extinction conditions in finite domains where L_c gives the minimum habitat size for survival.

For $\mu/\nu < 1$, numerical results indicate that a steady state exists for any L . Explicit solutions can be obtained in some particular cases, by directly solving Eq. (4-28), instead of inverting Eq. (4-32), as follows:

(i) When $\mu/\nu \rightarrow 0$, Eq. (4-28) becomes $Z'' + \nu = 0$, which has solutions $Z(x) = -\nu x^2/2 + Z^*$, that under the boundary conditions lead to

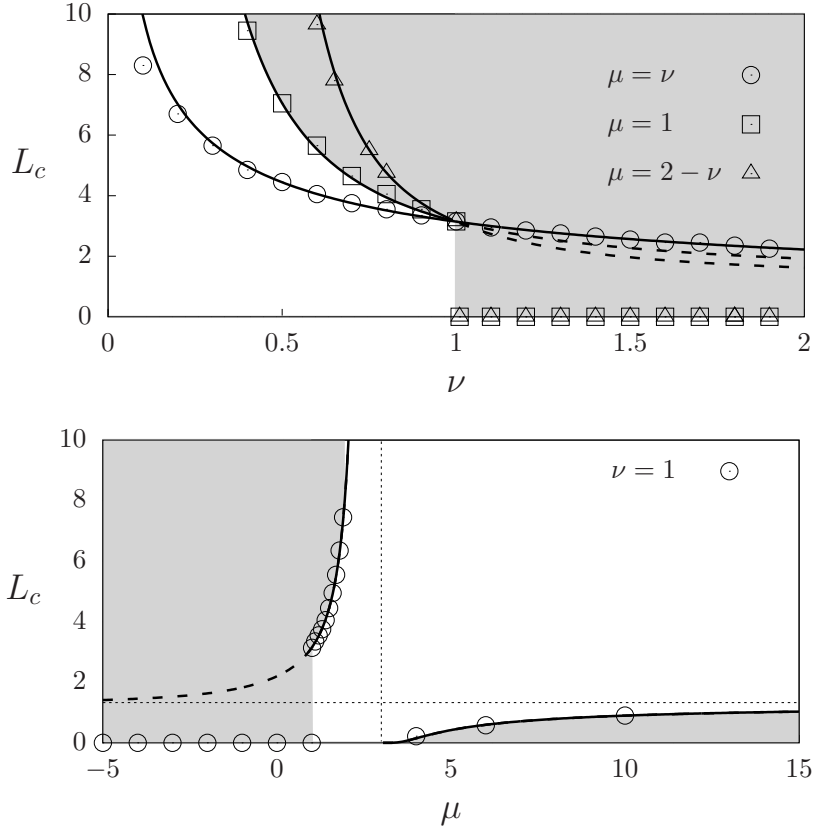


Figure 4.5: Critical habitat size L_c as a function of the exponents μ and ν . The shaded region indicates survival for the case $\mu = 1$ in the top panel and for $\nu = 1$ in the lower panel. The initial distribution is homogeneous with $N_0 = 1$. The solids lines are given by Eq. (4-37), with a fitted value of the proportionality factor. Notice that when $\mu/\nu < 1$ the critical size vanishes, signaling that the population survives for any L , but the theoretical prediction given by Eq. (4-37) still indicates when the population initially grows or decreases (dashed lines).

$$\rho(x) = (\nu L^2/8)^{1/\nu} (1 - 4x^2/L^2)^{1/\nu}. \quad (4-38)$$

Integrating this profile to obtain the steady total population N_s , one has, $L \propto N_s^{\nu/(\nu+2)}$, in accord with Eq. (4-37).

(ii) When $\mu/\nu = -3$, we obtain

$$\rho(x) = (\nu L^2/4)^{1/(4\nu)} [1 - 4x^2/L^2]^{1/(2\nu)}, \quad (4-39)$$

for which $L \propto N_s^{2\nu/(2\nu+1)}$, also in agreement with Eq. (4-37).

These theoretical profiles are compared to numerical results in Fig. 4.2. Let us remark that, for fixed μ/ν , the slope at the boundaries is finite for a critical value of ν , but vanishes (diverges) below (above) that value. For instance, when $\mu/\nu \rightarrow 0$, the critical value is $\nu = 1$, while for $\mu/\nu = -3$, it is $\nu = 0.5$.

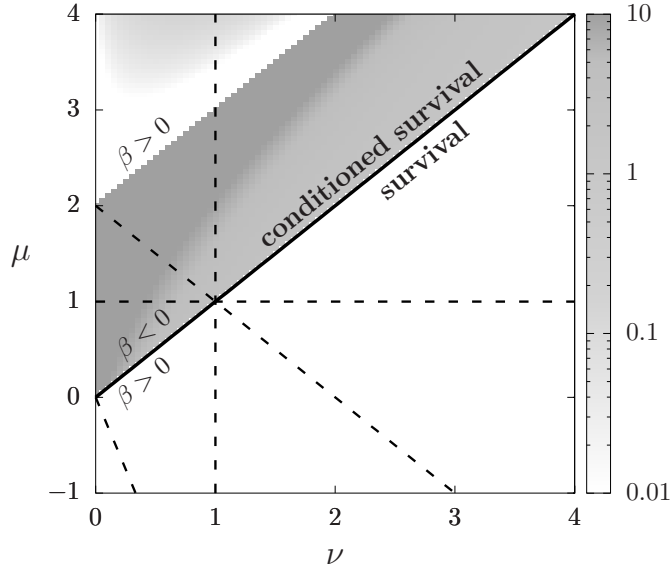


Figure 4.6: Gray-scale map of the habitat size L^* given by Eq. (4-37), in the plane (ν, μ) , for initial condition $N_0 = 1$. The solid line separates the phases where survival always occurs (below) or it is conditioned (above the line), while dashed lines highlight particular families analyzed numerically and analytically. We recall that in the survival phase ($\mu < \nu$), survival occurs for any L , meanwhile, in the conditioned phase, extinction occurs when $L < L_c$ (if $\nu < \mu < \nu + 2$ or $L > L_c$ (if $\mu > \nu + 2$), otherwise the population survives. Also recall that $\beta = 1 + 2/(\mu - \nu - 2)$, ruling the scaling relation between $L_c \sim N_0^\beta$.

In both cases (which belong to the region $\mu/\nu < 1$), a nontrivial steady state exists for any L , hence the population always survives. As a consequence, the critical size for survival is $L_c = 0$. Therefore, in this case, L^* in Eq. (4-37) is not associated to the survival-extinction dilemma, but it still reflects the threshold that separates the regimes in which the population grows or decays to attain the steady state (see Fig. 4.4, where $L^* = 1.64$).

A synthesis of our results is given in Fig. 4.6, in a gray-scale map representing the value of the critical habitat size L_c in the plane $\nu - \mu$. The solid line separates the two different regimes. Notice that although $\gamma = \mu/\nu$ determines that frontier, the critical size L_c is not uniquely determined by γ , neither is the inversion (dotted) line.

4.1.4

Role of initial conditions

Differently from the linear case, nonlinearities cause dependence on initial conditions. This feature has practical relevance, since when one tries to reintroduce an species in a given habitat, the initial quantity released changes the outcome of the ecological management [29].

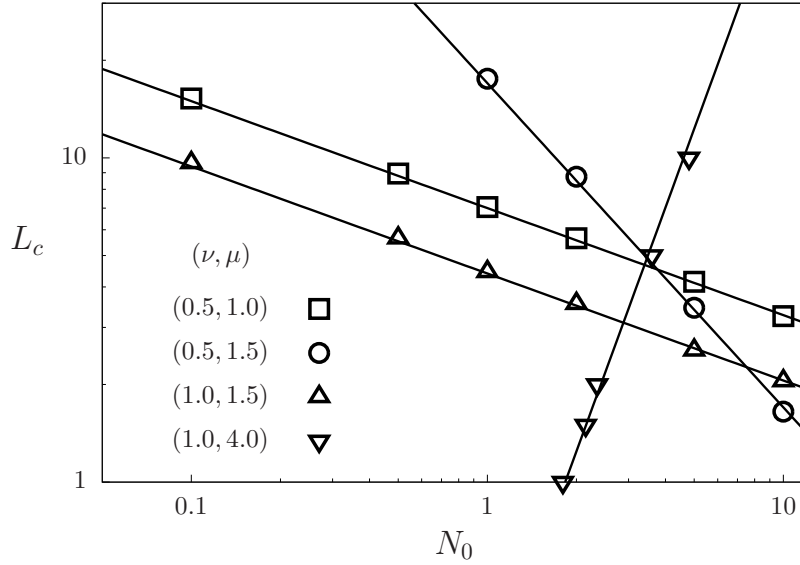


Figure 4.7: Critical habitat size as a function of the initial population size N_0 , when $\mu/\nu > 1$. Solid lines represent the scaling law provided by Eq. (4-37).

We considered a uniform initial population density, assuming that individuals are placed homogeneously within the full habitat domain. For such initial profile, we show in Fig. 4.7, the critical habitat size as a function of the initial total population N_0 , when $\mu/\nu > 1$. The degrees of nonlinearity change the sensitivity to the initial value N_0 , according to the scaling $L_c \sim N_0^\beta$, with $\beta = 1 + 2/(\mu - \nu - 2)$, following Eq. (4-37). The exponent β is a decreasing function of the difference $\mu - \nu$, diverging at $\mu - \nu = 2$. It vanishes only at $\nu = \mu$, in which case there is independence on the initial conditions, that would correspond to a (non plotted) horizontal line in the figure. The exponent β is negative in the interval $0 < \mu - \nu < 2$, producing negative slopes in the log-log plots of Fig. 4.7. This means that, as expected, when more individuals are introduced at early times (larger N_0), smaller habitat sizes are needed for survival where $L > L_c$. Differently, when $\mu - \nu > 2$, survival occurs for $L < L_c$, and, in addition, β is positive (see Fig. 4.6), therefore, the maximum habitat size L_c increases with the initial population density N_0 , which does not have any ecological benefits.

4.2 Higher order interactions

In this section, we present a brief discussion about the persistence of population considering higher order interactions. Higher order interaction are known to produce spatiotemporal patterns, as the ones seen in Sec. (3.3). In specific, the previous nonlocal competition discussed in Sec. (3.3) does not

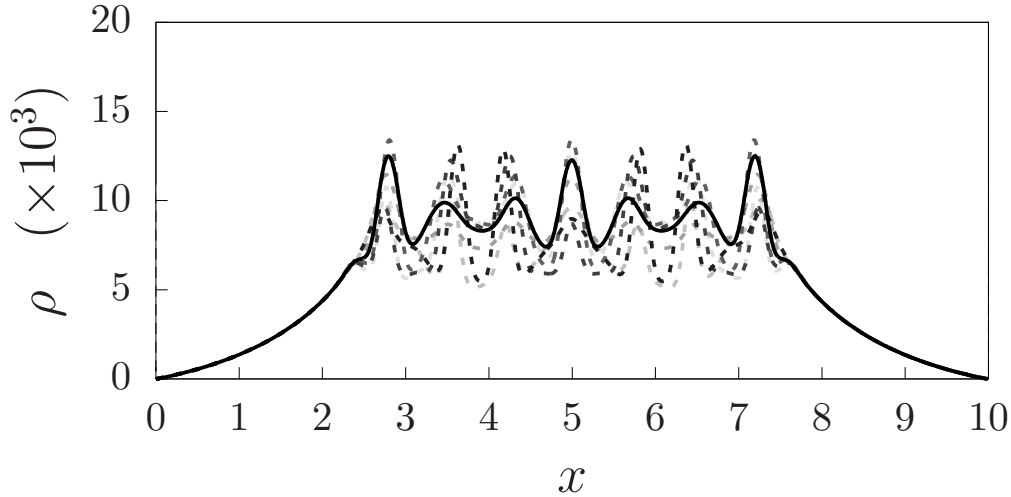


Figure 4.8: Long time population density distribution in a large habitat $L = 10 > L_c$ with $a = D = 1$, $\kappa = 10^{-4}$, $l = 3/\rho_0$, $\rho_0 = 10^5$. Dotted lines indicated the distribution evolution while color are darker for later time instants.

play a role in population conservation, since its impact vanishes near the null state. However, in a specific model for bacteria pattern formation, higher order interaction interfere in the critical habitat size L_c , as we will see. In Fig. 4.2 we show the a typical steady state formed for $L > L_c$.

Following a possible derivation for active matter from Cates et al. [52,87], we see that bacteria due to self-interaction exhibit density-dependent diffusion as well as surface tension term in the equation for the evolution of the population density distribution. Additionally, considering the logistic growth, we arrive that the aforementioned model,

$$\partial_t \rho(x, t) = \partial_x (D_{eff}(\rho) \partial_x \rho) + r\rho(1 - \rho/\rho_0) - \kappa \partial_x^4 \rho, \quad (4-40)$$

where $D_{eff}(\rho) = D(\rho) + \rho D'(\rho)$ with $D(\rho) = v(\rho)^2 \tau$ and $v(\rho) = v_0 \exp(-l\rho/2)$, such that

$$D_{eff}(\rho) = D(\rho)(1 - l\rho/2) \quad (4-41)$$

$$= (v_0 \tau)^2 \exp(-l\rho)[1 - l\rho/2] \quad (4-42)$$

$$= D_0 \exp(-l\rho)[1 - l\rho/2]. \quad (4-43)$$

Following the same methodology used in Sec. 3.2 and 3.3, the dispersion relation around the homogeneous ρ_0 can be obtained

$$\lambda(k) = -1 - D_{eff}(\rho_0)k^2 - \kappa k^4. \quad (4-44)$$

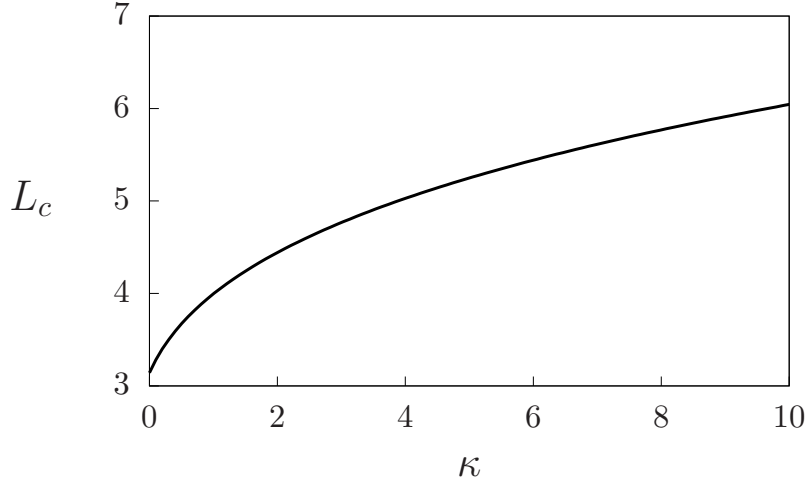


Figure 4.9: Critical habitat size L_c as a function of parameter κ with $a = D = 1$, $\kappa = 10^{-4}$, $l = 3/\rho_0$, $\rho_0 = 10^5$. Solid line is given by Eq. (4-49).

Patterns arise if $D_{eff} < 0$ due to density-dependent effects, while high modes growth is bounded by the surface tension term $\kappa > 0$. This can occur when

$$\Phi \equiv l\rho_0/2 > 1, \quad (4-45)$$

$$R \equiv D_0/\sqrt{r\kappa} > 2 \exp(2\Phi)/(\Phi - 1). \quad (4-46)$$

Eq. (4-44) provides the pattern stability condition that predict the periodic structures in Fig. 4.2.

Despite the interesting pattern formation phenomena that arises in this case [87], we will focus on the determination of the critical habitat size of this model. Note, that since population persistence is investigated in the low density regime (stability of the null state), pattern formation is not directly related to the following analysis (see Eq. (4-44)).

Assuming that we are in the limit of harsh conditions outside habitat domain, we set $\rho(\pm L/2) = 0$. The stability of the null state, in this case, is given by the dispersion relation

$$\lambda(k) = -D_0k^2 - \kappa k^4 + r, \quad (4-47)$$

such that $\tilde{\rho}(k, t) = \tilde{\rho}(k, 0)e^{\lambda(k)t}$ is the exact solution at low densities.

The dispersion relation given Eq. (4-47) is monotonically decreasing, with $\lambda(0) = r > 0$. Thus, for some k_0 the λ becomes negative. From Eq.(4-47) we find four possible solutions, but only two of them are suitable,

$$k_0^2 = \frac{-D_0 + \sqrt{D_0^2 + 4\kappa r}}{2\kappa}. \quad (4-48)$$

The correspondent $\lambda_0 = 2\pi/k_0$, is the smaller spatial scale. Then, survival occurs if $L > L_c$, with $L_c = \lambda_0$. In this case we find that

$$L_c = \frac{2\pi\sqrt{2\kappa}}{\sqrt{-D_0 + \sqrt{D_0^2 + 4\kappa r}}}. \quad (4-49)$$

In Fig. 4.9, we show the critical habitat size given by Eq. (4-49), which increases with κ .

The model discussed reproduces experimental results qualitatively well and might shed light into the positive deviations found in the measured Fisher critical size (Eq. 4-11) [17]. However, an interdisciplinary collaboration is needed to ensure that Eq. (4-44) has proper biological motivation. Moreover, it would be interesting to extend this result to the case where habitat heterogeneity is considered in a more realistic way $a \rightarrow a - A\Theta(|x| - L/2)$, as discussed at the beginning of this chapter.

4.3

Habitat temporal behavior

In order to predict the future of a given population in a particular habitat, it is necessary to take into account the nontrivial spatial distribution of resources, shelter, nutrients and other factors that compose the so called ecological landscape [28]. Moreover, the ecological factors change in time with a characteristic periodicity (seasonality) accompanied by random fluctuations. Then, the environment critical conditions for population survival rely on a combination of the spatial and temporal variability of the environment [22, 35, 36, 104–106]. Its time variability can have different origins. For instance, when the system is found in a natural habitat, it is typically subjected to inherent cycles of the ecosystem such as oscillations in sun light, seasonal changes, and other external dynamics that can interfere in the refuge conditions. For ecological reserves, the time scale can be introduced, for instance, by fishing (or hunting) prohibition laws that are made flexible during specific periods of the year. In the case of microorganisms, where artificially constructed landscapes can be made [17, 80], time scale might be introduced in the experimental setup via manipulation of a mask that can protect a population of bacteria from a harmful effect [17] (see Fig. 4.10).

Changes in size [15], position [107] or even rotations [16] of the refuge, as well as stochastic fluctuations [21, 42, 108] have been considered before. Continuing our discussion of this chapter, we proceed making basic assumptions about the population dynamics, we investigate population survival when there is an intermittent refuge of size L (see Fig. 4.10). We

consider that the refuge alternates, with period τ , between active and inactive states, such that the population can be protected or not, during intervals $\lambda\tau$ and $(1 - \lambda)\tau$ (where $0 \leq \lambda \leq 1$), respectively. We mainly investigate the requirements for survival as a function of the characteristic time scales and size of the refuge, aiming to provide general insights that can guide population management and conservation [14].

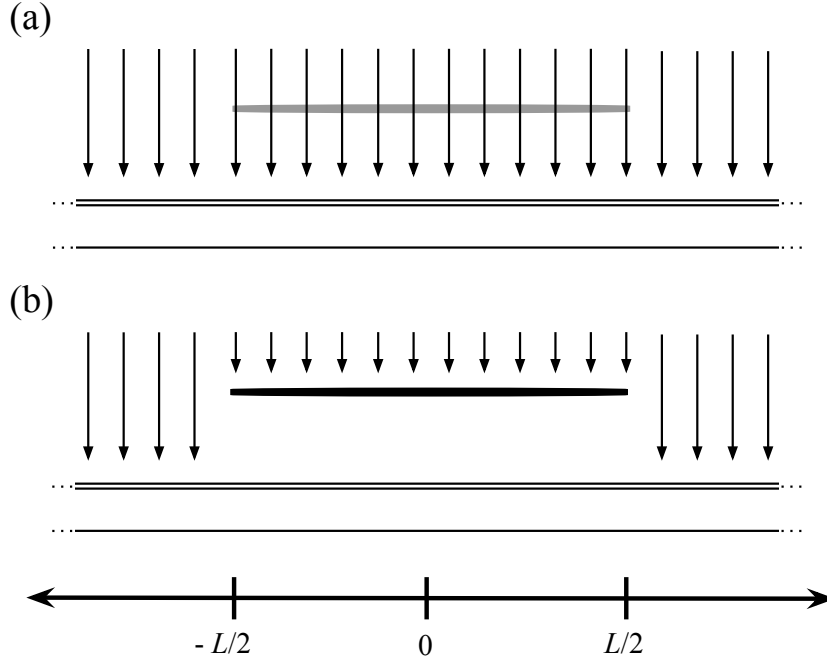


Figure 4.10: Pictorial representation of a one-dimensional habitat subject to an external harmful effect (downwards arrows) with a refuge (thick segment) of size L in the inactive (a) and active (b) states. In the active state, the refuge is able to block the harmful effect.

The temporal evolution of the population density distribution $\rho(x, t)$ is described by the Fisher-KPP equation [6, 56, 109] plus an additional term, namely,

$$\partial_t \rho(x, t) = D \partial_{xx} \rho(x, t) + f(\rho) + \psi(x, t) \rho(x, t), \quad (4-50)$$

where, as usual, D is the diffusion coefficient, $f(\rho)$ is the local growth rate given by the logistic or Verhulst expression $f(\rho) = a\rho(x, t) \left[1 - \frac{\rho(x, t)}{K}\right]$, with intrinsic growth rate a and carrying capacity K , which bounds population growth, inducing negative growth rates for $\rho > K$. For $\psi(x, t) = 0$, one recovers the standard Fisher-KPP equation. In our model,

$$\psi(x, t) = -A [1 - \Theta(L/2 - |x|)\varphi(t)], \quad (4-51)$$

with $A > a$. It contains the environment structure, pictorially represented in Fig. 4.10, where a harmful effect is always present (downwards arrows), contributing with an additional death rate in Eq. (4-50), but a refuge located at

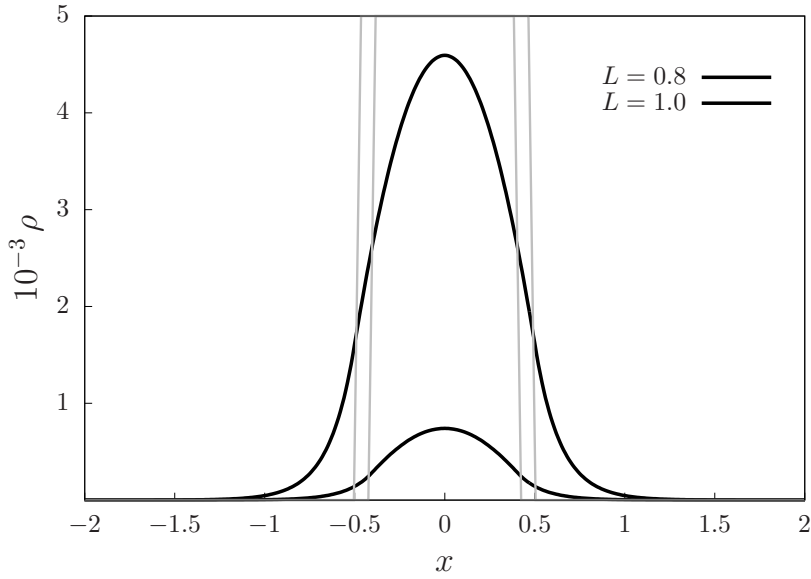


Figure 4.11: Asymptotic population distribution when the refuge is static, for two different refuge sizes L indicated in the figure. In this case, $L_c \simeq 0.73$, for our choice of the parameter values $a = 1$, $K = 10^4$, $D = 10^{-1}$, $A = 6$ defined in the beginning of the section. The gray vertical lines indicate the boundaries of the refuge for each refuge size.

$|x| \leq L/2$ can mitigate the effect. The factor $\varphi(t)$ embodies the time variability of the refuge. If the refuge is absent or inactive (Fig. 4.10.a), $\varphi(t) = 0$, then $\psi(x, t) = -A$ for all x . The refuge can protect the region $|x| \leq L/2$ (Fig. 4.10.b), either partially (when $0 < \varphi(t) < 1$) or totally (when $\varphi(t) = 1$). For simplicity, we assume a binary time behavior, such that $\varphi(t)$ can only take the values 0 and 1. Additional parameters λ and τ control the fraction of time that the harmful effect penetrates the refuge and the protocol time scale, respectively. Namely, during an interval $\lambda\tau$, the refuge is inactive, allowing the harmful effect to penetrate the refuge. Afterwards, the refuge becomes active, protecting the population during an interval $(1 - \lambda)\tau$.

Equation (4-50) will be numerically integrated by means of a standard fourth-order Runge-Kutta algorithm, together with spatial discretization, using $\Delta x = 10^{-2}$ and $\Delta t < 10^{-5}$, adequate for convergence. Along this section, we will focus mainly on population preservation at long times as a function of the refuge size L and time scale τ , keeping the remaining parameters fixed. Motivated by experiments for a nonchemotactic strain of *E. Coli* bacteria [17], we set $a = 1$, $K = 10^4$, $D = 10^{-1}$, $A = 6$, except when different values are explicitly indicated. Nevertheless, analytical expressions allow to extend the numerical results shown for that set of values.

4.3.1

Static refuge case

The case where the refuge is always active ($\varphi = 1$) is well known in the literature [12, 13] and has been analyzed in the previous section. The refuge imposes an heterogeneous spatial condition which is the spatial component of ψ . When the refuge has size L larger than a critical value L_c , the population survives achieving a nontrivial steady state. In Fig. 4.11 we show the distribution profiles for two values of L , with $L > L_c$.

The critical refuge size L_c can be obtained as shown in the beginning of this chapter and detailed in Sec. 4.1. Following Eq. (4-11), it is straightforward to obtain [12, 13, 18, 20]

$$L_c = L^* \equiv 2\sqrt{\frac{D}{a}} \arctan\left(\sqrt{\frac{A-a}{a}}\right). \quad (4-52)$$

In the literature, this result has been extended to modified forms of the static Eq. (4-50), including advection, nonlinear diffusion, other boundary conditions and functional forms of f [12–14, 18, 101, 110]. For instance, in the limit of harsh unfavorable conditions, $A \gg a$, Eq. (4-52) yields $L_c \propto \sqrt{D/a}$ [18]. For other cases, Eq. (4-52) still holds for effective values of the rates inside and outside the refuge [14, 101]. It is still a good reference even when demographic noise is included to account for the fact that the population is constituted by a finite number of individuals [21].

In this section, we present our results that show the influence of refuge temporal variability in population conservation. We consider a refuge whose temporal behavior is deterministic and periodic with period τ .

Figure (4.12) shows the temporal evolution of the total population size $N(t) = \int_{-\infty}^{\infty} \rho(x, t) dx$, starting from population densities well below the carrying capacity ($\rho(x, 0) \ll K$, for all x). We vary the time scale τ for fixed λ . Even if the fraction of time that the harmful effect penetrates the refuge is the same, we observe that, when subject to a fast varying environment, the population decays to extinction, but, differently, for large τ , the population grows and survives at long times. This drastic change from extinction to survival occurs because L is near enough a critical value, as we will see in subsection 4.3.2. However, increasing τ favors population growth for any L . In order to show these effects, we define the growth rate per capita

$$\Phi \equiv \dot{N}/N = \frac{d(\ln N)}{dt}, \quad (4-53)$$

whose average over one cycle is $\langle \Phi \rangle(t) = \frac{1}{\tau} \int_t^{t+\tau} \Phi(t') dt'$. After a short transient, while the population still remains low, this average attains a quasi-steady value

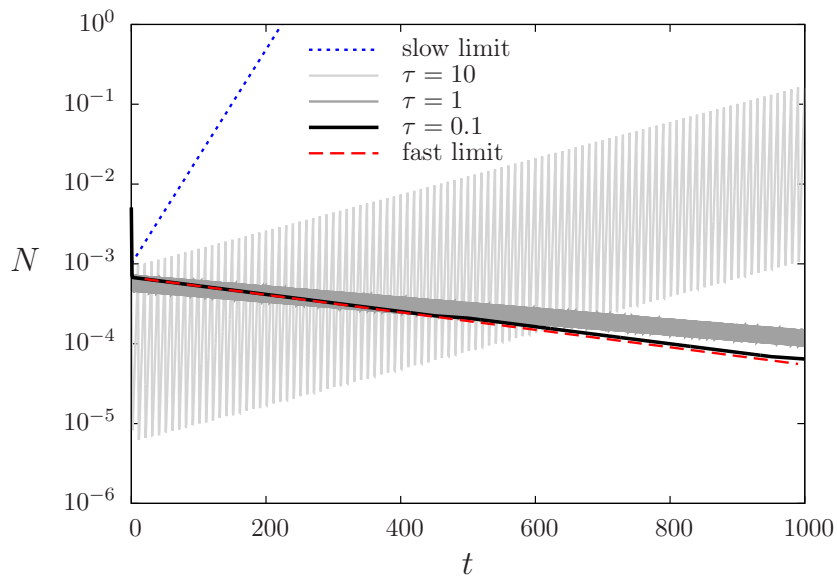


Figure 4.12: Temporal evolution of the total population size N , for different values of the period τ , fixed average rate $\lambda = 0.1$ and size $L = 1.28$ (for the values of the parameters used, $L_c = 1.295$). The dotted and dashed lines represent the slow and fast limit approximation (for details, see Sec. 4.3.2).

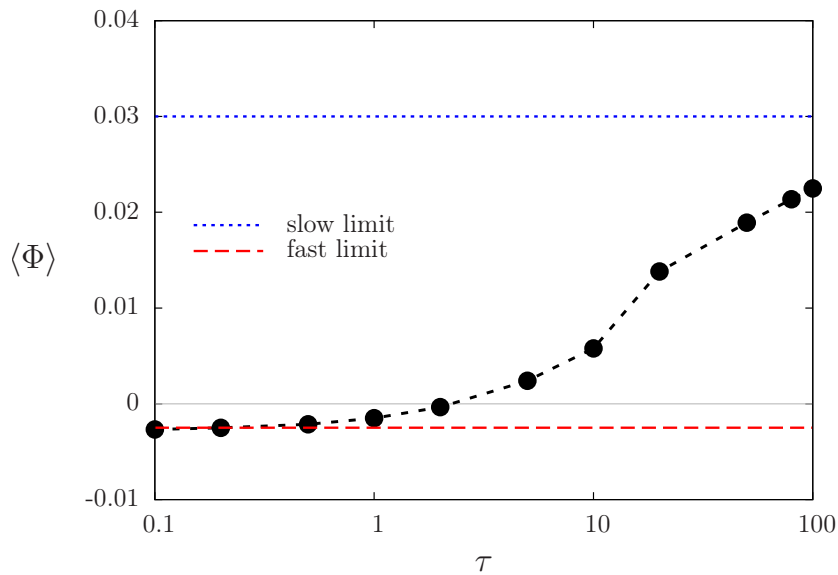


Figure 4.13: Average population growth rate $\langle \Phi \rangle$, computed over entire cycles, as a function of protocol period τ for $L = 1.28$ and $\lambda = 0.1$. The dashed and dotted lines represent the rates at the slow and fast limits (for details, see Sec. 4.3.2).

$\langle \Phi \rangle$, corresponding to the average slope of the curves plotted in Fig. (4.12). For negative $\langle \Phi \rangle$, its steady value will remain for long times, otherwise, it will decay at later times when the population becomes comparable to the carrying capacity and stops growing attaining a steady level. In Fig. 4.13, we show $\langle \Phi \rangle$ as a function of τ .

For the extreme cases of slow and fast time scales, we show, in Sec. 4.3.2, the derivation of the average growth rates, represented in Figs. 4.12 and 4.13. These limits provide the bounds of the influence of refuge temporal variability.

4.3.2

Slow and fast limits

First, we start by assuming that flashes occur in a very short time scale $\tau \ll \tau_S = 1/a$, such that the system does not have time to respond, where τ_S is the system time scale. In this limit, environment fluctuations can be locally averaged, producing an effective growth inside the refuge $(1 - \lambda)a - \lambda(A - a) = a - \lambda A$ (dashed line in Fig. 4.12). Substituting the intrinsic growth rate a by the effective one into Eq. (4-52), gives

$$L_c(\lambda; \tau \ll \tau_S) = 2\sqrt{\frac{D}{a - \lambda A}} \arctan\left(\sqrt{\frac{A - a}{a - \lambda A}}\right), \quad (4-54)$$

where $\tau_S \sim 1/a$ is the system response time. This result is expected to be independent on the microscopic details of the protocol, i.e. whether it is regular or stochastic behavior, being only dependent on its averaged behavior, characterized by parameter λ .

In order to estimate the slow-limit behavior, it is useful to observe the evolution of the growth rate Φ , for different time scales τ , as depicted in Fig. 4.14, where we have rescaled time t to facilitate the comparison of different periods τ . During the interval $\lambda\tau$, when the harmful effect penetrates the refuge, the growth is negative, constant and independent of time scale. When the harmful effect is blocked, the growth rate tends to attain a maximal value Φ_0 , which is achieved for large τ , $\tau \gg \tau_S$.

In this slow limit, we approximate the average growth rate by $\langle \Phi \rangle \approx (1 - \lambda)\Phi_0(L) - \lambda(A - a)$. Then, imposing $\langle \Phi \rangle = 0$, the critical refuge size under slow environmental changes can be written by using the inverse function of the growth rate, $L_c \simeq \Phi_0^{(-1)}[\lambda(A - a)/(1 - \lambda)]$.

The behavior of Φ_0 as a function of refuge size is shown in Fig. 4.15. Approximate expressions for $\Phi_0(L)$ are presented in appendix C.1. The numerical data can be well described by the heuristic expression (see appendix C.1)

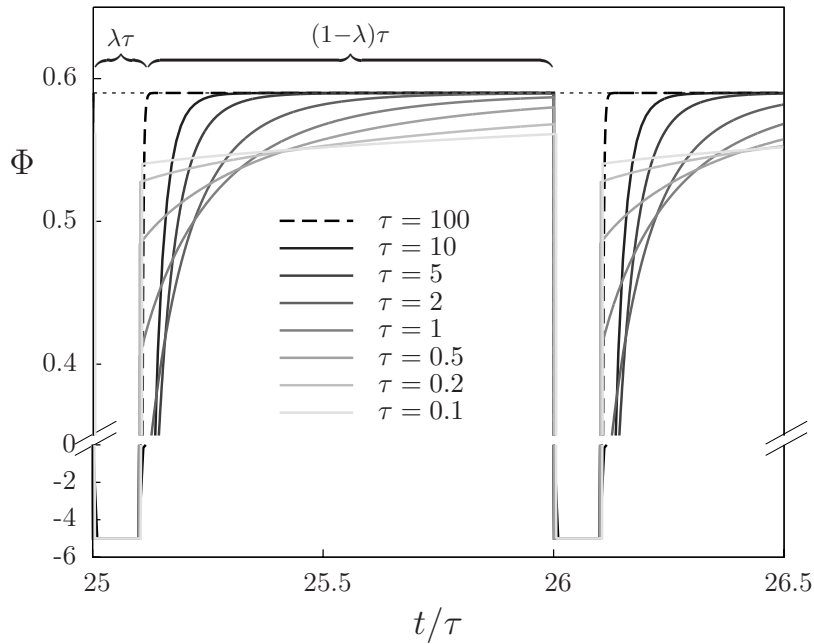


Figure 4.14: Temporal evolution of the growth rate Φ , for different time scales τ , with $L = 1.28$ and $\lambda = 0.1$. The dotted line denotes the maximal value Φ_0 .

$$\Phi_0(L) = a - \frac{A}{1 + \frac{A-a}{a}(L/L^*)^2}, \quad (4-55)$$

where L^* is the static case critical size given by Eq. (4-52). Explicitly, the critical refuge size for the slow limit becomes

$$L_c(\lambda; \tau \gg \tau_S) = L^* \sqrt{\frac{a}{a - \lambda A}}. \quad (4-56)$$

We summarize the results of this section in Fig. 4.16, where we show the upper and lower bounds for the critical size $L_c(\lambda; \tau \gg \tau_S) \leq L_c \leq L_c(\lambda; \tau \ll \tau_S)$, together with numerical results for different values of τ . The dashed region represents the possible range of L_c as a function of protocol temporal behavior. A critical value of τ , for which the average growth rate $\langle \Phi \rangle$ changes sign, always exists for L within that range.

Notice that when $\lambda = 0$, the bounds given by Eqs. 4-54 and 4-56 coincide, recovering the static value of L_c . In the limit $\lambda \rightarrow a/A < 1$, the critical size is divergent.

4.3.3 Spatial response

In this section, we will focus on the mechanism that connects the spatial and temporal components of the environment. Considering the low density

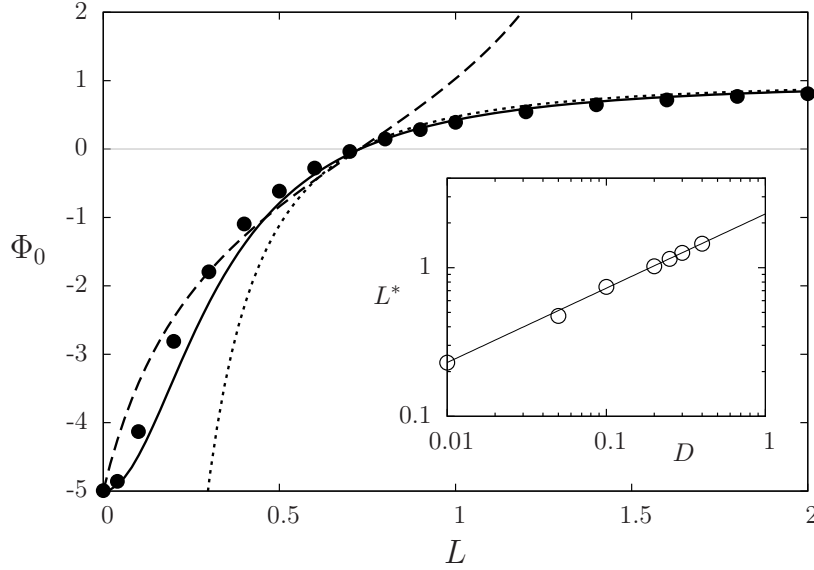


Figure 4.15: Population growth rate Φ_0 vs refuge size L (black circles). The solid line represents the ansatz given by Eq. (4-55), and the dotted line represents the growth rate in the limit case of harsh conditions outside the refuge, explicitly given by Eq. (C-9), and the dashed line the linear approximation given by Eq. (C-3). In the inset, we show that the fitting parameter L^* in the ansatz (4-55) follows Eq. (4-52).

regime $\rho \ll K$, and integrating Eq. (4-50) in space, we obtain that

$$\partial_t N = -(A - a)N_{out} + \{[a - A[1 - \varphi(t)]]\}N_{in}, \quad (4-57)$$

where N_{in} and N_{out} are the total populations inside and outside the refuge domain, respectively. Due to the fact that population growth occurs only inside the refuge, the external population is the result of the accumulated flux of individuals leaving the refuge. This makes the unfavorable neighborhood work as a reservoir of individuals. Explicitly, in the linear regime,

$$\dot{N}_{out}(t) = -(A - a)N_{out} + J \quad (4-58)$$

and

$$\dot{N}_{in} = \{[a - A[1 - \varphi(t)]]\}N_{in} - J. \quad (4-59)$$

where $J/D = -2(\pm\partial u/\partial x)|_{x=\pm L/2} = 2(V\rho)|_{x=\pm L/2}$ is the flux through the refuge boundary and V the net velocity outward the refuge. Due to the combination of a nonlinear spatial dynamics and heterogeneous environment, the flux J has a nonlinear dependency with N_{in} and N_{out} and it is also history-dependent. This means that attempts to define J as proportional to the population density difference $N_{in} - N_{out}$ ignore nonlinearities of the spatial

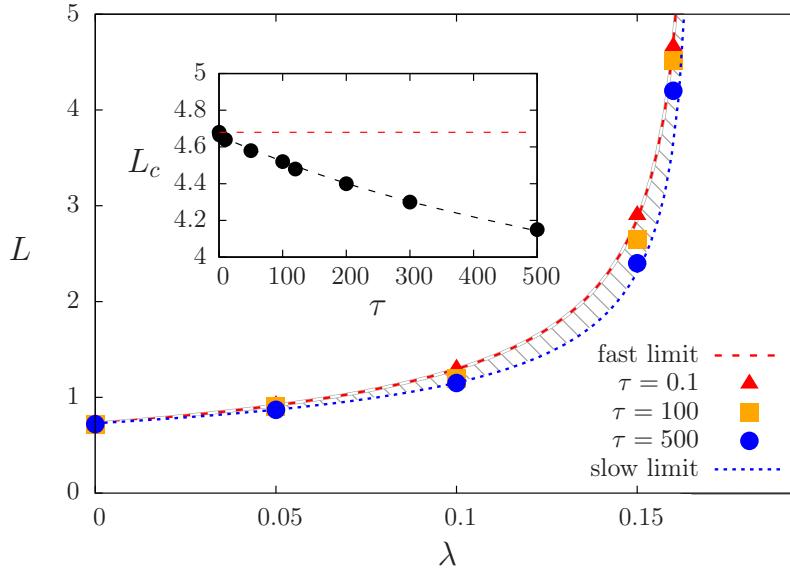


Figure 4.16: Theoretical predictions for the critical size L_c in the slow and fast protocol limits, given by Eqs. (4-56) and (4-54), respectively, together with numerical data for different τ . The striped region (black) between the curves represents the variability of L_c with τ . The inset shows L_c vs τ for $\lambda = 0.16$ and the slow limit approximation (blue dotted line).

dynamics and will not be suitable to model the system behavior (see Sec. 4.3.4), yielding τ -independent results.

For the case of a time periodic protocol, in Fig. 4.17, we show typical trajectories in the plane $\rho - V$, where the density and the velocity are evaluated at one of the boundaries. Time integration of these trajectories provides the total flux that left the refuge. The emergent cycles are induced by the protocol and their shape reveals the relation between the localized perturbation produced by the protocol and spatial changes in population distribution. First, when the condition inside the refuge changes from favorable to unfavorable, the population decays and its population tends to be flattened, as we see in Fig. 4.17, $V(x = L/2)$ decreases (decay period). When the refuge becomes active, the population inside the refuge starts to grow while the surrounding population is in constant process of extinction. This creates a fast stretch of the distribution, rapidly increasing the derivative of the population distribution at the refuge boundary (transient period). After the transient, relaxation towards the steady state occurs, where the velocity at the boundary is kept roughly constant (recovery period), $|V| = \sqrt{(A - a)/D} \approx 7.0$ in the case of the figure, as predicted by the linear approximation (see Appendix C.1).

As shown in Fig. 4.17, for $L > L_c$, in the steady state, these cycles are closed curves. In contrast, for $L < L_c$, the curves are not closed, although the

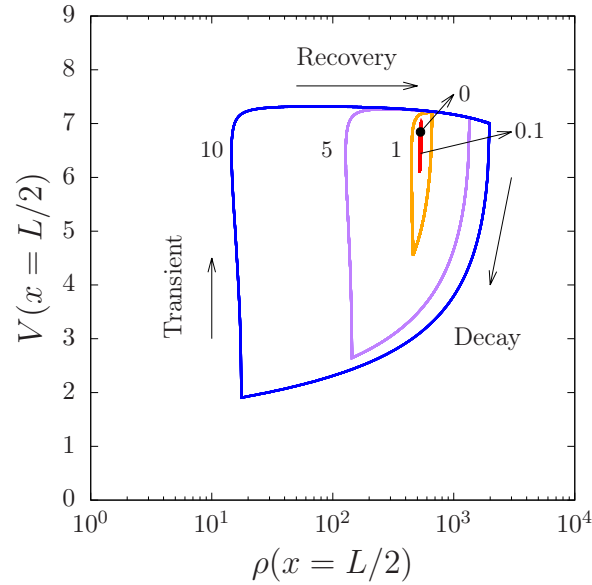


Figure 4.17: Velocity $V(x = L/2)$ vs population density $\rho(x = L/2)$ at the refuge boundary, for different values of τ indicated in the figure, with $\lambda = 0.1$ and refuge size $L = 2$ (hence, $L > L_c$). The single dot represents the limiting case $\tau \rightarrow 0$.

shape drawn in Fig. 4.17 remains essentially the same, but, at each period, the cycle is progressively shifted to the left (i.e., towards lower densities).

4.3.4 Recolonization process

We now proceed to investigate the recolonization process that occurs when all the population inside the refuge dies due to a catastrophic phenomenon. Such extreme situation allows us to follow in detail the recolonization process that takes place from the lateral population reservoirs formed during the period when the refuge was active. In Fig. 4.18, we show, for $L > L_c$, how the total flux at the borders and the population densities inside and outside the refuge behave during the recolonization process. Focusing on the temporal evolution of N_{in} , it is very clear that the population growth is maximal just after the reset ($t = 50$). This occurs due to the migration of the ‘stocked’ population in the vicinity of the refuge. This is confirmed by the change in the sign of the flux J , which becomes negative just after the reset, indicating that the net flux is inwards the refuge. Due to the fact that the source of the surrounding population is the flux of individuals from the refuge (see Eq. (4-57)), we can say that the environment spatial structure introduces a dependency on the history of the system. This is revealed by the non-monotonic response of J and N_{in} in Fig. 4.18. Moreover, comparing the flux J with the

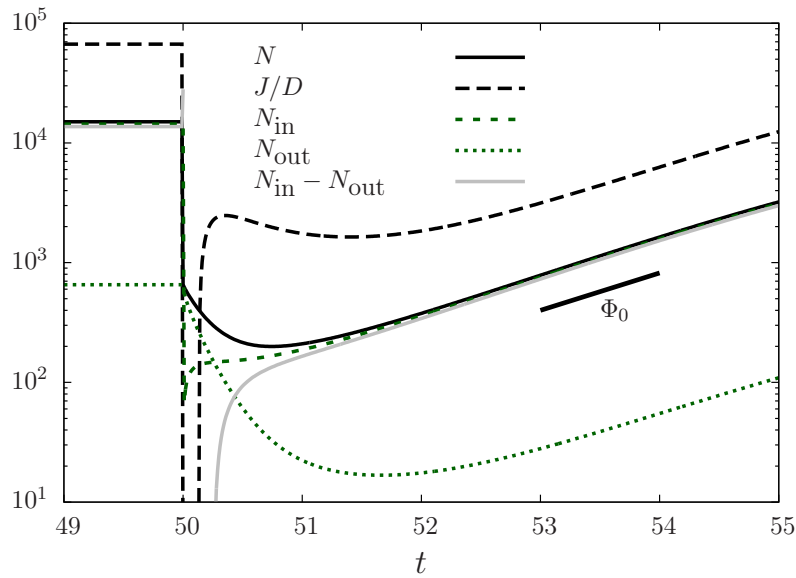


Figure 4.18: Temporal evolution of the total population N , the scaled flux J/D , the populations inside N_{in} and outside N_{out} the refuge (after resetting the population inside the refuge at $t = 50$) and their difference. In this case, the refuge size is $L = 2 > L_c$. After the transient, the population achieves the recovery state, growing with rate Φ_0 .

population difference $N_{\text{in}} - N_{\text{out}}$, it is clear that the simplification of Eq. (4-50) to a two-population model [24], defining $J \propto (N_{\text{in}} - N_{\text{out}})$ will not reproduce the observed behavior.

5 Metapopulation dynamics

Habitat fragmentation is commonly observed in nature associated with heterogeneity in the distribution of resources, e.g., water, food, shelter sites, physical factors such as light, temperature, moisture, and any feature able to affect the growth rate of the population of a given species [24]. A fragmented population made of subpopulations receives in the literature the suitable name of *metapopulation* [23, 24, 111]. These fragments, also known as patches, are not completely isolated as they are coupled, for instance, due to movements of individuals in space. For modeling purposes, as a first step one can adopt a single patch viewpoint, taking into account the impact of the surrounding population in an effective manner [33, 44, 47, 112]. As a further step beyond the single patch level, one can resort to a spatially explicit model. From this perspective, deterministic and stochastic theoretical models have been developed to obtain the macroscopic behavior of the whole population [11, 23, 113–116]. One of the main results is the detection of critical thresholds that delimit the conditions for the sustainability of the population, which occurs for a suitable combination of diverse factors, related to quality and spatial structure of the habitat, migration strategies and extinction rates. Here, we address related fundamental questions in metapopulation theory proposing a model that includes a general dispersion process, incorporating random and selective dispersal strategies. Additionally, we investigate the model dynamics on top of a complex ecological landscape whose spatial structure can be tuned, ranging from spread to aggregated patches [36].

Let us start from the local dynamics perspective. We assume that the rules that govern the dynamics of each patch can be modelled by the canonical model [33, 44, 48, 49]:

$$\dot{\rho}_i = [a_i + \sigma_\eta \bullet \eta_i(t)]\rho_i - b\rho_i^2 + \sigma_\xi \sqrt{\rho_i} \circ \xi_i(t), \quad (5-1)$$

where σ_η and σ_ξ are positive parameters, and η_i and ξ_i are assumed to be mutually independent zero mean and unit variance Gaussian white noises. Moreover each patch i can either be favorable if it induces positive growth at low densities (i.e., $a_i = A_i^+ > 0$) and unfavorable if it is adverse to support life (i.e., $a_i = A_i^- < 0$).

Now, introducing spatial coupling from migrations from one patch to another, the full model can be expressed by

$$\dot{\rho}_i = a_i \rho_i - b \rho_i^2 + D \Gamma_i[\rho] + \sigma_\eta \rho_i \bullet \eta_i(t) + \sigma_\xi \sqrt{\rho_i} \circ \xi_i(t), \quad (5-2)$$

where the additional term $D \Gamma_i[\rho]$, with $D > 0$, arises from the net flux towards patch i . It is the nonlocal term that couples the set of stochastic differential equations (5-1). We model the populational exchange between patches based on two behavioral strategies: one where the individuals spread in space diffusively, driven by density differences, and another where individuals transit selectively, mainly driven by patch-quality differences. The precise form of these exchanges will be presented in Sec. 5.1.

Finally, we construct a complex arrangement of favorable and unfavorable patches, that will be defined in Sec. 5.2. For the sake of simplicity, we consider a binary landscape, where sites can be in any of two states, $A_i^+ = -A_i^- = A > 0$, as assumed in previous studies [110, 117]. A typical configuration of the model system in a square lattice is illustrated in Fig. 5.1.

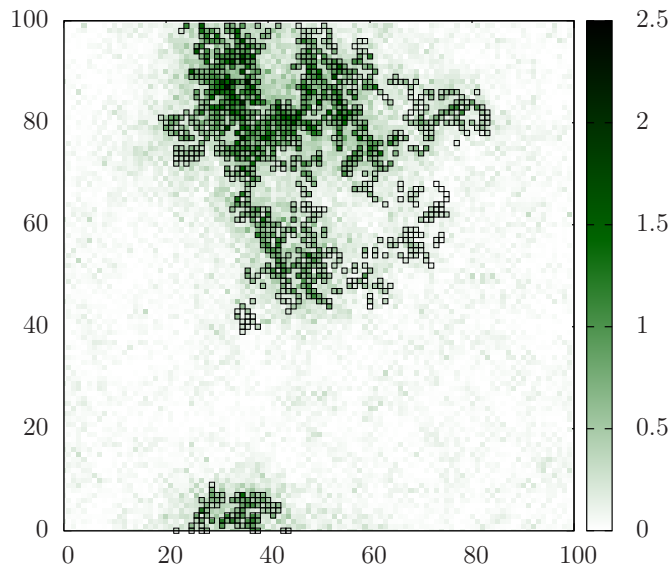


Figure 5.1: Ecological landscape and population distribution in a square lattice of linear size $L = 100$. Each lattice cell represents a patch. The landscape is defined by the configuration of favorable (positive growth rate) and unfavorable (negative growth rate) patches. A favorable patch is denoted by a black open square. The population density (number of individuals per unit area) is represented by shades of green.

5.1

Dispersal guided by habitat information

In order to define the coupling scheme let us state some considerations. First, let us assume that spatial spread is conservative, preserving the number of individuals during travels, and also that it is nonlocal, in the sense that individuals can travel long distances over the landscape, for example like butterflies and birds [11, 118].

Furthermore, it is reasonable to assume that active individuals like butterflies, birds and also terrestrial animals use their perception and memory to increase the efficiency in the search for viable habitats. Spatial knowledge can be acquired, for instance, by a direct visualization, previous visit or by the perception of the collective dynamics. The spatial information stored by the individuals can yield optimized routes between favorable regions. In fact, there is a relation between spatial memory and migration strategy [119]. We introduce this trait by allowing individuals to have access to information about the spatial distribution of patch quality. This will originate selective routes towards favorable patches and some directions will be preferred. Otherwise, if individuals do not have any information about the ecological landscape, or if they do not have memory, uncorrelated trajectories (random movements) can emerge. In fact, this has been the focus of works on animal foraging, where optimal efficiency in resource search occurs without previous knowledge of food distribution [120]. This type of behavior has isotropy as a main trait, indicating directional indifference.

We contemplate both scenarios by modeling spread through a diffusive component together with a contribution of direct routes connecting favorable patches, governed by quality differences. The relative contribution of both mechanisms is regulated by parameter δ , with $0 \leq \delta \leq 1$ tuning from the ecologically driven ($\delta = 0$) to the purely diffusive ($\delta = 1$) cases. Moreover, we assume that coupling is weighted by a factor $\gamma(d_{ij})$ that decays with the distance d_{ij} [121] between patches i and j , as will be defined below. Then, the flux J_{ij} from patch i to j is given by

$$J_{ij} = [\delta + (1 - \delta)\alpha_{ij}] \gamma(d_{ij}) \rho_i \geq 0, \quad (5-3)$$

where $\alpha_{ij} \equiv (a_j - a_i)/(4A) + 1/2$. Hence, the total flux is

$$\begin{aligned} \Gamma_i[\rho] &= \sum_{j \neq i} (J_{ji} - J_{ij}) \\ &= \sum_j \gamma(d_{ij}) [\delta(\rho_j - \rho_i) + (1 - \delta)(\alpha_{ji}\rho_j - \alpha_{ij}\rho_i)]. \end{aligned} \quad (5-4)$$

The total density is conserved by the exchanges described by Eq. (5-4), as can be seen by summing over i . It indicates that individuals tend to move towards patches with fewer individuals and better quality. For $\delta = 1$, Eq. (5-4) represents a generalization of the Fick's law for nonlocal dispersal driven by density gradients. For $\delta = 0$, with our definition of α_{ij} , and binary patch growth rate, the possible values of $\alpha_{ji}\rho - \alpha_{ij}\rho$ are

$j \backslash i$	A	$-A$
A	$(\rho_j - \rho_i)/2$	ρ_j
$-A$	$-\rho_i$	$(\rho_j - \rho_i)/2$

This means that, when the quality of two patches is different, the flux occurs in the direction of the higher quality, weighted by the out-flowing population density (lowest quality patch). Only when the quality is the same, diffusive exchange can occur, to allow a network of favorable patches.

Concerning the factor that takes into account the distance between patches, there is empirical evidence [11, 53] that the frequency of occurrence of flights between patches decays with the distance, which is reasonable due to the increase of energetic cost. Although diverse decay laws are possible, we will assume exponential decay of the weight γ with the traveled distance ℓ , as observed for some kinds of butterflies [11, 53, 54], that is

$$\gamma(\ell) = \mathcal{N}^{-1} \exp(-\ell/\ell_c), \quad (5-5)$$

where ℓ_c is a characteristic length (the average traveled distance) and the normalization constant \mathcal{N} is such that the sum of the contributions of all patches equals one. Operationally, we will truncate the exponential at $\ell \simeq 8\ell_c \ll L$, where L is the linear characteristic size of the landscape.

5.2

Complex landscape

In nature, the arrangement of the ecological landscape is built by many distinct processes, occurring in many time scales, creating complex spatiotemporal structures. Then, beyond the inclusion of the environmental noise η , it is also important to take into account the spatial organization of patches [11, 113, 122, 123].

Heterogeneity and patchiness are adequate to capture the complexity of diverse ecological systems [124–128]. Here we propose to use as complex ecological landscape a *Lévy dust* [120] distribution of favorable patches on a square domain of size $L \times L$ patches, with periodic boundary conditions. Over a background of adverse patches ($a_i = -A$), we construct a Lévy dust of

favorable patches ($a_i = A$) given by the sites visited by a Lévy random walk with step lengths ℓ drawn from the probability density function

$$p(\ell) \propto 1/\ell^\mu, \quad (5-6)$$

with $1 \leq \ell \leq L$. This protocol has been used in the study of different problems [120, 125, 126], but we apply it here in the study of metapopulation dynamics. It allows to mimic a general class of realistic conditions [124, 126–128] and to tune different habitat landscapes through parameter μ , from widely spread (for $\mu = 0$) to compactly aggregated in a few clusters separated by large empty spaces (for $\mu = 3$), as illustrated in Fig. 5.2. Moreover it is relevant to mention that the produced landscape pattern can be related to a fractal dimension, $d_f = \mu - 1$ (for $1 < \beta < 3$) [120].

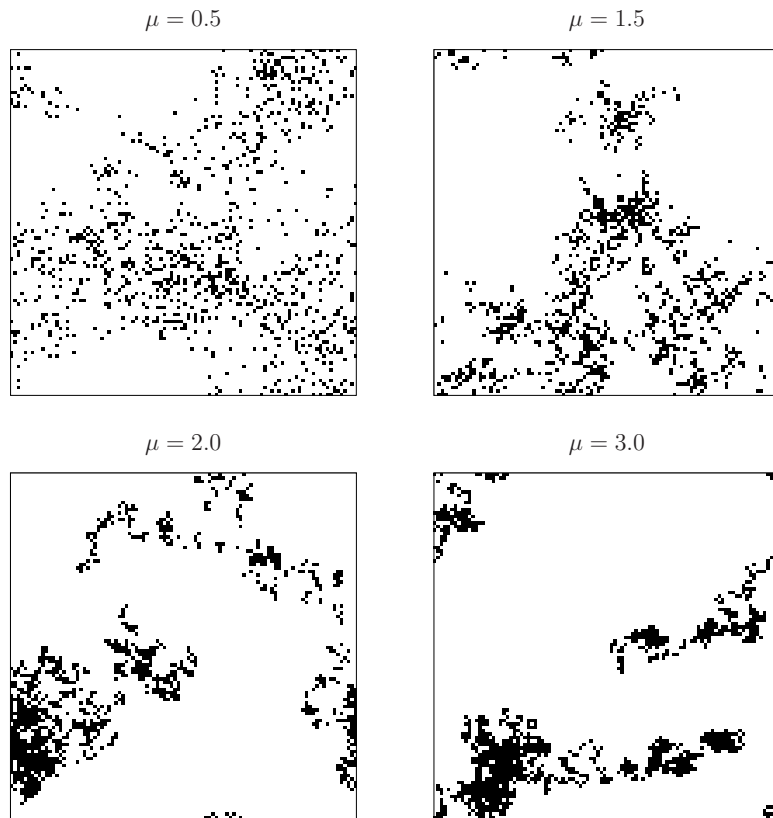


Figure 5.2: Ecological landscape for different values of the exponent μ that characterizes the distribution of Lévy jumps given by Eq. (5-6), used to build the configuration of favorable patches in a square domain with $L = 100$. Black cells indicate positive growth rate A (favorable patches) and white cells negative growth $-A$. In all cases the density of favorable patches is $h = 0.1$.

We quantify the change in the spatial structure by computing the probability distribution of the distance d between favorable patches $P_\mu(d)$ (see Fig. 5.3). For the density $h = 0.1$ used in the figure, when $\mu \lesssim 1$, patches are typically far from each other. For high values ($\mu \gtrsim 3$), the generating

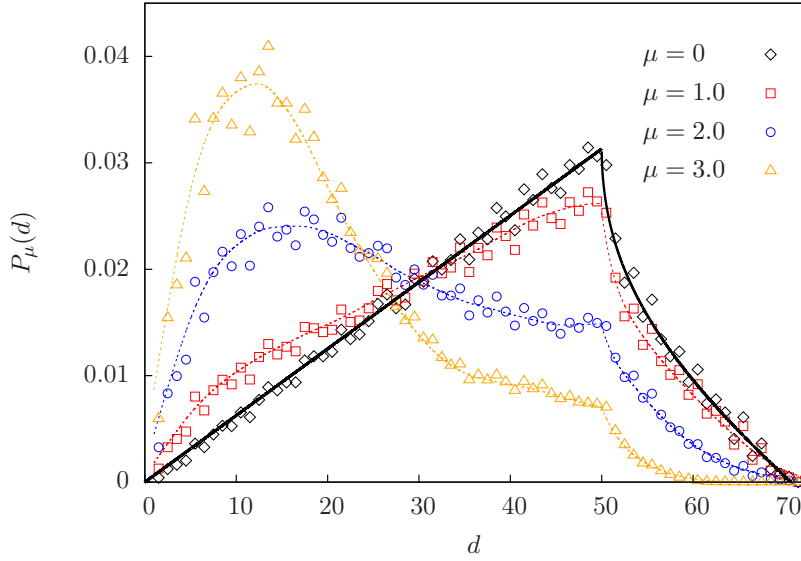


Figure 5.3: Probability distribution of the distance between favorable patches for different values of exponent μ in Eq. (5-6), for density $h = 0.1$ and lattice size $L = 100$ (200 configurations were used). Fluctuations are due to the discrete nature of the possible distances in the lattice. The dotted lines are a guide to the eye. The solid line represents the probability distribution for the distance between uniformly distributed random points in continuous space, drawn for comparison: $P(d) = 2\pi hd$ if $d < L/2$, $P(d) = 2\pi hd(1 - 4\arccos(L/[2d]))$, otherwise.

walk approaches the standard random walk, creating a much more clustered structure, evidenced by the peak at short distances. However the shape of $P_\mu(d)$ changes with h . When the patch density h is high, the shape of $P_\mu(d)$ resembles that of the uniform arrangement even for large μ , while at low densities $P_\mu(d)$ presents a peak at small d since the resulting configuration of patches is very localized even for small μ , as will be discussed in Sec. 5.4.3. Furthermore, $P_\mu(d)$ is also sensitive to L , but we kept L fixed ($L = 100$), even if some properties may have not attained the large size limit, as far as μ and h allow to scan many qualitatively different possibilities of landscape structure.

5.2.0.0

General considerations about the model

The set of parameters $\{D, \delta, \ell_c\}$ regulate the nonlocal dynamics. While D is the strength of the nonlocal coupling, δ controls the balance between diffusion and directed migration, and ℓ_c defines the coupling range. The ecological landscape is characterized by h and μ that set the density and the degree of clusterization, respectively.

In the results presented in the following sections, we will restrict

the analysis to a region of parameter space relevant to discuss the main phenomenology of the model. Thus, we will set $A = b = 1$ in all cases. We will also consider $L = 100$ and typically $h = 0.1$. Concerning the noise parameters, we set $\sigma_\eta = \sigma_\xi = 0$ to analyze the deterministic case in Sec. 5.3 and turn noise on by setting $\sigma_\eta = \sigma_\xi = 1$ in Sec. 5.4. This choice is based on previous works [44, 49]. Indeed, population size can be subject to large fluctuations as demonstrated by experimental data [118].

We performed numerical simulations of Eq. (5-2) on top of different landscapes, by preparing the system in the stationary state of the deterministic and uncoupled case, i.e., $\rho_i(0) = \max\{a_i/b, 0\}$ for all i , plus a small noise. Integration of Eq. (5-2) was carried out with Euler-Maruyama scheme with a time step $\Delta t = 10^{-3}$. Stratonovich noise was implemented by performing a shift in the drift to obtain the corresponding equivalent Itô version [129] (for more details see Appendix E).

5.3 Deterministic dynamics

Before proceeding to study the full model, we consider the deterministic case. Locally, when stochastic contributions are neglected, the asymptotic value of the population size for each patch is $\rho_i = a_i/b$. Introducing nonlocal effects, the population size might change. If population exchanges between patches are guided solely by their quality ($\delta = 0$), then, the favorable-patch network will conserve the initial population size, so no interesting phenomena occur from the viewpoint of extinction. However, when $\delta > 0$, the diffusive behavior induces exploration of the neighborhood independently of habitat quality, which leads to the occupation of unfavorable regions making likely the death of individuals.

By numerical integration of Eq. (5-2) we obtain the time evolution of the total population density $n(t) = \sum_{i=1}^{L^2} \rho_i(t)$. In Fig. 5.4 we show the outcomes for fixed values of the model parameters and different initial conditions (different landscapes). While some of the realizations lead to exponential decay of the population other ones attain finite values at long times. Several different non null steady states can be attained. Notice however, that the steady values of different realizations are all below that of the uncoupled case, $hL^2A/b = 1000$ for the parameters of the figure. Hence, diffusion favors the decrease of the total population density and the occurrence of extinctions, as expected.

In order to investigate how the fraction of survivals changes with the topology, we plot in Fig. 5.5 the number of survivals per realization, f_s , as function of the landscape parameter μ , for several values of the coupling coefficient D . Besides the initial condition used throughout this section (see

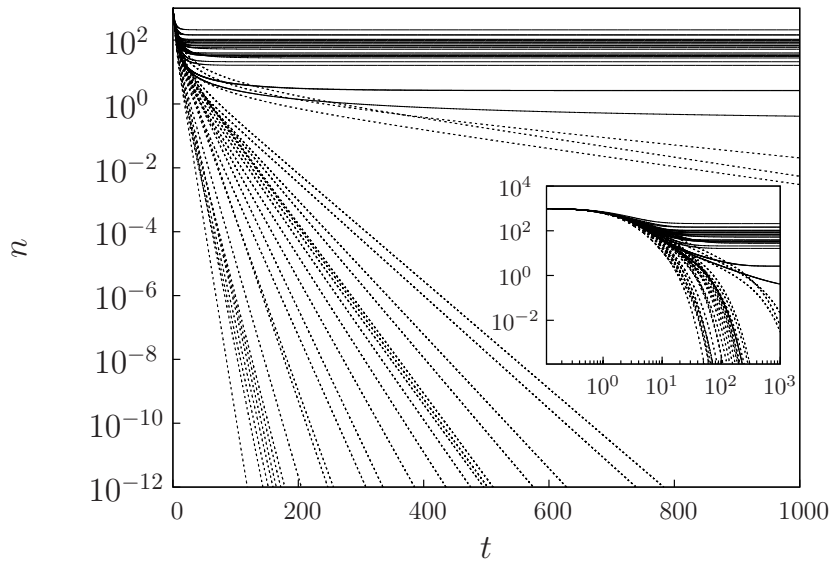


Figure 5.4: Deterministic ($\sigma_\eta = \sigma_\xi = 0$) time evolution of the total population density n in different initial landscapes, for $\delta = 1$, $h = 0.1$, $D = 10$, $\ell_c = 0.5$ and $\mu = 1.7$. This particular set of values of the parameters results in about half of 50 realizations leading to extinction. We use a dotted line to flag the ones that tend to extinction exponentially fast and a solid line for those that lead to population survival. Alternatively, the same data are represented as a log-log plot in the inset.

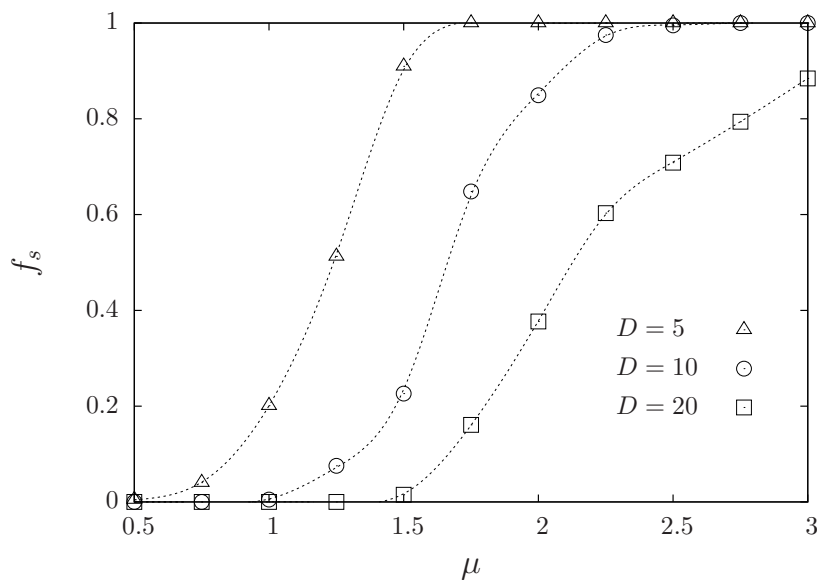


Figure 5.5: Fraction of surviving metapopulations f_s (over 100 realizations) in the deterministic case ($\sigma_\eta = \sigma_\xi = 0$) as a function of exponent μ in Eq. (5-6) that gives the degree of clusterization. The other parameters are $\delta = 1$, $h = 0.1$, $\ell_c = 0.5$, for the values of the coupling coefficient D indicated on the figure. In this and following figures, dotted lines are a guide to the eye.

Sec. 5.2), we observed that a perturbation of the null state also leads to the same results of Fig. 5.5. For given μ , increasing D favors the occurrence of extinctions as already commented above. For given D , below a threshold value of μ the population gets extincted in all the realizations, while above a second threshold it always survives (for the finite number of realizations done), between thresholds both states, the null and non null ones, are accessible. The number of non null stable states increases with μ .

Summing over all i the deterministic form of Eq. (5-2), one finds that the steady solution $\dot{n} = 0$ must satisfy $\sum_i a_i \rho_i = b \sum \rho_i^2$, which has infinite solutions between the fundamental null state and the uncoupled case solution (the only stable one for $D = 0$). The condition for stationarity of the total density depends only on the local parameters, since fluxes are only internal, however, the coupling and landscape can stabilize configurations other than the trivial ones. Furthermore, in the Appendix, we performed an approximate calculation to show that, for small D (recalling that $a_i = \pm A$), the null state is stable if

$$A - D(1 - \gamma_\mu) > 0, \quad (5-7)$$

where $0 \leq \gamma_\mu \leq 1$ is a factor that mirrors the topology, as defined in Eq. (D-3), varying from $\gamma_\mu = h$ for the uniform case $\mu = 0$ to $\gamma_\mu = 1$ in the limits of large μ or large h . Despite this approximate expression fails in providing accurate threshold values, it predicts that survival is facilitated by larger A and spoiled by increasing D . It also qualitatively predicts the impact of the topology, as far as it indicates that the destructive role of diffusion can be compensated by a large enough degree of clusterization of the resources given by large γ_μ .

5.4 Stochastic dynamics

First let us review some known results about the local (one site) dynamics, which is obtained in the limit $D \rightarrow 0$ of Eq. 5-2 (canonical model). In the deterministic case, the two-state habitat [110,117] leads to local extinction (if $a_i = -A$) or finite population A/b (if $a_i = +A$). The presence of stochastic contributions changes the stability of the patches. When $a_i = -A < 0$, the local extinction event predicted deterministically ($\dot{N}/N < 0$, when $t \rightarrow \infty$, see Sec. 2) is reinforced by noise. For $a_i = +A > 0$, the demographic (Itô) noise ξ (in the presence of the Stratonovich noise η) leads to extinction in a finite time. But this time diverges as $\sigma_\xi \rightarrow 0$ [44,47]. This divergence is due to the fact that when only the Stratonovich noise η is present, the null state is strictly not accessible, for any noise intensity, in the continuous model. That is, the external noise η reduces the most probable value of the population size,

that becomes very close to zero, but non null, when $\sigma_\eta > \sqrt{2A/b}$ [50].

The population stability can be quantified by the mean time to extinction \mathcal{T} averaged over realizations starting at $\rho(0)$. Recalling the results from Sec. 3.1, for Eq. (5-2) with $D = 0$, \mathcal{T} is given by [49],

$$\mathcal{T} = \int_0^{\rho(0)} \int_z^\infty \frac{\exp(\int_z^v \Psi(u) du)}{V(v)} dv dz, \quad (5-8)$$

where $\Psi(\rho) = 2M(\rho)/V(\rho)$, with $M(\rho) = a\rho - b\rho^2 + \sigma_\eta^2\rho/2$ and $V(\rho) = \sigma_\eta^2\rho^2 + \sigma_\xi^2\rho$. The results of Eq. (5-8) are in good accord with those from numerical simulations, as shown before Sec. 3.1.

5.4.1 Spatially extended system

In this section we investigate the effects introduced by patch coupling, i.e., when $D \neq 0$. Nonlocal contributions redistribute the individuals in space, driven by density and quality gradients. In Fig. 5.7 we show that $D \neq 0$ prevents the extinction events that occur when $D = 0$ (see Fig. 5.6). Therefore, in contrast to the deterministic case, now spatial coupling is constructive. On the other hand, noise has also a constructive role when $D \neq 0$, differently to the uncoupled case, not only preventing extinction but also contributing to the increase of the population (as in the case $D = 10$). In a Sec. 3.3, we already

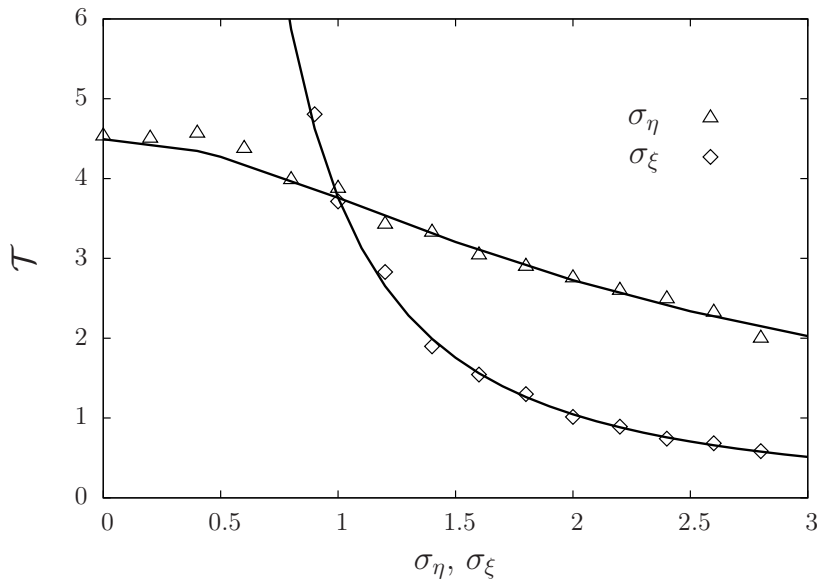


Figure 5.6: Single patch dynamics. Mean extinction \mathcal{T} time vs noise strengths σ_η (fixing $\sigma_\xi = 1$, triangles), that modulates the fluctuations in the growth rate, and σ_ξ (fixing $\sigma_\eta = 1$, diamonds), that modulates the demographic noise. Symbols correspond to numerical simulations averaged over 500 samples and the full lines to the theoretical prediction given by Eq. (5-8). The curve for variable σ_ξ diverges in the limit $\sigma_\xi \rightarrow 0$.

observed the constructive role in population growth of linearly multiplicative Stratonovich noise in contrast with the destructive behavior of its Itô version. Therefore, environmental noise and coupling have a positive feedback effect on population growth, as shown in Fig. 5.7.

We will compute the long-time total population density $n_\infty \equiv \lim_{t \rightarrow \infty} n(t)$, which is useful to be compared with the initial value $n_0 \equiv n(0) = hL^2\rho_0 = hL^2(A/b)$, that represents the asymptotic total density in the deterministic uncoupled case. Then we will measure the long-time relative total population density $E \equiv \langle n_\infty \rangle / n_0$, that represents a kind of efficiency, where the brackets indicate average over landscapes and noise realizations.

In the upper panel of Fig. 5.8 we plot the long-time relative value E as a function of D . We see that for very small values of D , the population is non null, although the final relative population density E is smaller than one. Moreover, for given D , the long-time relative value E is smaller when the diffusive component is absent ($\delta = 0$). In all cases, E first increases with D and even exceeds the value $E = 1$, indicating again that not only the noise has a constructive role in preventing extinction but also in promoting the increase of the initial total population. When the diffusive strategy is present ($\delta > 0$), the increase of E occurs up to an optimal value of the coupling D (with $E > 1$), above which the E decays. Hence, there is a nonlinear effect that does

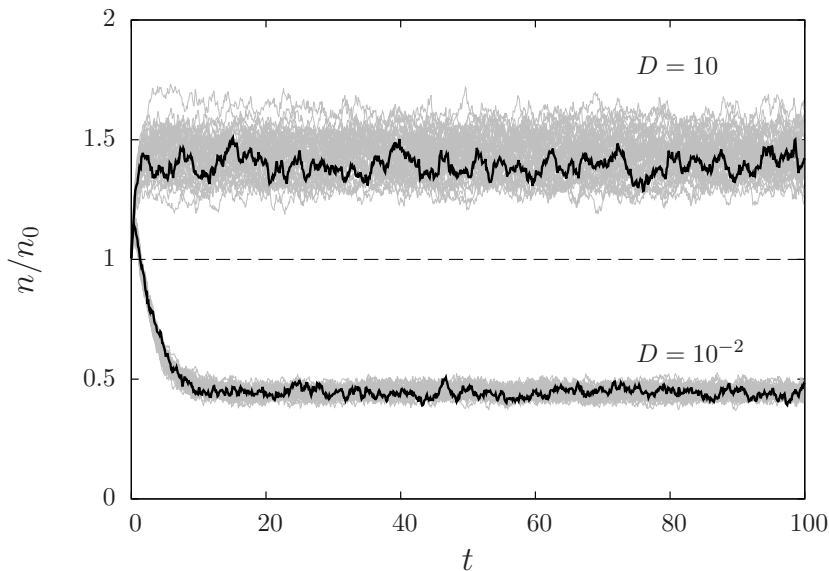


Figure 5.7: Temporal evolution of n/n_0 , the total population density relative to the initial value n_0 (set as the uncoupled deterministic value). For $\delta = 0.5$, $h = 0.1$, $\ell_c = 0.5$, $\mu = 2.0$, $\sigma_\eta = \sigma_\xi = 1$ and values of the coupling coefficient D indicated on the figure. We highlight a single realization (black full line) for each set of 50 realizations (gray lines). The dashed line at $n = n_0$ is plotted for comparison.

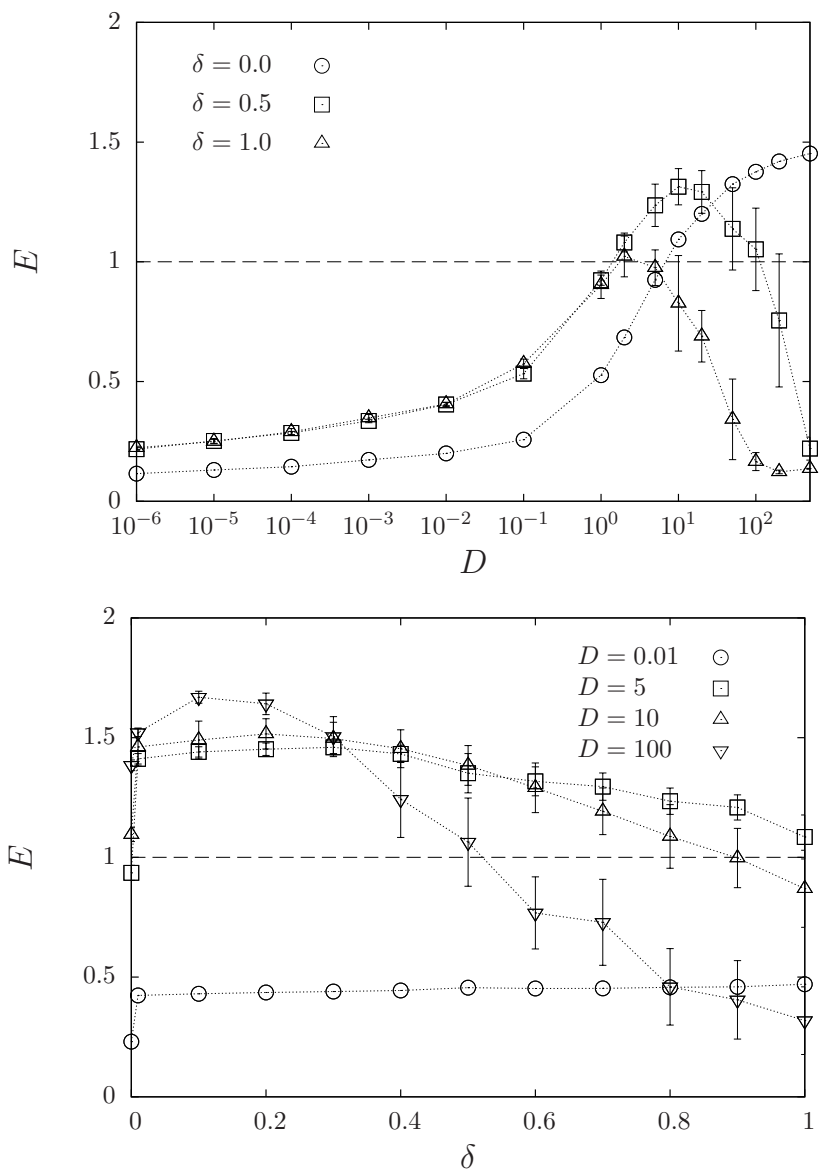


Figure 5.8: Long-time relative total population density, $E \equiv \langle n_\infty \rangle / n_0$, as a function of the coupling coefficient D , for different values of δ (upper panel) and E as a function of δ , for different values of D (lower panel). Recall that parameter δ regulates the balance between the diffusive ($\delta = 1$) and selective ($\delta = 0$) strategies. The other parameters are $h = 0.1$, $\ell_c = 0.5$, $\mu = 2.0$ and $\sigma_\eta = \sigma_\xi = 1$. The symbols represent the average over 20 samples and the vertical bars the standard error. The dashed line at $E = 1$ is plotted for comparison.

not reflect the linear combination in Eq. (5-3), as shown in the lower panel of Fig. 5.8. The diffusive component, despite being much less efficient, like in placing individuals in unfavorable regions, acts with greater connectivity. Then, for small D , the nonlocal contribution of the diffusive coupling is much higher than in the $\delta = 0$ case, leading to a higher population size. In fact, the abrupt transition in the connectivity of the spatial coupling is mirrored in the abrupt change suffered by E as δ becomes non null. Contrarily, for high values of D , $\delta = 0$ is more efficient due to high damage caused by an intense dispersal towards unfavorable regions, which in the case of Fig. 5.8 are the majority of the sites. All these observations highlight the importance of the diffusive strategy, that can become more efficient than the ecological pressure driven by the quality gradient.

5.4.2

Habitat topology and coupling range

The nonlocal contribution results from the combination of the spread strategies, interaction range and topology, characterized by δ , ℓ_c and μ , respectively. Fig. 5.9 shows the long-time relative population density E as function of μ with different values of ℓ_c for $\delta = 1$ and $\delta = 0$.

$E > 1$ means that the combination of habitat topology and spatial coupling range leads the population to profit from the environment fluctuations, increasing its size. The region $E > 1$ is bigger when individuals are selective with respect to their destinations ($\delta = 0$) and increases with ℓ_c . For the diffusive strategy ($\delta = 1$), $E > 1$ is attained only in a clustered habitat (large μ) together with short-range dispersal (small ℓ_c). We have already seen that in a sparse habitat, diffusion represents a waste, specially if the dispersal is long-range. Instead, when $\delta = 0$, the habitat does not need to be so clustered or the range so short for population growth. In this instance, the optimal combination occurs in a clustered habitat but with long-range coupling. Finally note that, as ℓ_c increases, E becomes independent of the topology.

5.4.3

Density of favorable patches

Another important issue is the influence of the density h of favorable patches in the dynamics. Until now, we have kept it constant to highlight the effects of the heterogeneity of the habitat and of the coupling schemes in the longtime behavior of the total population size. In terms of the protocol used to generate the ecological landscape, h not only changes the proportion of favorable patches but also reshapes the distribution of distances between

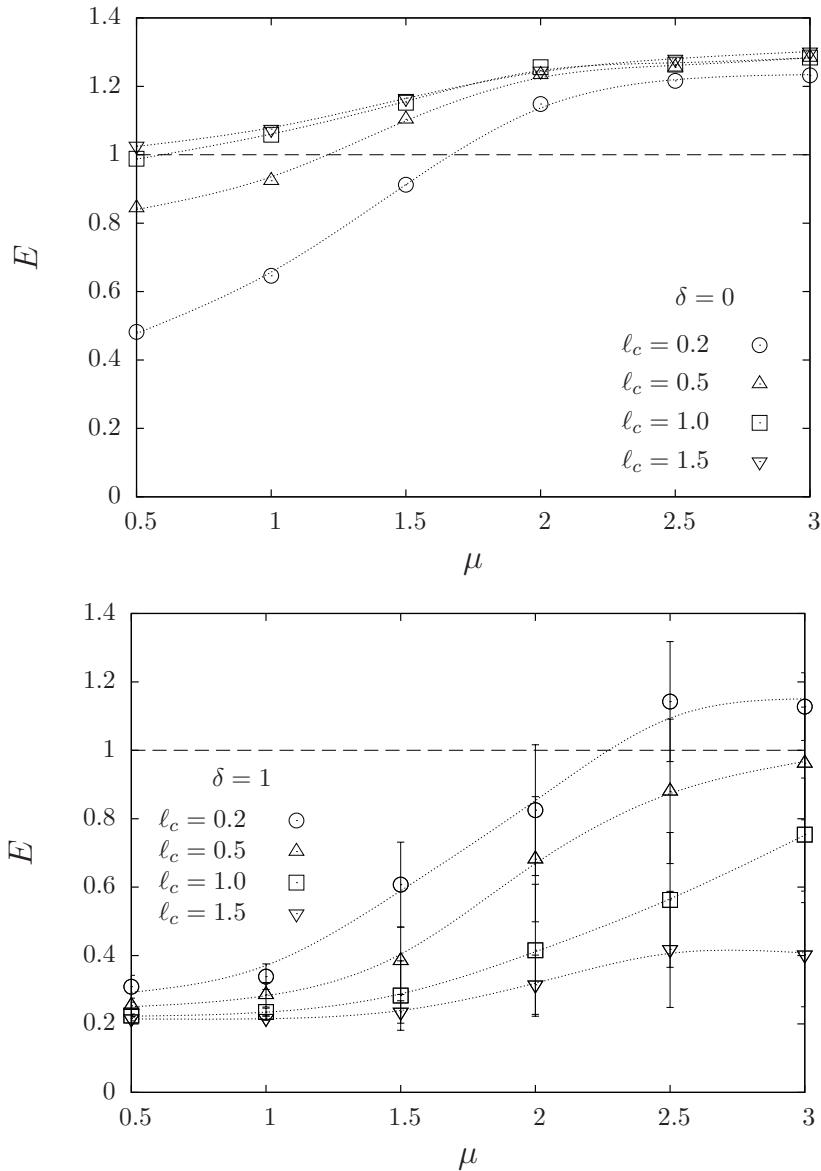


Figure 5.9: Long-time relative total population density, $E \equiv \langle n_\infty \rangle / n_0$, as a function of exponent μ in Eq. (5-6) for different values of the coupling range l_c , when $\delta = 0$ (selective strategy, upper panel) and $\delta = 1$ (diffusive strategy, lower panel), with $h = 0.1$, $D = 20$ and $\sigma_\eta = \sigma_\xi = 1$. The symbols represent the average over 20 samples and the vertical bars the standard error. The dashed line at $E = 1$ is plotted for comparison.

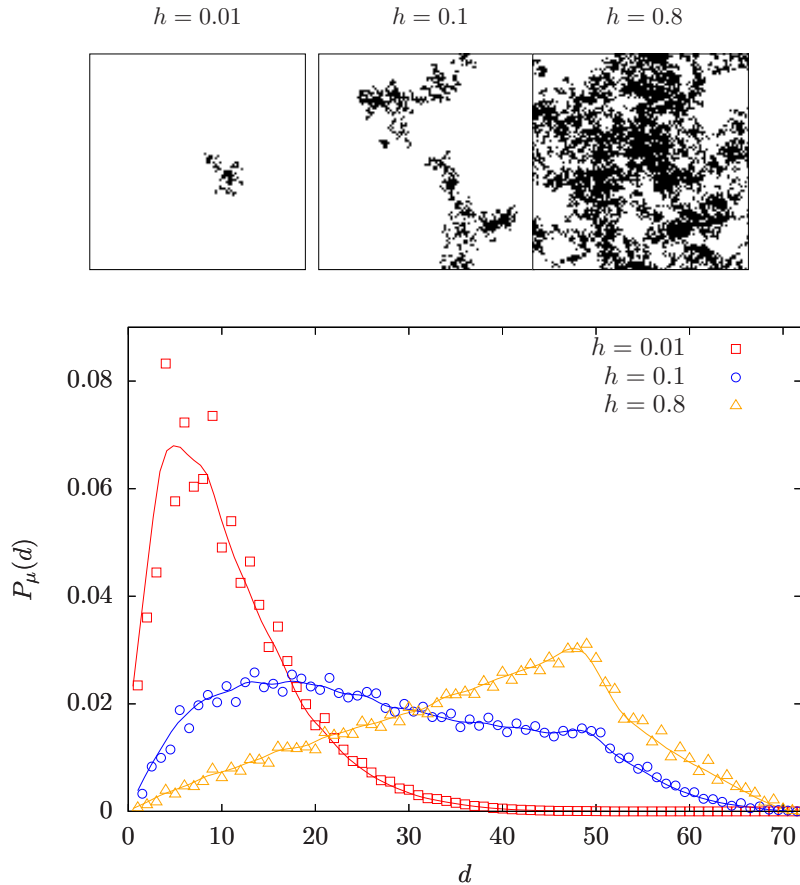


Figure 5.10: Ecological landscape (upper panels), with favorable patches in black, probability distribution of the distance between favorable patches, averaged over 100 landscapes (lower panel). Three different values of h , indicated on the figures, were considered. In all cases, Lévy exponent $\mu = 2$.

favorable patches. In Fig. 5.10 we show three different outcomes of the spatial structure and the corresponding distance distribution for a fixed value of $\mu = 2$. For low h , patches organize in a kind of archipelago structure, that is much smaller than the system size, and the distance resembles that obtained for large μ when $h = 0.1$. For high h , many points of the domain are visited creating a distance distribution that approaches the homogeneous form. For μ higher than the value of the figure, profiles very similar to those shown in Fig. 5.10 are obtained. Meanwhile, for small values of μ , the distribution is almost invariant with h , being very close to that of the uniform case. This is due to frequent flights with lengths of the order of system size. Concerning the factor γ_μ that reflects the topology, as defined in Eq. (D-3), it can be affected by h more through the amount of favorable patches n_v than by its indirect consequences on the spatial distribution P_μ .

In Fig. 5.11, we show E as a function of h for the case $\mu = 2$. By comparing the outcomes for different values of δ , we see the impact of distinct

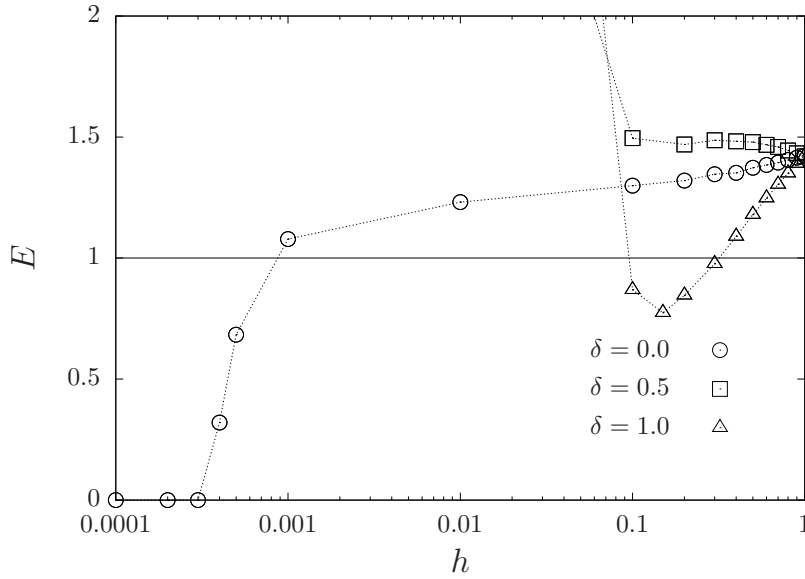


Figure 5.11: Long-time relative total population density, $E \equiv \langle n_\infty \rangle / n_0$ as a function of the favorable-patch density h . Different values of the strategy balance parameter δ were also considered as indicated on the figure. Recall that δ allows to tune from the purely diffusive strategy ($\delta = 1$) to the selective one ($\delta = 0$). The remaining parameters are $A = b = 1$, $D = 20$, $\ell_c = 0.5$, $\mu = 2.0$, $\sigma_\eta = \sigma_\xi = 1$ and $L = 100$. The symbols represent the average over 20 samples and the vertical bars the standard error. The horizontal line represents $E = 1$.

connectivities. In order to interpret this figure, recall that the initial population density n_0 is proportional to the number of favorable patches n_v , namely $n_0 = n_v A/b = hL^2$.

For $\delta = 1$, E presents a minimum value for $h \simeq 0.15$. Beyond this value, E grows with h attaining the value of the full favorable lattice. In the opposite limit of vanishing h (no favorable patches), E diverges as far as, according to the model, (intrinsically) favorable patches are not necessary to promote growth, due to the noisy growth rate. However, if noise is reduced, then the stochastic dynamics approaches the deterministic one, where the population will certainly go extinct.

Now, turning our attention to the $\delta = 0$ case, E is monotonically increasing with h , also attaining a limiting value when $h \rightarrow 1$. Differently from the diffusive case, there exists a critical value $h_c = 4 \times 10^{-4}$ ($n_v = 4$) for population survival.

For small h , it is curious that the role played by the connectivity, according to the model, makes the diffusive behavior more efficient, while selective moves are important at high values of h . In this case, when the system is approaching a fully favorable landscape, the long-time relative population density E tends to be the same for different values of δ . For intermediate values

of h , we see that the selective strategy overcomes the diffusive one (but never overcomes the combined scheme).

5.5

Extracting metapopulation heterogeneity from ensemble data

Metapopulation experimental data has different kind of limitations due to the large ecological time scale and technical difficulties [24]. This issue is reflected in low spatial statistics, such that at patch level no statistics can be performed. It is necessary, then, to study the ensemble statistics of the metapopulation [118, 130], with a mean-field perspective of the system. This procedure groups data from different patches, causing loss of information about the microscopic details of the environment, included in the ecological landscape [28]. Nevertheless, here we propose a methodology to restore the distribution of patch characteristics from the ensemble data, such as the variability of environmental conditions and migration rate among patches. We will focus our approach in the experimental data from a bird meta-population in United States [118]. The data provides the lifetime probability distribution of the ensemble set (all patches in the same sample). Our task will be to identify patch variability from the ensemble set statistics.

As it has been argued, along the previous chapters, the idea of providing a direct connection between patch and macroscopic levels has been a central issue in metapopulation dynamics studies [24]. However, a rigorous mathematical treatment for stochastic spatial explicit models face challenges to provide expressions for macroscopic quantities. Thus, analytical calculation relying on approximation methods such as moment closure or perturbative expansions around the mean-field solution [131]. In order to bypass this challenges, we will use an effective description to each patch dynamics to predict the ensemble data.

The approach discussed here can be applied in cases in which the metapopulation is in a quasi-steady state and patch temporal variability and migration fluxes are weakly correlated in space [11]. That is expected to be true for a large metapopulation and when migration is discrete with events fairly spaced [132]. Our proposal can be adjusted to a particular problem, including features as the Allee effect, cooperation, additional species [6, 109].

Deconvolution of the ensemble data

In the ensemble data, the observed lifetimes from each patch are mixed together in the same set. In order to obtain some preliminary properties of the

ensemble set, consider that for each patch i the set $\mathcal{E}_i = \{T_{i,1}, T_{i,2}, \dots\}$ contains the extinction times at the respective location. The metapopulation ensemble data set is defined by $\bar{\mathcal{E}} \equiv \mathcal{E}_0 \cup \mathcal{E}_1 \cup \dots \cup \mathcal{E}_N$. The size $|\mathcal{E}_i|$ of each set is the number of extinction events. Defining τ_i the mean extinction time in patch i , the average set size is $|\mathcal{E}_i| = T_o/\tau_i$, where T_o is the total observation time. Due to the fact that in practical situations $T_o \sim \tau_i$, a statistical analysis cannot be performed locally (for each patch).

Nevertheless, if patches are grouped by same characteristics, we can construct the set $\mathcal{E}(m)$ of patches with $m \in [m - \Delta m, m + \Delta m]$, which has size $|\mathcal{E}(m)| = \frac{p(m)}{\tau(m)} NT_o$, where $\tau(m)$ provides the mean extinction time as a function of the characteristic m . In the limit of large N , $NT_o \gg 1$, we can obtain a probability distribution of the lifetimes given m , $P(T|m)$.

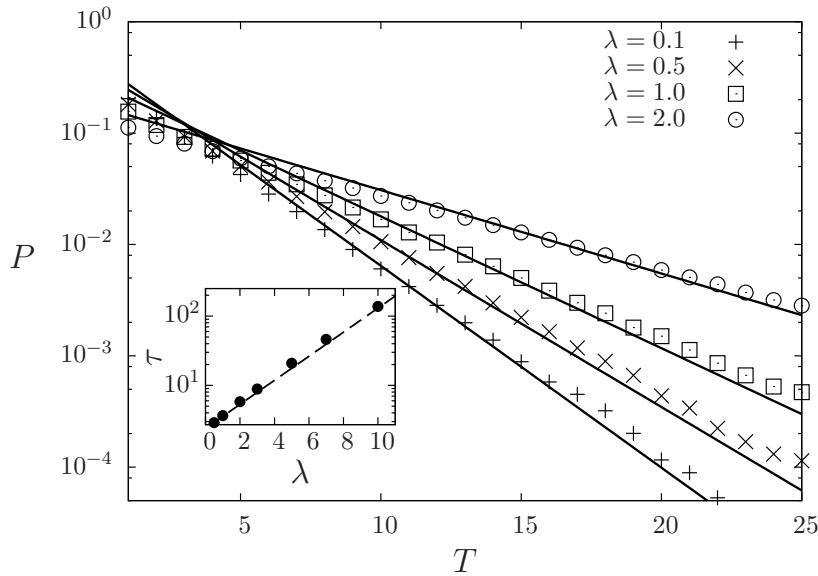


Figure 5.12: Probability distribution of patch lifetimes P for different average migration rates λ . Solid lines represent the approximation in Eq. (B-13), considering the migration term ζ as a Poisson shot noise with rate λ and fixed amplitude. In the inset, we show the behavior of τ as a function of λ . The dashed line represent an exponential fit, $\tau(\lambda) = 2.39 \exp(0.4\lambda)$.

By performing an ensemble average we can obtain the probability distribution of lifetime for the metapopulation. Explicitly, the ensemble average is given by

$$\mathcal{P}(T) \equiv \frac{1}{\sum_i w_i} \sum_i w_i P_i(T).$$

where $w_i \sim 1/\tau_i$. In the limit where N is large, we can rewrite the above average in the characteristic space. Assuming that a continuous probability

distribution $p(m)$ exists for the set $m = \{m_1, m_2, \dots\} \in \Omega$, then

$$\mathcal{P}(T) \propto \int_{\Omega} \frac{p(m)}{\tau(m)} P(T|m) dm. \quad (5-9)$$

The mixing of probability distributions can yield different outcomes depending on the structural heterogeneity p and population dynamics through $\tau(m)$.

The particular form for the local lifetime probability distribution arises from patch characteristics, such as amount of resources, quality of environment conditions and the intensity of the migration between neighboring patches. In order to provide a link between the probability distribution and patch characteristic we recall the effective model described in Eq. (3-11),

$$\dot{\rho}(t) = f(\rho) + \eta(t) \bullet \rho(t) + \xi(t) \circ \sqrt{\rho(t)} + \zeta(t), \quad (5-10)$$

where the effective noise ζ is a function of patch connectivity and dispersal rates, while the rest of the terms refer to the local properties. In Fig. 5.5 we illustrate this approach.

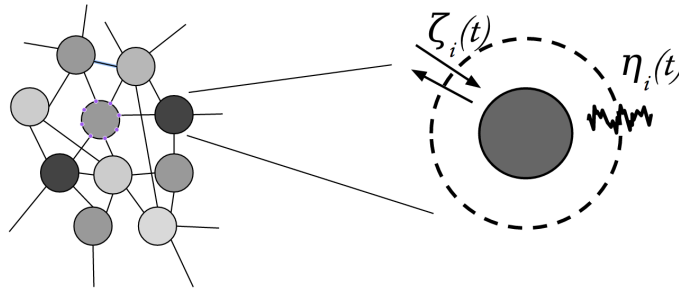


Figure 5.13: Effective modeling of patch dynamics. For each node in the metapopulation network, one can approximate the external fluxes and environment fluctuations by suitable stochastic variables.

In Fig. (5.12) we show different probability distributions for Eq. (3-11) with ζ being a Poisson shot noise with rate λ . For local effective models the probability distribution of lifetimes of a given patch has exponential tails. This occurs due to the formulation with Markov chains (see Sec. (3.1)) [130].

For our canonical choice (Eq. 3-28), the mean lifetime $\tau(\lambda)$ grows exponentially with λ for the Gaussian and Poisson shot noises [44, 49, 132, 133], and diverge as $1/\lambda$ at a maximum value for the constant migration rate (not shown). This result is confirmed by Eq. (3-12) and numerical simulations.

Numerical simulations of metapopulation, in the limit of weakly coupled patches (small D in Eq. (5-2)), show this same result but the migration rate

is interpreted in terms of patch connectivity C , $C_i \equiv \sum_j \gamma(|x_i - x_j|)$. In Fig. (5.14), we show that the mean lifetime increases exponentially as more connected the patch is.

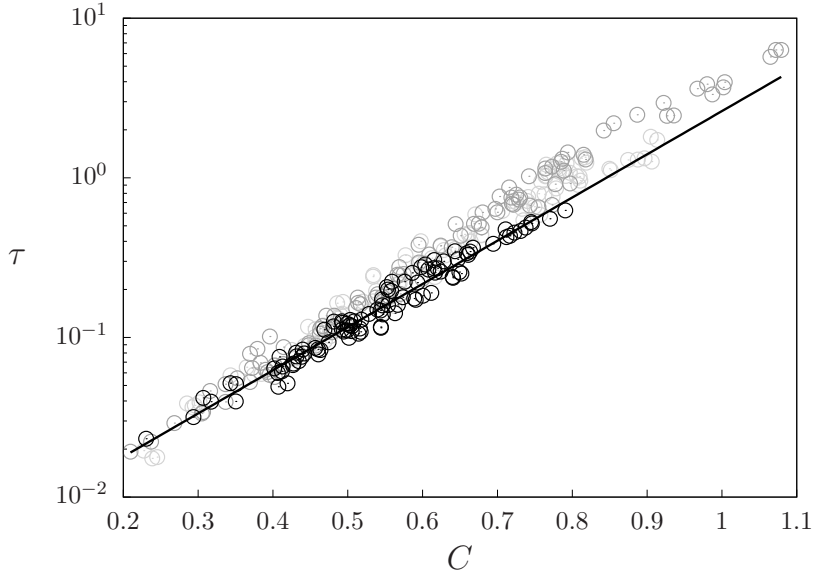


Figure 5.14: Mean lifetime τ vs. patch connectivity C for a random landscape ($\mu = 0$, see Sec. (5.2)) with $\rho = 1$. Black dots represent cases with $D = 0.01$ and gray dots $D = 1$.

Due to this evidence, we proceed assuming that the local extinction probability follows an exponential distribution with mean extinction time $\tau(m)$, given by a particular mathematical model, such as Eq. (5-10). In this case, Eq. (5-9) becomes

$$\mathcal{P}(T) \propto \int_{\Omega} \frac{p(m)}{\tau^2(m)} e^{-T/\tau(m)} dm. \quad (5-11)$$

After performing a change of variable, $s(m) = 1/\tau(m)$, Eq. (5-11) becomes

$$\mathcal{P}(T) \propto \int_{s(0)}^{s(\infty)} p(m(s)) s^2 m'(s) e^{-Ts} ds. \quad (5-12)$$

Now, assuming that the particular patch features considered m are directly related to population persistence, such as migration and connectivity, then we can approximate $s(\infty) = 0$ and $s(0) = \infty$. That is, with high migration, patch lifetime diverges, while for low migration, it goes to zero.

Thus,

$$\mathcal{P}(T) \propto - \int_0^\infty p(m(s)) s^2 m'(s) e^{-Ts} ds \quad (5-13)$$

$$\mathcal{P}(T) \propto -L[p(m(s)) s^2 m'(s)]. \quad (5-14)$$

where L refers to the Laplace transform. Finally,

$$p(m) \propto - \left. \frac{L^{-1}[\mathcal{P}(T)]}{m'(s)s^2} \right|_{s=1/\tau(m)} = \left(\frac{d\tau(m)}{dm} \right) L^{-1}[\mathcal{P}(T)]_{s=1/\tau(m)}, \quad (5-15)$$

$$p(m) \propto h(m) L^{-1}[\mathcal{P}(T)]_{s=1/\tau(m)} \quad (5-16)$$

where $h(m) \equiv \frac{d\tau(m)}{dm}$.

Eq. (5-15) provides the *indirect* transformation, that gives the metapopulation heterogeneity $p(m)$ from the ensemble probability distribution \mathcal{P} . Keep in mind that the Laplace transform connects $T \leftrightarrow s$, so after the transformation we set $s = 1/\tau(m)$.

Applications

Now we focus on the variation of a single patch feature, keeping the remaining ones fixed. Also, let us consider that the dynamical model provides $\tau(m)$ such that it covers the integral range in Eq. (5-13), as imposed for the derivation of Eq. (5-15). That is, $\tau(0) = 0$ and $\tau(\infty) = \infty$. Motivated by the previous observation in Figs. 5.12 and 5.14, a possible choice would be $\tau(m) = e^{cm} - 1$. But also a power-law form for τ would satisfy the necessary requirements. Now assuming particular ensemble lifetime probability distribution we shall use Eq. (5-15) to access information about the metapopulation migration network.

Let us consider some particular cases. From Eq. (5-15), assuming that \mathcal{P} is exponential, automatically $p(m) \sim \delta(m - m^*)$. This can also be seen from Eq. (5-11). If \mathcal{P} is for instance proportional to $e^{-T/\tau_c}/T$, p will have a cutoff in values of m . Below we list some relevant cases.

$\mathcal{P}(T)$	$p(m)$
e^{-T/τ_c}	$h(m)\delta(1/\tau(m) - 1/\tau_c)$
$e^{-T/\tau_c}/T$	$h(m)\Theta(\Delta m)$ where $\Delta m \equiv 1/\tau(m) - 1/\tau_c$
$e^{-T/\tau_c}/(\tau_0 + T)^\beta$	$h(m)\Theta(\Delta m)\Delta m^{\beta-1}e^{-\Delta m\tau_0}$

The last case in the above table corresponds to the one observed in experimental data for the North American Breeding Bird Survey with $\beta = 1.6$ and $\tau_c = 14$ (years) [118]. In Fig. 5.5, we show the probability distributions for p as a function of the exponent β . This result relates a macroscopic property

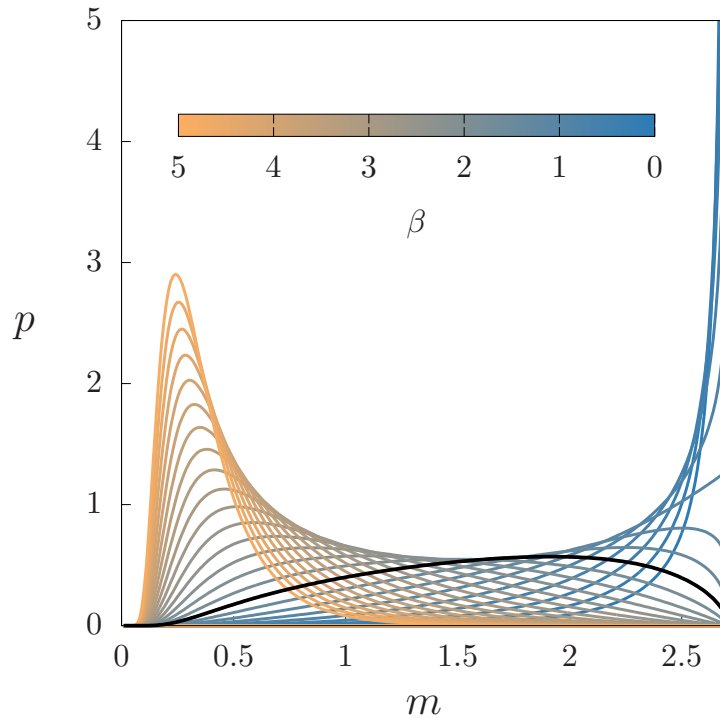


Figure 5.15: Probability distribution p for a given patch characteristic m . The distribution are obtained applying Eq. (5-15) with $\tau(m) = e^{cm} - 1$. In this case p can be interpreted as the distribution of migration rates m among the metapopulation patch set. Solid line indicate the case $\beta = 1.6$.

β to the metapopulation heterogeneity p . It has been a matter of debate the origins of the power-law observed in the ensemble lifetime probability distribution [118, 134]. In one hand, it is attractive to argue that power-laws emerge from near-criticality phenomena, that produce long-range interactions. However, here we see that spatial variability can also be the cause for this power-laws. For instance, small exponents in tails of the ensemble lifetime probability distribution \mathcal{P} indicate that the majority of patches have its characteristic concentrated that the maximum allowed values of m . For higher values of the exponent patches characteristic shifts towards the minimum value. For values in between these limits, the patch characteristics are roughly homogeneous distributed between the allowed interval.

Eq. (5-15) provides interesting hints about the heterogeneity. However, a systematic validation of Eq. (5-15), using metapopulation models such as the one discussed in the previous section still lacking to proof the range of validity of the approach.

6

Final remarks on population dynamics

In the present study, the role of environment heterogeneity in the collective dynamics of living beings was investigated.

In Chapter 2, we introduced the mathematical framework used to describe the system. We also defined important concepts about the environment modeling and a proper definition of the population persistence is presented.

In Chapter 3, we started by considering an homogeneous environment and analyzed how stochasticity can trigger a self-organization process, affecting the spatial distribution of the population. In this case, nonlocal competitive interactions are the main mechanism for pattern formation, while environment fluctuations affect different features of this phenomenon. Using analytical and numerical techniques, we obtained the transition from homogeneous to patterned population distribution. We showed that external fluctuations can shift the transition point (a noise induced shift transition [108]). Besides that, there is an optimal intensity of the fluctuations that tune patterns in space-time, generating large temporal correlation.

In Chapter 4, we discussed the case in which the environment landscape is composed by a single habitat domain. In Sec. 4.1, we showed that the ecological statement that population survives for habitats larger than a minimum values L_c is not valid in general. When nonlinearities are present, population may survive for $L > L_c$, $L < L_c$, or even for any $L > 0$, depending on the model parameters. In Sec. 4.2, we presented a brief discussion on population conservation when higher order interactions are present. In Sec. 4.3, introducing habitat seasonality, we obtained significant corrections to the critical habitat size L_c . Particularly, we found that L_c decreases with habitat oscillation period, that is, slow environments (with same average conditions) make population perform better.

In Chapter 5, we developed a more sophisticated model, considering a complex environment structure and information based dispersal. Regarding habitat spatial structure, we showed, for instance, that population survives in fragmented environments that are clustered enough (high fractal dimension). About dispersal, we showed that random movement, up to a certain amount,

introduces a positive feedback in population size. Then, counter-intuitively, we see that population size becomes larger when individuals partially neglect habitat information, choosing to visit locations that do not have the best environment conditions, or even, where harmful factors are present. In Sec. 5.5, we present an approximation to connect theory and experimental data, bypassing difficult mathematical challenges. This way, we were able to show that intriguing power-laws in the metapopulation extinction times might not be exclusively due to near-criticality phenomena, but due to metapopulation heterogeneity.

In summary, recalling the general model (Eq. (2-3)), different cases were presented assuming different population dynamics \mathcal{L} and environment spatiotemporal structure M . For instance, in Chapter 4 environment is characterized by its spatial and temporal scales, $M = (L, \tau)$, where L is the size and τ the period of oscillation of the habitat. In Chapter 5, the landscape is determined by $M = (\mu, h)$, where μ represents the degree of clusterization, while the parameter h represent the fraction of space considered viable for population development. In all these cases, we found that there is a critical line M_c in the environment parameter space that separates the extinction and survival phases. The exact determination of M_c was one of the main objectives of previous chapters. The results explore fundamental features, relevant to other disciplines, such as theoretical ecology and, in practical situations, it might guide management and conservation protocols of natural habitats.

Finally, I would like to acknowledge the financial support of the FAPERJ and CAPES agencies and PUC-Rio Physics department, that enable this research.

A Master equation

In order to represent the reactions in Eq. (3-1), we write the master equation of the probability $P_N(t)$ of having N individuals at instant t ,

$$P_N(t + dt) = P_N(t) + \sum_n [W(n \rightarrow N)P_n(t) - W(N \rightarrow n)P_N(t)]dt, \quad (\text{A-1})$$

$$P_0(t + dt) = P_0(t) + \sum_n W(n \rightarrow 0)P_n(t)dt. \quad (\text{A-2})$$

From Eq. (3-1), we identify the rates, such that

$$W(n \rightarrow n + 1) = a_b n, \quad (\text{A-3})$$

$$W(n \rightarrow n - 1) = (a_d + b n)n. \quad (\text{A-4})$$

Then,

$$\begin{aligned} \partial_t P_n(t) &= W(n - 1 \rightarrow n)P_{n-1}(t) + W(n + 1 \rightarrow n)P_{n+1}(t) \\ &\quad - [W(n \rightarrow n - 1) + W(n \rightarrow n + 1)]P_n(t) \\ &= [a_b(n - 1)]P_{n-1}(t) + [(a_d + b(n + 1))(n + 1)]P_{n+1}(t) \\ &\quad - [(a_b + a_d + b n)n]P_n(t). \end{aligned}$$

Taking the continuous limit, using that $\partial_n f = [f(n + 1) - f(n - 1)]/2$ and that $\partial_{nn} f = [f(n + 1) + f(n - 1) - 2f(n)]$,

$$\partial_t P_n = \partial_n \left[-(a_b - a_d - b n)n P_n + \frac{1}{2} \partial_n (a_b + a_d + b n)n P_n \right], \quad (\text{A-5})$$

which recovers Eq. (3-4) in the form

$$\partial_t P(n, t) = -\partial_n [f(n)P(n, t)] + \frac{1}{2} \partial_n [g(n)P(n, t)]. \quad (\text{A-6})$$

For more details see Appendix B.

B Mean extinction time

Assuming that the system is Markovian, we can write the temporal evolution of the probability density distribution [135]

$$P(u, t + \tau) = \int_0^\infty W(u, t + \tau | u', t) P(u', t) du, \quad (\text{B-1})$$

with the population density $u \in [0, \infty]$ and $W(u, t + \tau | u', t)$ is the transition probabilities $(u', t) \rightarrow (u, t + \tau)$.

Through the characteristic function method, using the Fourier transform, we see that

$$\tilde{W}(q, t, \tau) \equiv \int_{-\infty}^\infty e^{iq(u-u')} W(u, t + \tau | u', t), \quad (\text{B-2})$$

$$= 1 + \sum_{n=0}^\infty \frac{(iq)^n}{n!} \langle (u - u')^n \rangle, \quad (\text{B-3})$$

thus,

$$W(u, t + \tau | u', t) = \int_{-\infty}^\infty e^{-iq(u-u')} \tilde{W}(q, t + \tau), \quad (\text{B-4})$$

$$= \left[1 + \sum_{n=0}^\infty \left(-\frac{\partial}{\partial u} \right)^n W_n \right] \delta(u - u'), \quad (\text{B-5})$$

where we define

$$W_n = \frac{\langle [u(t + \tau) - u(t)]^n \rangle |_{u(t)=u'}}{n!} = \frac{\omega_n \tau}{n!} + \mathcal{O}(\tau^2), \quad (\text{B-6})$$

where $\langle [u(t + \tau) - u(t)]^n \rangle$ are the jump moments [135] and ω_n the first term in the expansion of order τ . Finally, substituting (B-5) into (B-1), we obtain in the limit of $\tau \rightarrow 0$,

$$\partial_t P(u, t) = \sum_{n=0}^\infty \left(-\frac{\partial}{\partial u} \right)^n W_n(u, t, \tau) P(u, t). \quad (\text{B-7})$$

Pawula's theorem shows, that if fluctuations are Gaussian, we can truncate the sum in Eq. (B-7) at $n = 2$ [135]. This gives rise to the well-known Fokker-Planck equation, such as Eq. (3-8).

The presence of stochasticity brings uncertainty to population size allowing extinction. We proceed now to obtain the population mean lifetime

\mathcal{T} [44].

The total flow towards extinction in interval τ [135] is given by

$$\mathcal{P}(\tau|t) \equiv \int_0^\infty W(0, t + \tau|u', t) du'. \quad (\text{B-8})$$

Due to the properties of the fluctuations considered, the system is invariant over time inversion. Thus, for convenience, we use the reverse version of Eq. (B-5) for the temporal evolution of the probability distribution for W ,

$$W(u, t + \tau|u') = [W_1 \partial_u W(u, t|u') + W_2 \partial_{uu} W(u, t|u')] \delta(u - u') \quad (\text{B-9})$$

in the limit $\tau \rightarrow 0$,

$$\dot{W}(u|u', t) = [\bar{f}(u) \partial_u W(u, t|u') + \frac{1}{2} g^2(u) \partial_{uu} W(u, t|u')] \delta(u - u'), \quad (\text{B-10})$$

Integrating for all u' , we obtain

$$\dot{\mathcal{P}} = \bar{f}(u) \partial_u \mathcal{P} + \frac{1}{2} g^2(u) \partial_{uu} \mathcal{P}, \quad (\text{B-11})$$

integrating from $t = 0$ up to $t = \infty$ and noting that $\int_0^\infty \dot{\mathcal{P}} = \mathcal{P}(\infty) - \mathcal{P}(0) = -1$ and that $\mathcal{T} = -\int_0^\infty t \dot{\mathcal{P}} dt = \int_0^\infty \mathcal{P} dt$, we obtain

$$\bar{f}(u) \partial_u \mathcal{T} + g^2(u) \partial_{uu} \mathcal{T} = -1. \quad (\text{B-12})$$

Integrating in \mathcal{T} and fixing the initial population size $u(0)$, we arrive at

$$\mathcal{T} = \int_0^{u(0)} \int_z^\infty \frac{2 \exp(\int_z^v \Psi(u) du)}{g^2(v)} dv dz, \quad (\text{B-13})$$

with $\Psi(u) = 2\bar{f}(u)/g^2(u)$. [48, 49, 135].

C Time-dependent habitat

C.1 Population growth in heterogeneous static environment

Assuming that population density is low, such that we can neglect the second order term from the carrying capacity, the temporal evolution of the population spatial distribution in Fourier space, $\tilde{\rho}$, from Eq. (4-50), is given by

$$\partial_t \tilde{\rho}(k, t) = (-Dk^2 + a)\tilde{\rho}(k, t) + [\tilde{\psi} \star \tilde{\rho}](k), \quad (\text{C-1})$$

where the symbol \star denotes the convolution operation, i.e., $\tilde{\psi} \star \tilde{\rho} = \int \tilde{\psi}(k - k', t)\tilde{\rho}(k', t)dk'$. From the protocol definition in Sec. 4.3, we obtain $\tilde{\psi}(k, t) = -A \left[\delta(k) - 2 \frac{\sin(kL/2)}{k} \right]$, where we consider the static case, setting $\varphi(t) = 1$ for all t . The growth rate of the total population size is obtained by taking $k = 0$,

$$\partial_t \tilde{\rho}(0, t) = (a - A)\tilde{\rho}(0, t) + A \int_{-\infty}^{\infty} \frac{2 \sin(kL/2)}{k} \tilde{\rho}(k, t) dk. \quad (\text{C-2})$$

In Sec. 4.3.3, the analysis of the spatial dynamics has shown, among other results, that, when the population grows during the recovery time, the spatial distribution changes but preserving its shape (see Fig. 4.17). Therefore, we assume that $\rho(x, t) = N(t)\rho_s(x)$. Then, $\tilde{\rho}(k, t) = \tilde{\rho}(0, t)\tilde{\rho}_s(k)$, where we have arbitrarily set $\tilde{\rho}_s(0) = 1$. As a consequence, we can write Eq. (C-2) as $\partial_t \tilde{\rho}(0, t) = \Phi_0(L)\tilde{\rho}(0, t)$, with the intrinsic population growth rate being

$$\Phi_0(L) = a + A[S(L) - 1], \quad (\text{C-3})$$

where

$$S(L) \equiv \int_{-\infty}^{\infty} \frac{2\tilde{\rho}_s(k) \sin(kL/2)}{k} dk. \quad (\text{C-4})$$

First, we see that, independently of the shape of the distribution $\tilde{\rho}_s$, if $L \rightarrow 0$, then $S(L) \rightarrow 0$, and as a consequence $\Phi_0 \rightarrow a - A$. Second, in the limit of large refuge $L \rightarrow \infty$, we have $\tilde{\psi} \rightarrow \delta(k)$, then $S(L) = 1$, giving $\Phi_0 = a$.

We proceed obtaining an approximate expression for the distribution $\rho_s(x)$. We start by recalling the steady solution of Eq. (4-50), in the static case, for $L = L_c = L^*$ (see Eq. (4-52)):

$$\rho(x, t) = \begin{cases} c_1 \cos(\beta_+ x) & |x| \leq L_c/2, \\ c_2 e^{-\beta_- |x|} & |x| > L_c/2, \end{cases} \quad (\text{C-5})$$

where the parameters that regulate the spatial scale are $\beta_+ = \sqrt{a/D}$, $\beta_- = \sqrt{(A-a)/D}$ and the constants c_1 and c_2 are such that $\rho(x, t)$ is continuous and differentiable at $x = \pm L_c/2$. Eq. (C-5) can be used as a base to estimate the shape of the distribution in the recovery period, for other values of L . In order to do that, we keep the simple form of the critical solution but flexibilize the conditions at the boundary of the refuge, allowing discontinuity of the first derivative. This yields $c_1 = c_2 \exp(-L_c \beta_-/2) / \cos(\beta_+ L_c/2)$. Normalization of Eq. (C-5) provides the value of $c_2(L)$ (expression not shown). Then, the Fourier transform $\tilde{\rho}_k$ can be computed and substituted into Eq. (C-4), giving

$$S(L) = c_2(L) \exp(\beta_- L/2) \tan(\beta_+ L/2) / \beta_+. \quad (\text{C-6})$$

This expression is exact for L_c , where $\Phi_0(L_c) = 0$ and captures the main contributions for $L < L_c$, since the presence of higher modes in the limit of small L is filtered by the shape $\tilde{\psi}$. For $L > L_c$, the trigonometric solution loses its validity and the distribution tends to flatten. For this case, small values of k (long wavelenghts) have a significant impact on $S(L)$. In order to provide an analytical expression for small and large values of L , we propose the suitable ansatz

$$S(L) = 1 - \frac{1}{1 + \frac{A-a}{a}(L/L^*)^2}, \quad (\text{C-7})$$

therefore

$$\Phi_0(L) = a - \frac{A}{1 + \frac{A-a}{a}(L/L^*)^2}, \quad (\text{C-8})$$

where L^* is the critical refuge size in the static case. The expression in Eq. (C-8) recovers the known result for harsh conditions when $A \rightarrow \infty$, the asymptotic behavior for large L , and the condition $\Phi_0(L_c) = 0$. Comparison between Eq. (C-3) (assuming $S(L)$ as in Eq. (C-6)), our proposal Eq. (C-8) and numerical data is shown in Fig. 4.15.

C.2

Slow and fast limits with harsh conditions outside the refuge

In the limit of harsh conditions outside the refuge, the population density goes to zero at the refuge boundary, i.e., $\rho(|x| > L/2) = 0$. Under this boundary condition, it is straightforward to obtain the largest eigenvalue which determines the value of the growth rate Φ_0 [12, 101],

$$\Phi_0 = a - \frac{\pi^2 D}{L^2}. \quad (\text{C-9})$$

The condition $\Phi_0 = 0$ gives $L^* = \pi \sqrt{D/a}$.

Following the same procedure described in Sec. (4-56), in the fast limit, we assume that the growth rate is locally averaged, then

$$L_c(\lambda; \tau \ll \tau_S) = \pi \sqrt{\frac{D}{a - \lambda A}} = L^* \sqrt{\frac{a}{a - \lambda A}}. \quad (\text{C-10})$$

In the slow limit, we assume that population growth switches between $a - A < 0$, during the harmful action, and Φ_0 , during the recovery period. Then, $\langle \Phi \rangle = (a - A)\lambda + \left(a - \frac{\pi^2 D}{L^2}\right)(1 - \lambda)$. When $\langle \Phi \rangle = 0$, hence $L = L_c$, we find that

$$L_c(\lambda; \tau \gg \tau_S) = \pi \sqrt{\frac{D(1 - \lambda)}{a - \lambda A}} = L^* \sqrt{\frac{a(1 - \lambda)}{a - \lambda A}}. \quad (\text{C-11})$$

Therefore, the ratio between the critical refuge sizes in the slow and fast limits is

$$\frac{L_c(\lambda; \tau \ll \tau_S)}{L_c(\lambda; \tau \gg \tau_S)} = \frac{1}{\sqrt{1 - \lambda}}. \quad (\text{C-12})$$

This means that, even in this case, where we neglect the role of the surrounding population, the spatial dynamics distinguishes slow from fast environment perturbations. Nevertheless, the ratio is only $\frac{L_c(\lambda; \tau \ll \tau_S)}{L_c(\lambda; \tau \gg \tau_S)} = 1.091$, for $\lambda = a/A$. Therefore, there is a relative difference of about 9% in refuge critical size due to temporal variability of the environment. However, when conditions are not harsh outside, like in the case of Fig. 4.16, the change in L_c with τ can reach 30%.

D Metapopulation stability

To study how steady state stability is affected by spatial coupling, let us assume that the population is located at the favorable patches, which is true for small D (that is, close to the uncoupled case), and that the coupling is purely diffusive ($\delta = 1$). For a favorable patch, the deterministic form of Eq. (5-2) reads

$$\begin{aligned}\dot{\rho}_i &= A\rho_i - b\rho_i^2 + D \sum_{j \neq i} (\rho_j - \rho_i) \gamma(d_{ij}) \\ &= (A - D)\rho_i - b\rho_i^2 + D \sum_{j \neq i} \rho_j \gamma(d_{ij}),\end{aligned}\quad (\text{D-1})$$

recalling that $\sum_{j \neq i} \gamma(d_{ij}) = 1$. To estimate the last term, that represents the flow of individuals from the neighborhood towards patch i , J_i^{in} , we consider that $\rho_j \approx \rho_i$. In this case

$$J_i^{in} = \rho_i \sum_{j \neq i} \gamma(d_{ij}), \quad (\text{D-2})$$

where the sum effectively runs over the n_v favorable patches. The average over arrangements of a landscape $\gamma_\mu \equiv \langle \sum_{j \neq i} \gamma(d_{ij}) \rangle$ can be estimated as

$$\gamma_\mu = n_v \int P_\mu(\ell) e^{-\ell/\ell_c} d\ell. \quad (\text{D-3})$$

It depends on μ and on the density h , such that it varies from h (when $\mu = 0$) to 1, in the extreme cases of either maximal density or very large μ . That is, γ_μ increases with μ , with h and with ℓ_c too. Then, Eq. (D-1) can be approximated by

$$\dot{\rho}_i \simeq (A - D[1 - \gamma_\mu])\rho_i - b\rho_i^2 \equiv G\rho_i - b\rho_i^2. \quad (\text{D-4})$$

If $G > 0$, the population will grow and assume a finite value, bounded by the carrying capacity. Meanwhile, D diminishes the effective growth rate G , that becomes negative for sufficiently large D , namely for

$$D > A/(1 - \gamma_\mu), \quad (\text{D-5})$$

indicating decrease of the population. In fact, notice in Fig. 5.5 that, the smaller D , the less frequent the extinction events, for a given μ . This effect

can be mitigated by the landscape, through parameter γ_μ , when the density of favorable sites or clusterization associated with large μ increases. Eq. D-5 also provides the linear stability condition for the null state. If $G < 0$, the population will decrease and go extinct.

E Numerical method for partial differential equations

The numerical integration of the stochastic partial differential equations investigated in this work (Eq. 2-3) were performed following standard finite difference scheme known in the literature [79]. Here we present the method in more details.

Given a partial differential equation such as

$$\partial_t \rho(x, t) = F(\rho) + \Gamma[\rho], \quad (\text{E-1})$$

we start discretizing the population density distribution, writing

$$\rho_{i,n} = \rho(i\Delta x, n\Delta t), \quad (\text{E-2})$$

where i and n are the space and temporal indexes.

To rewrite Eq. (E-1), we need first to note that the temporal derivative can be cast as

$$\partial_t \rho(x, t) \simeq \frac{\rho_{i,n} - \rho_{i,n+1}}{\Delta t}, \quad (\text{E-3})$$

with small Δt . Then, in first order

$$\rho_{i,n+1} = \rho_{i,n} + \mathcal{L}[\rho|M]\Delta t, \quad (\text{E-4})$$

$$= \rho_{i,n} + (F(\rho|M) + \Gamma[\rho|M])\Delta t. \quad (\text{E-5})$$

The correct discrete forms of the local F and Γ contributions are presented below.

From the dynamical operator \mathcal{L} in Eq. (3-7), we have that the local contributions F come from deterministic and stochastic sources. Moreover, the stochastic terms have different interpretations and this should be taken into account in the numerical integration. For the investigated model the local contribution becomes

$$F(\rho)\Delta t = \left(f(\rho_{i,n}) + \frac{\rho_{i,n}}{\Delta x} \right) \Delta t + \eta_d \rho_{i,n} + \xi_d \sqrt{\rho_{i,n}}. \quad (\text{E-6})$$

where

$$\eta_d = \eta_{i,n} \sqrt{\frac{\Delta t}{\Delta x}} \quad (\text{E-7})$$

and

$$\xi_d = \xi_{i,n} \sqrt{\frac{\Delta t}{\Delta x}}, \quad (\text{E-8})$$

with η and ξ being zero mean white Gaussian noises. Note that Stratonovich noise induces a shift in the deterministic term, due to its non-null correlation [46]. For more details see Ref. [79].

The spatial contribution Γ in operator \mathcal{L} is either written in terms of spatial derivatives or convolutions. Respectively, we have that

$$(\partial_x)^{2m} \rho \simeq \frac{1}{(\Delta x)^{2m}} \sum_{j=0}^{2m} (-1)^j \binom{2m}{j} u \left(x + \left(\frac{m}{2} - j \right) \Delta x \right), \quad (\text{E-9})$$

and

$$\int_{-\infty}^{\infty} g(x - x') \rho(x') dx' \simeq \sum_{n'=-\infty}^{\infty} f((n - n') \Delta x) \rho_{i,n} \Delta x. \quad (\text{E-10})$$

At last, Eqs. (E-6), (E-9) and (E-10) sum up typical contribution used in all previous chapters. In order to give a concrete example, consider, for instance, the stochastic Fisher equation $\partial_t \rho = D \partial_{xx} \rho + a \rho - b \rho^2 + \eta \bullet \rho + \sqrt{\rho} \circ \xi$. In this case

$$\begin{aligned} \rho_{i,n+1} &= \rho_{i,n} + (a \rho_{i,n} - b \rho_{i,n}^2 + \rho_{i,n} / \Delta x) \Delta t + \eta_d \rho_{i,n} + \xi_d \sqrt{\rho_{i,n}} \\ &+ D \frac{\rho_{i+1,n} + \rho_{i-1,n} - 2 \rho_{i,n}}{\Delta x^2}, \end{aligned} \quad (\text{E-11})$$

where in order to obtain convergence $\frac{2D\Delta t}{\Delta x^2} < 1$. In other cases, the convergence criteria is not clear, then a systematic investigation needs to be made.

The method described above can be straightforwardly applied in the case of lattices, as done in Chapter 5. In some extreme situations studied, more robust methods might be adequate, such as second or forth order methods [79], to avoid a very small Δt (see Sec. 4.3), making simulation last beyond a feasible computational time.

Bibliography

- [1] NICOLIS, G.; PRIGOGINE, I. **Self-organization in nonequilibrium systems: from dissipative structures to order through fluctuations**. A Wiley-Interscience Publication. Wiley, 1977.
- [2] MARCHETTI, M. C.; JOANNY, J. F.; RAMASWAMY, S.; LIVERPOOL, T. B.; PROST, J.; RAO, M. ; SIMHA, R. A. **Rev. Mod. Phys.** Hydrodynamics of soft active matter, journal, v.85, p. 1143–1189, Jul 2013.
- [3] CASTELLANO, C.; FORTUNATO, S. ; LORETO, V. **Rev. Mod. Phys.** Statistical physics of social dynamics, journal, v.81, p. 591–646, May 2009.
- [4] MATURANA, H. R.; VARELA, F. J. **Autopoiesis and cognition: The realization of the living**, volume 42. Springer Science & Business Media, 1991.
- [5] ANDERSON, P. W. **Science**. More is different, journal, v.177, n.4047, p. 393–396, 1972.
- [6] MURRAY, J. D. **Mathematical Biology: I. An Introduction**. Interdisciplinary Applied Mathematics. Springer, 2002.
- [7] TURCHIN, P. **Quantitative Analysis of Movement: Measuring and Modeling Population Redistribution in Animals and Plants**. Beresta Books, 2015.
- [8] OVASKAINEN, O.; FINKELSHTEIN, D.; KUTOVIY, O.; CORNELL, S.; BOLKER, B. ; KONDRATIEV, Y. **Theoretical Ecology**. A general mathematical framework for the analysis of spatiotemporal point processes, journal, v.7, n.1, p. 101–113, Feb 2014.
- [9] MACARTHUR, R. H.; WILSON, E. O. **The theory of island biogeography**. Princeton University Press, 2016.
- [10] LEVIN, S. A. **Annual Review of Ecology and Systematics**. Population dynamic models in heterogeneous environments, journal, v.7, p. 287–310, 1976.

- [11] HANSKI, I.; KUUSSAARI, M. ; NIEMINEN, M. **Ecology**. Metapopulation structure and migration in the butterfly *melitaea cinxia*, journal, v.75, n.3, p. pp. 747–762, 1994.
- [12] SKELLAM, J. G. **Bulletin of Mathematical Biology**. Random dispersal in theoretical populations, journal, v.53, p. 135–165, 1991.
- [13] LUDWIG, D.; ARONSON, D. ; WEINBERGER, H. **Journal of Mathematical Biology**. Spatial patterning of the spruce budworm, journal, v.8, n.3, p. 217–258, 1979.
- [14] HOLMES, E. E.; LEWIS, M. A.; BANKS, J. ; VEIT, R. **Ecology**. Partial differential equations in ecology: spatial interactions and population dynamics, journal, p. 17–29, 1994.
- [15] BALLARD, M.; KENKRE, V. M. ; KUPERMAN, M. N. **Phys. Rev. E**. Periodically varying externally imposed environmental effects on population dynamics, journal, v.70, p. 031912, Sep 2004.
- [16] NEICU, T.; PRADHAN, A.; LAROCHELLE, D. A. ; KUDROLLI, A. **Phys. Rev. E**. Extinction transition in bacterial colonies under forced convection, journal, v.62, p. 1059–1062, Jul 2000.
- [17] PERRY, N. **Journal of The Royal Society Interface**. Experimental validation of a critical domain size in reaction–diffusion systems with *escherichia coli* populations, journal, v.2, n.4, p. 379–387, 2005.
- [18] KENKRE, V.; KUPERMAN, M. **Physical Review E**. Applicability of the Fisher equation to bacterial population dynamics, journal, v.67, n.5, p. 051921, May 2003.
- [19] ARTILES, W.; CARVALHO, P. G. S. ; KRAENKEL, R. A. **Journal of Mathematical Biology**. Patch-size and isolation effects in the fisher–kolmogorov equation, journal, v.57, n.4, p. 521–535, 2008.
- [20] KENKRE, V. M.; KUMAR, N. **Proceedings of the National Academy of Sciences**. Nonlinearity in bacterial population dynamics: Proposal for experiments for the observation of abrupt transitions in patches, journal, v.105, n.48, p. 18752–18757, 2008.
- [21] BERTI, S.; CENCINI, M.; VERGNI, D. ; VULPIANI, A. **Phys. Rev. E**. Extinction dynamics of a discrete population in an oasis, journal, v.92, p. 012722, Jul 2015.

- [22] HANSKI, I.; OVASKAINEN, O. **Nature**. The metapopulation capacity of a fragmented landscape, journal, v.404, n.6779, p. 755–758, 04 2000.
- [23] HANSKI, I. **Nature**. Metapopulation dynamics, journal, v.396, n.6706, p. 41–49, Nov. 1998.
- [24] HANSKI, I. **Metapopulation Ecology**. Oxford series in ecology and evolution. Oxford University Press, 1999.
- [25] MAY, R. M. **Stability and complexity in model ecosystems**, volume 6. Princeton university press, 2001.
- [26] SAUNDERS, D. A.; HOBBS, R. J. ; MARGULES, C. R. **Conservation Biology**. Biological consequences of ecosystem fragmentation: A review, journal, v.5, n.1, p. 18–32, 1991.
- [27] CRUTZEN, P. J. **The “anthropocene”**. In: EARTH SYSTEM SCIENCE IN THE ANTHROPOCENE, p. 13–18. Springer, 2006.
- [28] TURNER, M. G.; GARDNER, R. H.; O’NEILL, R. V. ; OTHERS. **Landscape ecology in theory and practice**, volume 401. Springer, 2001.
- [29] SEDDON, P. J.; ARMSTRONG, D. P. ; MALONEY, R. F. **Conservation Biology**. Developing the science of reintroduction biology, journal, v.21, n.2, p. 303–312, 2007.
- [30] CONDIT, R.; ASHTON, P. S.; BAKER, P.; BUNYAVEJCHEWIN, S.; GUNATILLEKE, S.; GUNATILLEKE, N.; HUBBELL, S. P.; FOSTER, R. B.; ITOH, A.; LAFRANKIE, J. V.; LEE, H. S.; LOSOS, E.; MANOKARAN, N.; SUKUMAR, R. ; YAMAKURA, T. **Science**. Spatial patterns in the distribution of tropical tree species, journal, v.288, n.5470, p. 1414–1418, 2000.
- [31] DE OLIVEIRA SANTOS, M.; STOSIC, T. ; STOSIC, B. D. **Physica A: Statistical Mechanics and its Applications**. Long-term correlations in hourly wind speed records in pernambuco, brazil, journal, v.391, n.4, p. 1546 – 1552, 2012.
- [32] RIASCOS, A. P. **Phys. Rev. E**. Universal scaling of the distribution of land in urban areas, journal, v.96, p. 032302, Sep 2017.
- [33] DA SILVA, L. A.; COLOMBO, E. H. ; ANTENEODO, C. **Phys. Rev. E**. Effect of environment fluctuations on pattern formation of single species, journal, v.90, p. 012813, Jul 2014.

- [34] COLOMBO, E.; ANTENEODO, C. **Journal of Theoretical Biology**. Nonlinear population dynamics in a bounded habitat, journal, v.446, p. 11 – 18, 2018.
- [35] COLOMBO, E. H.; ANTENEODO, C. **Phys. Rev. E**. Population dynamics in an intermittent refuge, journal, v.94, p. 042413, Oct 2016.
- [36] COLOMBO, E. H.; ANTENEODO, C. **Phys. Rev. E**. Metapopulation dynamics in a complex ecological landscape, journal, v.92, p. 022714, Aug 2015.
- [37] HERNÁNDEZ-GARCÍA, E.; LÓPEZ, C. **Phys. Rev. E**. Clustering, advection, and patterns in a model of population dynamics with neighborhood-dependent rates, journal, v.70, p. 016216, Jul 2004.
- [38] KEYMER, J. E.; GALAJDA, P.; MULDOON, C.; PARK, S. ; AUSTIN, R. H. **Proceedings of the National Academy of Sciences**. Bacterial metapopulations in nanofabricated landscapes, journal, v.103, n.46, p. 17290–17295, 2006.
- [39] GIOMETTO, A.; ALTERMATT, F.; MARITAN, A.; STOCKER, R. ; RINALDO, A. **Proceedings of the National Academy of Sciences of the United States of America**. Generalized receptor law governs phototaxis in the phytoplankton euglena gracilis, journal, v.112, n.22, p. 7045–7050, 06 2015.
- [40] GARCIA, R. R.; DUNKERTON, T. J.; LIEBERMAN, R. S. ; VINCENT, R. A. **Journal of Geophysical Research: Atmospheres**. Climatology of the semiannual oscillation of the tropical middle atmosphere, journal, v.102, n.D22, p. 26019–26032, 1997.
- [41] PENG, C.-K.; BULDYREV, S. V.; HAVLIN, S.; SIMONS, M.; STANLEY, H. E. ; GOLDBERGER, A. L. **Phys. Rev. E**. Mosaic organization of dna nucleotides, journal, v.49, p. 1685–1689, Feb 1994.
- [42] ESCUDERO, C.; BUCETA, J.; DE LA RUBIA, F. J. ; LINDENBERG, K. **Phys. Rev. E**. Extinction in population dynamics, journal, v.69, p. 021908, Feb 2004.
- [43] ASSAF, M.; MEERSON, B. **Physical Review E**. Extinction of metastable stochastic populations, journal, v.81, n.2, p. 021116, 2010.
- [44] OVASKAINEN, O.; MEERSON, B. **Trends in Ecology & Evolution**. Stochastic models of population extinction, journal, v.25, n.11, p. 643–652, 2014/08/20.

- [45] VERHULST, P. F. **Correspondance mathématique et physique**. Notice sur la loi que la population poursuit dans son accroissement, journal, v.10, p. 113–121, 1838.
- [46] KAMPEN, N. **Journal of Statistical Physics**. Itô versus stratonovich, journal, v.24, n.1, p. 175–187, 1981.
- [47] MEERSON, B.; OVASKAINEN, O. **Phys. Rev. E**. Immigration-extinction dynamics of stochastic populations, journal, v.88, p. 012124, Jul 2013.
- [48] HAKOYAMA, H.; IWASA, Y. **Journal of Theoretical Biology**. Extinction risk of a density-dependent population estimated from a time series of population size, journal, v.204, n.3, p. 337 – 359, 2000.
- [49] HAKOYAMA, H.; IWASA, Y. **Journal of Theoretical Biology**. Extinction risk of a meta-population: aggregation approach, journal, v.232, n.2, p. 203 – 216, 2005.
- [50] HORSTHEMKE, W.; LEFEVER, R. **Noise-Induced Transitions: Theory and Applications in Physics, Chemistry, and Biology**. Springer complexity. Physica-Verlag, 2006.
- [51] COLOMBO, E. H., L. D. S.; ANTENEODO, C. **Unpublished**. Stochastic ressonance in population extinction times, journal.
- [52] TAILLEUR, J.; CATES, M. E. **Phys. Rev. Lett**. Statistical mechanics of interacting run-and-tumble bacteria, journal, v.100, p. 218103, May 2008.
- [53] BAGUETTE, M. **Ecography**. Long distance dispersal and landscape occupancy in a metapopulation of the cranberry fritillary butterfly, journal, v.26, n.2, p. 153–160, 2003.
- [54] FRIC, Z.; KONVICKA, M. **Basic and Applied Ecology**. Dispersal kernels of butterflies: Power-law functions are invariant to marking frequency, journal, v.8, n.4, p. 377 – 386, 2007.
- [55] EDWARDS, A. M.; PHILLIPS, R. A.; WATKINS, N. W.; FREEMAN, M. P.; MURPHY, E. J.; AFANASYEV, V.; BULDYREV, S. V.; DA LUZ, M. G.; RAPOSO, E. P.; STANLEY, H. E. ; OTHERS. **Nature**. Revisiting lévy flight search patterns of wandering albatrosses, bumblebees and deer, journal, v.449, n.7165, p. 1044, 2007.
- [56] FISHER, R. **Annals of Eugenics**. The Wave of Advance of Advantageous Genes., journal, v.7, p. 355–369, 1937.

- [57] KOLMOGOROV, A. N.; PETROVSKII, I. G. ; PISKUNOV, N. S. **Bjul. Moskovskogo Gos. Univ.** A study of the equation of diffusion with increase in the quantity of matter, and its application to a biological problem, journal, v.1, n.7, p. 1–26, 1937.
- [58] THERAULAZ, G.; BONABEAU, E.; NICOLIS, S. C.; SOLÉ, R. V.; FOURCASSIÉ, V.; BLANCO, S.; FOURNIER, R.; JOLY, J.-L.; FERNÁNDEZ, P.; GRIMAL, A.; DALLE, P. ; DENEUBOURG, J.-L. **Proceedings of the National Academy of Sciences.** Spatial patterns in ant colonies, journal, v.99, n.15, p. 9645–9649, 2002.
- [59] TONER, J.; TU, Y. **Phys. Rev. Lett.** Long-range order in a two-dimensional dynamical XY model: How birds fly together, journal, v.75, p. 4326–4329, Dec 1995.
- [60] RUDGE, T. J.; FEDERICI, F.; STEINER, P. J.; KAN, A. ; HASELOFF, J. **ACS Synthetic Biology.** Cell polarity-driven instability generates self-organized, fractal patterning of cell layers, journal, v.2, n.12, p. 705–714, 2013.
- [61] ALIM, K.; AMSELEM, G.; PEAUDECERF, F.; BRENNER, M. P. ; PRINGLE, A. **Proceedings of the National Academy of Sciences.** Random network peristalsis in physarum polycephalum organizes fluid flows across an individual, journal, v.110, n.33, p. 13306–13311, 2013.
- [62] FERNANDEZ-OTO, C.; CLERC, M.; ESCAFF, D. ; TLIDI, M. **Physical review letters.** Strong nonlocal coupling stabilizes localized structures: an analysis based on front dynamics, journal, v.110, n.17, p. 174101, 2013.
- [63] MARTÍNEZ-GARCÍA, R.; CALABRESE, J. M.; HERNÁNDEZ-GARCÍA, E. ; LÓPEZ, C. **Philosophical transactions. Series A, Mathematical, physical, and engineering sciences.** Minimal mechanisms for vegetation patterns in semiarid regions, journal, v.372, n.2027, p. 20140068, Oct. 2014.
- [64] DA CUNHA, J. A. R.; PENNA, A. L. A. ; OLIVEIRA, F. A. **Physical Review E.** Pattern formation and coexistence domains for a nonlocal population dynamics, journal, v.83, n.1, p. 15201, Jan. 2011.
- [65] FUENTES, M. A.; KUPERMAN, M. N. ; KENKRE, V. M. **Physical Review Letters.** Nonlocal Interaction Effects on Pattern Formation in Population Dynamics, journal, v.91, n.15, p. 158104, Oct. 2003.

- [66] FUENTES, M. A.; KUPERMAN, M. N. ; KENKRE, V. M. **The Journal of Physical Chemistry B**. Analytical Considerations in the Study of Spatial Patterns Arising from Nonlocal Interaction Effects†, journal, v.108, n.29, p. 10505–10508, May 2004.
- [67] MENDOZA-COTO, A.; STARIOLO, D. A. ; NICOLAO, L. **Phys. Rev. Lett.** Nature of long-range order in stripe-forming systems with long-range repulsive interactions, journal, v.114, p. 116101, Mar 2015.
- [68] RATKOWSKY, D. A.; OLLEY, J.; MCMEEKIN, T. A. ; BALL, A. J. **Bacteriol.** Relationship between temperature and growth rate of bacterial cultures., journal, v.149, n.1, p. 1–5, Jan. 1982.
- [69] FARRELL, J.; ROSE, A. **Annual Reviews in Microbiology**. Temperature effects on microorganisms, journal, v.21, n.1, p. 101–120, 1967.
- [70] FERNANDEZ-OTO, C.; TLIDI, M.; ESCAFF, D. ; CLERC, M. G. **Philosophical Transactions of the Royal Society of London A: Mathematical, Physical and Engineering Sciences**. Strong interaction between plants induces circular barren patches: fairy circles, journal, v.372, n.2027, 2014.
- [71] TARNITA, C. E.; BONACHELA, J. A.; SHEFFER, E.; GUYTON, J. A.; COVERDALE, T. C.; LONG, R. A. ; PRINGLE, R. M. **Nature**. A theoretical foundation for multi-scale regular vegetation patterns, journal, v.541, n.7637, p. 398, 2017.
- [72] TURELLI, M. **Theoretical Population Biology**. Random environments and stochastic calculus, journal, v.12, n.2, p. 140 – 178, 1977.
- [73] CROSS, M.; HOHENBERG, P. **Pattern formation outside of equilibrium**, volume 65. American Physical Society, July 1993, 851–1112p.
- [74] PIGOLOTTI, S.; LÓPEZ, C.; HERNÁNDEZ-GARCÍA, E. ; ANDERSEN, K. H. **Theoretical Ecology**. How gaussian competition leads to lumpy or uniform species distributions, journal, v.3, n.2, p. 89–96, 2010.
- [75] COLOMBO, E. **Master dissertation**. Formação de padrões espaciais na dinâmica de populações., journal, 2012.
- [76] RIDOLFI, L.; D’ODORICO, P. ; LAIO, F. **Noise-induced phenomena in the environmental sciences**. Cambridge University Press, 2011.

- [77] IBAÑES, M.; GARCÍA-OJALVO, J.; TORAL, R. ; SANCHO, J. M. **Linear instability mechanisms of noise-induced phase transitions**. In: STOCHASTIC PROCESSES IN PHYSICS, CHEMISTRY, AND BIOLOGY, p. 247–256. Springer, 2000.
- [78] NOVIKOV, E. A. **JETP**. Functionals and the random-force method in turbulence theory, journal, v.20, n.5, p. 1290, 1965.
- [79] SAGUÉS, F.; SANCHO, J. ; GARCÍA-OJALVO, J. **Reviews of Modern Physics**. Spatiotemporal order out of noise, journal, v.79, n.3, p. 829–882, July 2007.
- [80] KEYMER, J. E.; GALAJDA, P.; MULDOON, C.; PARK, S. ; AUSTIN, R. H. **Proceedings of the National Academy of Sciences**. Bacterial metapopulations in nanofabricated landscapes, journal, v.103, n.46, p. 17290–17295, 2006.
- [81] MACIEL, G. A.; LUTSCHER, F. **The American Naturalist**. How individual movement response to habitat edges affects population persistence and spatial spread, journal, v.182, n.1, p. 42–52, 2013.
- [82] NEWMAN, W. I. **Journal of Theoretical Biology**. Some exact solutions to a non-linear diffusion problem in population genetics and combustion, journal, v.85, n.2, p. 325 – 334, 1980.
- [83] GALAKTIONOV, V. A.; VÁZQUEZ, J. L. **Discrete and continuous dynamical systems**. The problem of blow-up in nonlinear parabolic equations, journal, v.8, n.2, p. 399–434, 2002.
- [84] FUJITA, H. **J. Fac. Sci. Univ. Tokyo Sec. 1A Math**. On the blowing up of solutions of the cauchy problem for $u_t = \Delta u + u^{1+\alpha}$, journal, v.16, p. 105, 1966.
- [85] PRESS, W. H.; TEUKOLSKY, S. A.; VETTERLING, W. T. ; FLANNERY, B. P. **Numerical Recipes 3rd Edition: The Art of Scientific Computing**. 3. ed., New York, NY, USA: Cambridge University Press, 2007.
- [86] COURCHAMP, F.; CLUTTON-BROCK, T. ; GRENFELL, B. **Trends in Ecology & Evolution**. Inverse density dependence and the allee effect, journal, v.14, n.10, p. 405 – 410, 1999.
- [87] CATES, M.; MARENDUZZO, D.; PAGONABARRAGA, I. ; TAILLEUR, J. **Proceedings of the National Academy of**

- Sciences. Arrested phase separation in reproducing bacteria creates a generic route to pattern formation, journal, v.107, n.26, p. 11715–11720, 2010.
- [88] MURRAY, J. D. **Mathematical Biology: I. An Introduction**. Interdisciplinary Applied Mathematics. Springer, 2002.
- [89] GURTIN, M. E.; MACCAMY, R. C. **Mathematical Biosciences**. On the diffusion of biological populations, journal, v.33, n.1, p. 35 – 49, 1977.
- [90] KAREIVA, P. **Oecologia**. Local movement in herbivorous insects: applying a passive diffusion model to mark-recapture field experiments, journal, v.57, n.3, p. 322–327, 1983.
- [91] TSALLIS, C.; BUKMAN, D. J. **Physical Review E**. Anomalous diffusion in the presence of external forces: Exact time-dependent solutions and their thermostistical basis, journal, v.54, n.3, p. R2197–R2200, Sept. 1996.
- [92] ANTENEODO, C. **Physica A: Statistical Mechanics and its Applications**. Non-extensive random walks, journal, v.358, n.2, p. 289 – 298, 2005.
- [93] LENZI, E.; ANTENEODO, C. ; BORLAND, L. **Physical Review E**. Escape time in anomalous diffusive media, journal, v.63, n.5, p. 051109, 2001.
- [94] SOSA-HERNÁNDEZ, J. E.; SANTILLÁN, M. ; SANTANA-SOLANO, J. **Phys. Rev. E**. Motility of escherichia coli in a quasi-two-dimensional porous medium, journal, v.95, p. 032404, Mar 2017.
- [95] MUSKAT, M.; WYCKOFF, R. D. ; OTHERS. **Flow of homogeneous fluids through porous media**. McGraw-Hill Book Company, Inc., 1937.
- [96] TSALLIS, C.; BUKMAN, D. J. **Physical Review E**. Anomalous diffusion in the presence of external forces: Exact time-dependent solutions and their thermostistical basis, journal, v.54, n.3, p. R2197–R2200, Sept. 1996.
- [97] NEWMAN, W. I.; SAGAN, C. **Icarus**. Galactic civilizations: Population dynamics and interstellar diffusion, journal, v.46, n.3, p. 293–327, 1981.
- [98] ANTENEODO, C. **Physical Review E**. Brownian motors in nonlinear diffusive media, journal, v.76, n.2, p. 021102, 2007.

- [99] WALKER, M.; HALL, A.; ANDERSON, R. M. ; BASÁÑEZ, M.-G. **Parasites & Vectors**. Density-dependent effects on the weight of female ascaris lumbricoides infections of humans and its impact on patterns of egg production, journal, v.2, p. 11–11, 2009.
- [100] TRONCOSO, P.; FIERRO, O.; CURILEF, S. ; PLASTINO, A. **Physica A: Statistical Mechanics and its Applications**. A family of evolution equations with nonlinear diffusion, verhulst growth, and global regulation: Exact time-dependent solutions, journal, v.375, n.2, p. 457 – 466, 2007.
- [101] RYABOV, A. B.; BLASIUS, B. **Mathematical Modelling of Natural Phenomena**. Population growth and persistence in a heterogeneous environment: the role of diffusion and advection, journal, v.3, p. 42–86, 1 2008.
- [102] MARRO, J.; DICKMAN, R. **Nonequilibrium phase transitions in lattice models**. Cambridge University Press, 2005.
- [103] ABRAMOWITZ, M.; STEGUN, I. A. ; OTHERS. **Handbook of mathematical functions with formulas, graphs, and mathematical tables**, volume 9. Dover, New York, 1972.
- [104] KEYMER, J. E.; MARQUET, P. A.; VELASCO-HERNÁNDEZ, J. X. ; LEVIN, S. A. **The American Naturalist**. Extinction thresholds and metapopulation persistence in dynamic landscapes, journal, v.156, n.5, p. 478–494, 2000.
- [105] REIGADA, C.; SCHREIBER, S. J.; ALTERMATT, F. ; HOLYOAK, M. **The American Naturalist**. Metapopulation dynamics on ephemeral patches, journal, v.185, n.2, p. 183–195, 2015.
- [106] CORNELL, S. J.; OVASKAINEN, O. **Theoretical Population Biology**. Exact asymptotic analysis for metapopulation dynamics on correlated dynamic landscapes, journal, v.74, n.3, p. 209 – 225, 2008.
- [107] LIN, A. L.; MANN, B. A.; TORRES-OVIEDO, G.; LINCOLN, B.; KÄS, J. ; SWINNEY, H. L. **Biophysical Journal**. Localization and extinction of bacterial populations under inhomogeneous growth conditions, journal, v.87, n.1, p. 75 – 80, 2004.
- [108] MÓNDEZ, V.; LLOPIS, I.; CAMPOS, D. ; HORSTHEMKE, W. **Theoretical Population Biology**. Extinction conditions for isolated populations affected by environmental stochasticity, journal, v.77, n.4, p. 250 – 256, 2010.

- [109] MURRAY, J. D. **Mathematical Biology II: Spatial Models and Biomedical Applications**. Interdisciplinary Applied Mathematics. Springer, 2003.
- [110] FONSECA, C. R.; COUTINHO, R. M.; AZEVEDO, F.; BERBERT, J. M.; CORSO, G. ; KRAENKEL, R. A. **PLoS ONE**. Modeling habitat split: Landscape and life history traits determine amphibian extinction thresholds, journal, v.8, n.6, p. e66806, 06 2013.
- [111] LEVINS, R. **Bulletin of the ESA**. Some demographic and genetic consequences of environmental heterogeneity for biological control, journal, v.15, n.3, p. 237–240, 1969.
- [112] HAMBÄCK, P. A.; ENGLUND, G. **Ecology Letters**. Patch area, population density and the scaling of migration rates: the resource concentration hypothesis revisited, journal, v.8, n.10, p. 1057–1065, 2005.
- [113] HANSKI, I.; OVASKAINEN, O. **Nature**. The metapopulation capacity of a fragmented landscape, journal, v.404, n.6779, p. 755–758, 04 2000.
- [114] CORNELL, S. J.; OVASKAINEN, O. **Theoretical Population Biology**. Exact asymptotic analysis for metapopulation dynamics on correlated dynamic landscapes, journal, v.74, n.3, p. 209 – 225, 2008.
- [115] NORTH, A.; OVASKAINEN, O. **Oikos**. Interactions between dispersal, competition, and landscape heterogeneity, journal, v.116, p. 1106–1119, 2007.
- [116] OVASKAINEN, O.; FINKELSHTEIN, D.; KUTOVIY, O.; CORNELL, S.; BOLKER, B. ; KONDRATIEV, Y. **Theoretical Ecology**. A general mathematical framework for the analysis of spatiotemporal point processes, journal, v.7, n.1, p. 101–113, 2014.
- [117] KRAENKEL, R.; DA SILVA, D. P. **Physica A: Statistical Mechanics and its Applications**. Stochastic skellam model, journal, v.389, n.1, p. 60 – 66, 2010.
- [118] KEITT, T. H.; STANLEY, H. E. **Nature**. Dynamics of north american breeding bird populations, journal, v.393, n.6682, p. 257–260, 05 1998.
- [119] BERBERT, J. M.; FAGAN, W. F. **Ecological Complexity**. How the interplay between individual spatial memory and landscape persistence can generate population distribution patterns, journal, v.12, n.0, p. 1 – 12, 2012.

- [120] FERREIRA, A.; RAPOSO, E.; VISWANATHAN, G. ; DA LUZ, M. **Physica A: Statistical Mechanics and its Applications**. The influence of the environment on lévy random search efficiency: Fractality and memory effects, journal, v.391, n.11, p. 3234 – 3246, 2012.
- [121] Given that the boundary conditions are periodic, distances obey the so called minimum image convention. See M. P. Allen and D.J. Tildesley, *Computer simulation of liquids* (Oxford university press, 1989). Distances are measured in unit cell side length.
- [122] GILARRANZ, L. J.; BASCOMPTE, J. **Journal of Theoretical Biology**. Spatial network structure and metapopulation persistence, journal, v.297, n.0, p. 11 – 16, 2012.
- [123] BASCOMPTE, J.; SOLE, R. V. **Journal of Animal Ecology**. Habitat fragmentation and extinction thresholds in spatially explicit models, journal, v.65, n.4, p. 465–473, 07 1996.
- [124] FORMAN, R. T. **Landscape Ecology**. Some general principles of landscape and regional ecology, journal, v.10, n.3, p. 133–142, 1995.
- [125] MIRAMONTES, O.; BOYER, D. ; BARTUMEUS, F. **PLoS ONE**. The effects of spatially heterogeneous prey distributions on detection patterns in foraging seabirds, journal, v.7, n.4, p. e34317, 04 2012.
- [126] KENKEL, N.; WALKER, D. **Abst. Bot.** Fractals and ecology, journal, v.17, p. 53–70, 1993.
- [127] SUGIHARA, G.; MAY, R. M. **Trends in Ecology & Evolution**. Applications of fractals in ecology, journal, v.5, n.3, p. 79 – 86, 1990.
- [128] **Journal of Oceanography**. TSUDA, A., journal, v.51, n.3, p. 261–266, 1995.
- [129] GARCÍA-OJALVO, J.; SANCHO, J. **Noise in spatially extended systems**. Springer Science & Business Media, 2012.
- [130] PIGOLOTTI, S.; FLAMMINI, A.; MARSILI, M. ; MARITAN, A. **Proceedings of the National Academy of Sciences of the United States of America**. Species lifetime distribution for simple models of ecologies, journal, v.102, n.44, p. 15747–15751, 2005.
- [131] OVASKAINEN, O.; FINKELSHTEIN, D.; KUTOVIY, O.; CORNELL, S.; BOLKER, B. ; KONDRATIEV, Y. **Theoretical Ecology**. A general

- mathematical framework for the analysis of spatiotemporal point processes, journal, v.7, n.1, p. 101–113, 2014.
- [132] DRURY, K.; DRAKE, J.; LODGE, D. ; DWYER, G. **Ecological Modelling**. Immigration events dispersed in space and time: Factors affecting invasion success, journal, v.206, n.1–2, p. 63 – 78, 2007.
- [133] LAIO, F.; PORPORATO, A.; RIDOLFI, L. ; RODRIGUEZ-ITURBE, I. **Phys. Rev. E**. Mean first passage times of processes driven by white shot noise, journal, v.63, p. 036105, Feb 2001.
- [134] ALLEN, A.; LI, B.-L. ; CHARNOV, E. **Ecology Letters**. Population fluctuations, power laws and mixtures of lognormal distributions, journal, v.4, n.1, p. 1–3, 2001.
- [135] VAN KAMPEN, N. **Stochastic Processes in Physics and Chemistry**. North-Holland Personal Library. Elsevier Science, 2011.